Shanghai HIgh repetitioN rate XFEL and Extreme light facility (SHINE)

Technical Design Report of FEL-II beamline

September 2021

Directory

1. Beamline introduction

The energy range covered by the FEL-II (soft X-ray) beamline is 0.2-3keV, optimized energy range of 0.4-3 keV, where the energy range covered by monochromatic beam is 0.4-2 keV. The beamline is mainly composed of three parts: the front-end area, the beam transmission system and the online diagnosis system, supplemented by the control system, personal and equipment safety system, etc., to deliver high brightness and high coherence soft X-ray laser to the Atomic and Molecular Reaction Imaging Experimental Station (AMO), the Soft X-ray High Resolution Resonance Scattering Experimental Station (SSS), and the Electronic Structure Experimental Station (SES) according to the experimental requirements.

The front-end area is an important part of the beamline, which is the transition between the undulator and the beam transmission area, and its function is to guide the free electron laser to the beam transmission area, ensure the safety of vacuum and radiation, and carry out real-time diagnosis of luminous flux attenuation, beam intensity and position, but at the same time, it must take into account the various requirements given by other related systems, such as beam position interlocking threshold, gas pressure, etc.; In addition to the relationship with the oscillator and beamline, it also involves buildings, utilities, etc., and the requirements, conditions, and parameters they provide must be considered in the front-end design. Specifically, its main functions include: (1) component safety protection: to ensure that FEL pulses will not be directly irradiated on unprotected components; (2) Beam diagnosis: real-time monitoring and diagnosis of FEL luminous flux and beam position; (3) Flux attenuation: The X-rays generated by the oscillator are mainly attenuated in the beamline debugging stage to protect the safety of downstream components; (4) Vacuum protection: provide two-way vacuum interlocking protection for accelerator and beam line; (5) Personal protection: block high-energy ductile radiation, high-energy spontaneous radiation and neutron radiation, and provide reliable radiation shielding for the staff and instruments and equipment in the beam transmission and experimental area. The main equipment in the front-end area is: 1. Isolation valve, fast valve and slow valve that play the role of vacuum protection; 2. Movable photon light shield used to ensure that the vacuum protection system and safety shutter are damaged by the action of the laser; 3. A fixed diaphragm that protects the follow-up components from direct irradiation of FEL pulses when the oscillator beam drifts, and its absorber is boron carbide material; 4. The safety shutter is used to block the radiation, gas toughness radiation and synchrotron radiation generated when the electronic and equipment hardware of the linear accelerator collides, so as to ensure the personal safety of the staff entering the diagnostic area during injection or operation; 5. Gas flux attenuator: the necessary attenuation of the incident laser intensity, especially in the equipment installation and commissioning stage of the beam transmission area, the effective reduction of the laser intensity through the attenuator can avoid the damage caused by excessive instantaneous radiation damage to the subsequent optical components and the saturation of the detector.

After passing through the front-end area, the X-ray laser enters the beam delivery system. The beam delivery system is mainly composed of an offset mirror group, a grating monochromator, a deflection mirror and three KB focusing systems. Its main function is to transmit FEL pulses to each experimental station, and to monochromatize and focus the FEL pulses as required according to the different experimental station.

The optical elements on the beamline are mainly composed of an offset mirror group, a grating monochromator, a deflection mirror, and three KB focusing systems: the main function of the offset mirror group is to separate the high-energy radiation coming out of the upstream accelerator and the X-ray free electron laser beam. The offset mirror set consists of two groups of three mirrors to cover the photon energy range of 0.2-2keV and 2-3keV, respectively. The three mirrors are all plane type mirrors. The main function of the grating monochromator, which covers the photon energy range of 0.4-2keV, is to provide the required high-resolution monochromatic beam for the experimental station adopting the variable angle mode. The variable line distance grating with aberration correction function is selected to focus the beam in the vertical direction to the exit slit. And the plane mirror can be moved out of the optical path, so that the straight-through beam could directly transmit to the subsequent optical element without passing through the monochromator. The deflection mirror is composed of two mirrors, in which the plane mirror deflects the beam to the SES experimental station, and the elliptical cylindrical mirror focuses the beam to the SSS experimental station while deflecting the beam. The KB focusing system will focus the upstream FEL pulse to the sample point according to the different needs of each experimental station.

2. Design basis

2.1 Design specification

Table 2.1-1 shows the specification of FEL-II beamline.

Table 2.1-1 FEL-II beamline specification

	Nominal	Objective
Photon energy	0.2-3keV	0.5-2keV
Energy resolving power	>15000@867eV	>10000@867eV
Single-pulse photon transmission efficiency	30%@1keV（No monochromators）	15%@1keV（No monochromators）
Spot size at the sample	<10μm x 6μm （HxV, FWHM）	<20μm x 12μm （HxV, FWHM）

The above indicators are all the results of the electron energy of 8 GeV, in which the design value of the photon energy range is the energy range that can be covered by the monochromator, and the photon energy range that finally reaches the experimental station also depends on the photon energy radiated by the front-end oscillator.

2.2 Experimental station requirements

The FEL-II beamline needed to provide the required high-quality FEL pulses for the four experimental stations, all of which were located in the near-experimental hall of the SHINE unit approximately 350 meters from the FEL-II oscillator light source. Among the three experimental stations, the Electronic Structure of Matter Experimental Station (SES) and the Soft X-ray High Resolution Resonance Scattering Experimental Station (SSS) are located in the branch line, and these two experimental stations require monochromatic light incidence. The Atomic and Molecular Reaction Imaging Experiment (AMO) is located in the through line, and these two stations do not require monochromatic light incidence, but can use pink light. Among the above-mentioned experimental stations, the AMO experimental station contains three sub-experimental systems, and the SES experimental station contains two sub-experimental systems. The specifications of each experimental station are shown in Table 22-1.

Table 2.2-1 Specification of each experimental station in the FEL-II beamline

The name of the experimental station	The name of the parameter	Design metrics	Acceptance indicators
Atomic and Molecular Reaction Imaging Experiment Station (AMO).	Ionic momentum resolution	≤3%	≤5%
Electronic Structure of Matter Experimental Station (SES).	Spatial resolution	≤100nm	≤500nm
	Temporal	≤60fs	≤80fs

	resolution		
Soft X-ray High Resolution Resonance Scattering Experiment (SSS).	Energy resolution of the spectrometer	50meV@1000 eV	100meV@1000eV

*This resolution is the resolution that can be achieved by the spatial geometry of the experimental station design, and the actual imaging resolution depends on the brightness of the light source and the performance of the detector.

According to the different scientific objectives and specific experimental conditions of each experimental station, each experimental station also puts forward different specific requirements for the energy resolution of the incident light, the size of the focused spot and other parameters, and the specific requirements of each experimental station are shown in Table 2.2-2.

Table 2.2-2 Specific requirements of the experimental station

			SSS	AMO	SES
1	Energy range		0.2-3 keV[1]	0.2~3 keV	0.2~3keV[1]
2	Optimize energy points or ranges		0.4~1.7keV	0.3 ~2keV	0.4~1.5keV
3	Energy resolution requirements		⩾50000@930eV	/	⩾ 40000@0.4keV&0.93keV
4	Single-pulse transmission efficiency		0.4%@900eV (800l/mm)	30%[2]	/
5	Higher harmonic content		/	⩽10% (400eV-1000eV) ⩽1% (1000eV-3000eV)	/
6	Sample point focus spot size requirements （H×V, FWHM）		>25 μ m (H)@900eV[2] <1.8 μ m (V) @900eV[2]	The 1st focal point < 2 μm × 2μm @900 eV The 2nd focal point < 4μm × 4μm @900 eV The 3rd focal point < 6μm× 6μm @900 eV	The 1st focal point < 10μm × 10μm @ 0.4keV The 2nd focal point < 20μm × 20μm @0.4keV
7	Spot divergence angle requirement (FWHM).		⩽26mrad	/	/
8	Spot stability (RMS).		⩽1μm [3] [4]	⩽10 μm [3]	⩽4 μm [3]
9	Working distance		⩾1m	The distance between the trifocal and the last outlet flange of the KB mirror box is 1.5 m, 3.4 m and 5.2 m	Bifocal: PEM is about 4.5m from the center of the KB case, and TAP is 8.5m from the center of the KB case
10	Single pulse width		⩽200 fs	10-30 fs (Accelerator 25-36 fs).	/
11	Attenuation demand		3 orders of magnitude adjustable	3 orders of magnitude adjustable	4 orders of magnitude adjustable
12	Diagnostic requirements	Pulse energy measurement repeatability	⩽10% (Accumulation mode)	⩽10%	/
13		Pulsed spectra	/	Single-pulse spectroscopy is required,	/
14		Diagnostic time accuracy	Arrival time measurement repeatability: better than 30fs (RMS).	Arrival Time Measurement Repeatability: Better than 30fs (RMS) Pulse length measurement repeatability: better than 30fs (RMS)	Arrival time measurement repeatability: better than 30fs (RMS).

15		Wavefront diagnostic repeatability (RMS).	/	/	λ/50@λ=3nm

(1) No monochromator above 2keV (2) Thermal load correction ability is not considered (3) Calculated according to the mirror angular stability of 50nrad, the position jitter of the light source point is calculated according to 10% (no signed contact sheet) (4) The comprehensive stability is in the vertical component.

2.3 Source Parameters

The FEL-II undulator utilizes the proven and reliable vacuum outdoor planar undulator technology and the principle of soft X-ray self-seeding. The line places two APPLE-X undulator with adjustable polarization state behind the plane undulator to realize the adjustment of the output polarization.

The FEL-II undulator will be installed approximately 450 meters upstream of the experimental hall for a total length of 100 meters. The undulator magnet gap can be adjusted to provide photons of different energies, and after theoretical optimization, the period length of the undulator is selected to be 55mm, and the operating magnetic gap is greater than 7mm (the minimum gap corresponds to the minimum photon energy of 400 eV at 8 GeV electron energy).

Using the three-dimensional analytical theory of free electron laser, Figure 2.3-1 shows the saturation length and saturation power of FEL-II at 0.4-3keV output photon energy.

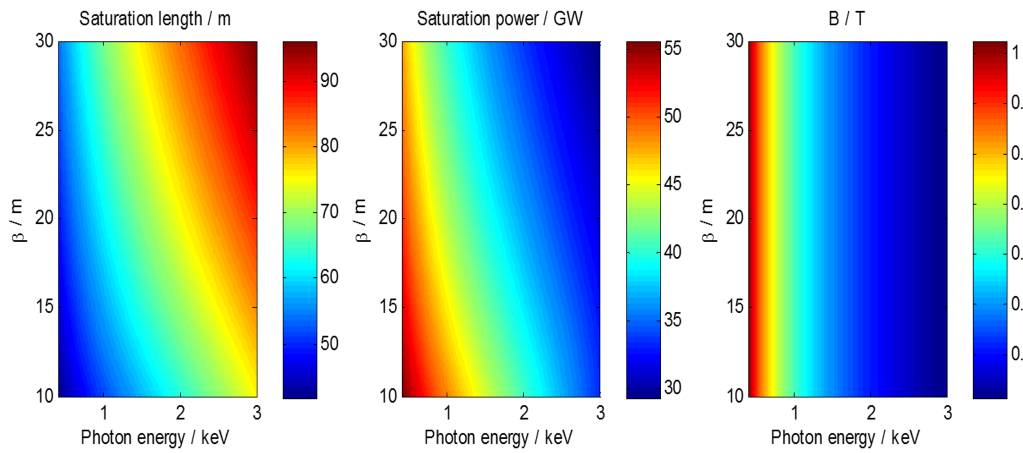

Figure 2.3-1 Optimization results of FEL-II saturation length and saturation power

In the nearly 100-meter-long beamline, the saturation point of the radiation pulse energy is not the same, and its variation curve with distance in the undulator is shown in Figure 2.3-2. The difference between the saturation point of the low-energy photon and the high-energy photon in the undulator is about 50 meters.

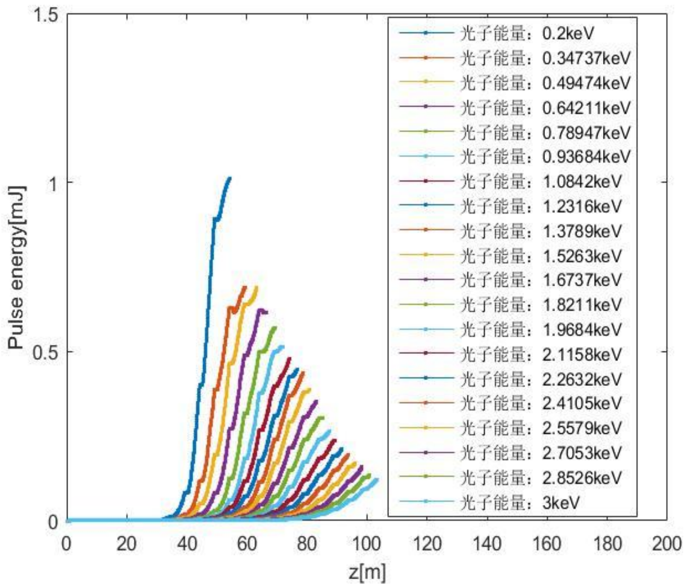

Figure 2.3-2 Variation of FEL-II radiated pulse energy with distance

Table 2.3-1 shows the parameters of the FEL-II light source in different operating modes.

Table 2.3-1 Parameters of FEL-II beamline source in SASE mode (non-taper)

Energy (eV)	Wavelength (nm)	Saturation p oint (m)	Peak power(GW)	FWHM pulse length (fs)	FWHM bandwidth (0.1%)	Pulse energy(μJ)	FWHM source size (μm)	FWHM source divergence (μrad)	Coherence degree
200	6.20	65.50	27.41	35.25	4.10	515.30	249.86	28.15	2.57
400	3.10	80.50	44.58	36.05	5.64	447.98	200.26	14.65	2.14
600	2.07	60.85	20.57	29.65	2.99	330.28	107.16	16.41	1.93
900	1.38	70.89	13.72	34.41	1.62	358.27	104.12	11.57	1.98
1200	1.03	75.89	16.60	32.49	1.96	296.83	86.24	8.96	1.70
1600	0.77	87.57	12.31	33.23	1.06	243.54	77.10	7.21	1.63
2000	0.62	90.58	20.92	22.82	0.98	279.30	86.03	6.31	1.98
2500	0.50	108.57	16.30	24.99	1.05	297.64	82.12	5.46	2.04
3000	0.41	110.54	12.27	25.20	0.74	139.81	77.98	4.45	1.90

The above light source parameters are those in which the accelerator is running in high charge mode and there is no taper, which will also bethe general parameters for the operation of the SHINE accelerator, so the design of the FEL-II beamline is based on the source parameters in the above table.

3. Schematic design

3.1 International investigation

Due to the excellent performance of X-ray free electron laser and its wide application in the field of basic discipline development and scientific and technological innovation, many countries and institutions have vigorously invested in the construction of XFEL devices. At present, the XFEL devices that have been completed and put into use include the FLASH soft X-ray free electron laser facility (FLASH) of the Electron Synchrotron Laboratory (DESY) in Germany, the linear accelerator coherent light source (LCLS) of the SLAC National Accelerator Laboratory in the United States, and the SACLA device of the RIKEN in Japan (SACLA), Italy FERMI Soft X-ray Free Electron Laser Facility (FERMI), European X-ray Free Electron Laser Facility (European-XFEL), South Korea Pohang Free Electron Laser Facility (PAL-XFEL).and the Swiss Free Electron Laser Facility (SwissFEL). In addition to this, many countries are building or planning to build X-ray free electron lasers in the near future, such as the Shanghai Soft X-ray Free Electron Laser Facility (SXFEL) under construction, and the American Linear Accelerator Coherent Light Source Phase II (LCLS-II). Except for European-XFEL and LCLS-II, all of the above devices are low-repetition frequency free electron laser devices. The operating mode of the European-XFEL is Pulse train mode, the frequency of the train is 10 Hz, and the pulse is 2700 in each train. The equivalent maximum repetition frequency can reach 4.5MHz, and the device contains three beamlines, including two hard X-ray beamlines and one soft X-ray beamline; the LCLS-II and SHINE devices under construction are both operating in CW mode with a maximum repetition rate of 1MHz, and the LCLS-II device includes a soft X-ray beamline and a hard X-ray beamline, which can switch between low repetition rate and high repetition rate accelerators, A single pulse of several millijoules can be obtained at low repetition rates. Table 3.1-1 lists the energy range and repetition rate of the soft X-ray band beamlines in the major free electron laser facilities described above.

Table 3.1-1 Energy range and repetition rate of soft X-ray beamlines in major

free electron laser facilities in the world

device	FLASH	LCLS	SACLA	STOP	PAL-XFEL	SXFEL	European-XFEL
Country	Germany	United States	Japan	Italy	Korea	China	Germany
Fundamental Range (nm)	6.9-47	0.6-2.2	8-60	4-100	0.85-4	2-20	0.4-4.7
Repetition rate (Hz)	5	120	60	10	60	50	27000

3.2 Scheme layout

As mentioned above, the FEL-II beamline beam transmission system is mainly composed of an offset mirror group, a grating monochromator, a deflection mirror and a KB focusing system, in which the offset mirror group (M1, M2a, M2b) is located at 165-167.05 meters from the light source point, and two groups are used, corresponding to 02-2keV vs. 2-3keV. The planar grating monochromator (PGM) is located 200 meters away from the light source point, and uses 3 variable line distance plane gratings to correspond to different energy resolution requirements. The deflector (M3) is located at 267 m from the light source point and is used to deflect/focus the FEL pulses to the SES/SSS experimental station. The monochromatic light slit is 295 meters away from the light source. After the monochromatic light slit, a total of three KB focusing systems provide the station with different sizes of focusing spots as required. The optical path of the FEL-II beamline beam transmission system is shown in Figure 3.2-1, the mechanical layout of the FEL-II beamline and the experimental station is shown in Figure 3.2-2 and 3, and the layout of all equipment on the beamline is shown in Figure 3.2-4.

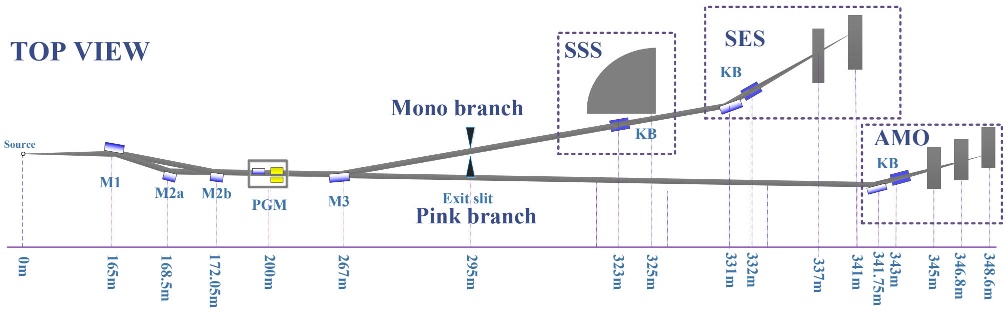

Figure 3.2-1 Optical layout of the FEL-II beamline

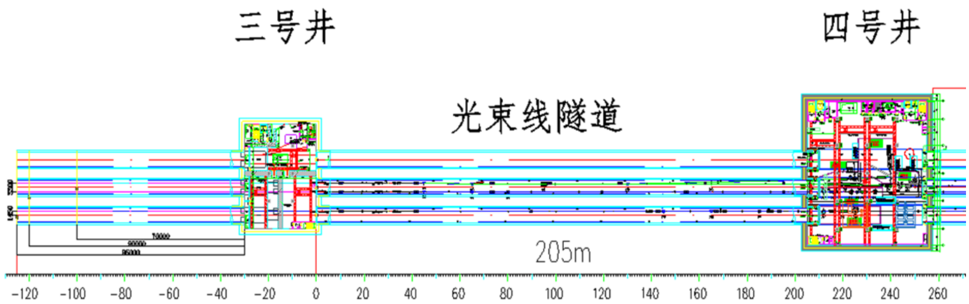

Figure 3.2-2 Mechanical layout of FEL-II beamline

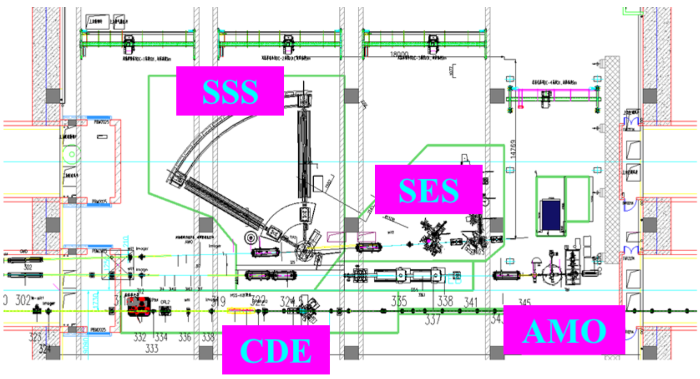

Figure 3.2-3 Mechanical layout of the FEL-II experimental station

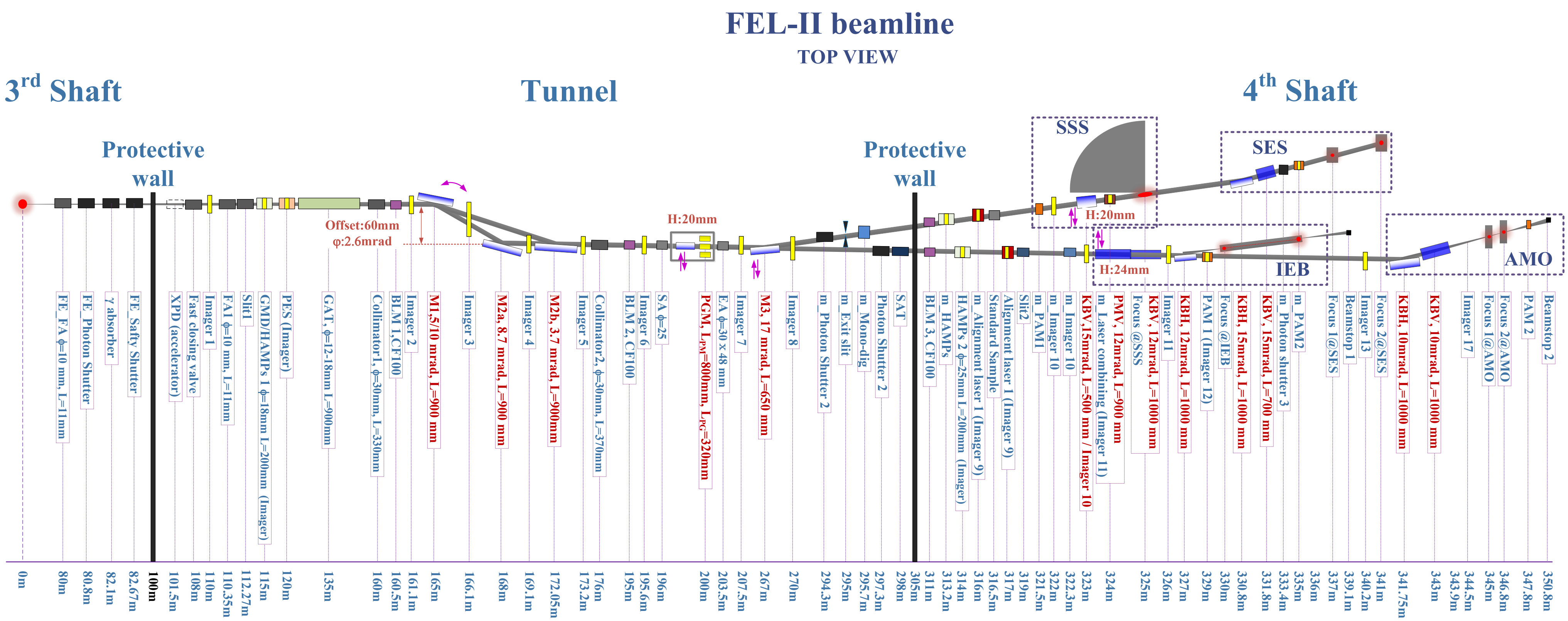

Figure 3.2-3 Layout of all devices in FEL-II beamline

3.3Physical design

3.3.1 Selection of optical component receiving aperture and coating

Due to the good spatial coherence of the FEL light source, the receiving aperture of the optical element will affect the focused spot at the sample point, when the receiving aperture of the optical element is too small, the focused spot will be affected by the diffraction effect of the beam, and it is difficult to achieve ideal focusing, in addition, the photon flux and peak intensity are also affected by the receiving aperture of the optical element. Therefore, one of the design principles is to maintain the flux density of the FEL pulses at the sample point when designing the beamline. In order to maintain the flux density of the FEL pulses at the sample point, a reasonable requirement needs to be made for the clear aperture of the beamline. Figure 3.3-1 shows the effect of different receiving aperture on photon flux and peak intensity of the focused spot.

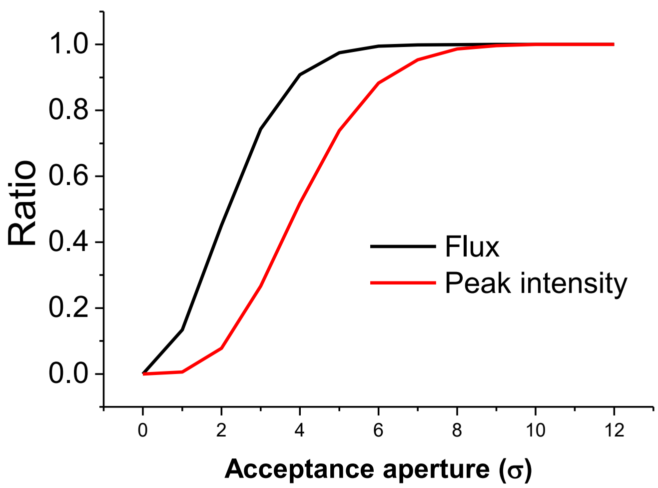

Figure 3.3-1 Photon flux and peak intensity of focused spot at different receiving apertures

As shown in the figure, when the receiving aperture of the optical element reaches the 4 σspot size, the photon flux transmitted by the system can reach 90%, but the peak intensity of the focused spot only reaches 50% of the maximum value, which is unacceptable for some experimental stations that require strong peak intensity, such as AMO. When the receiving aperture of the optical element reaches 6σ spot size, the photon flux transmitted by the system can reach 99%, and the peak intensity of the focused spot can also reach 90% of the maximum value, so the receiving aperture of all optical elements on the beam line needs to reach 6σ spot size.

When it comes to the coating of optical components, two factors need to be considered: the reflection efficiency in the corresponding energy range, and the resistance to radiation damage under high-intensity FEL pulses. Figure 3.3-2 shows the radiation damage thresholds for different materials, and Figure 3.3-3 shows the reflectivity of the coating materials commonly used in the FEL-II beamline band. In the case of comprehensive consideration of radiation damage and reflection efficiency, combined with international practice, B4C is selected as the coating material of optical components.

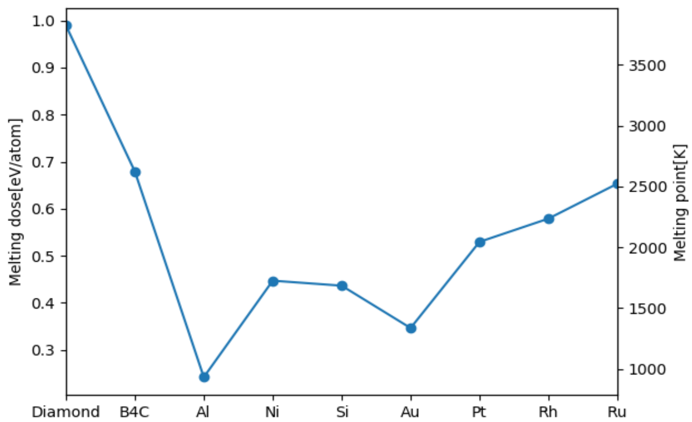

Figure 3.3-2 Radiation damage thresholds for different materials

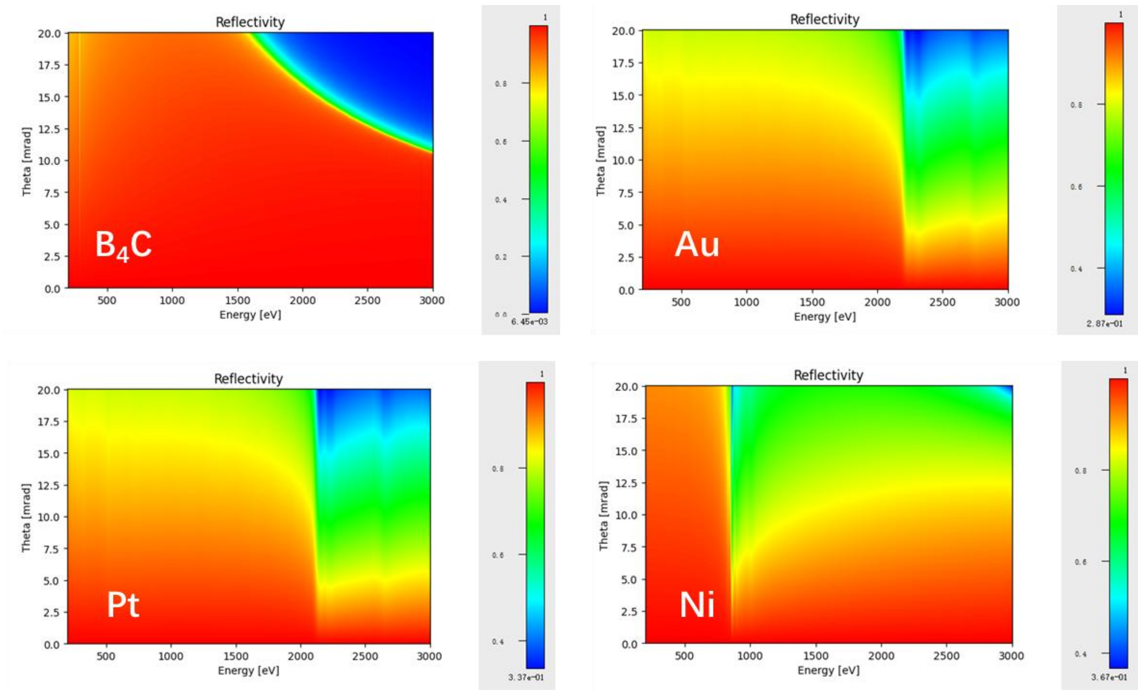

Fig. 3.3-3 Reflectance curves of different coating materials at different grazing angles in the range of 200-3000 eV

3.3.2 Pink beam slit

Due to the limitation of the size of the optical element, it is difficult for the beamline to receive the full 6 σ spot at all energy points, so a white light slit is required to limit the receiving angle of the beamline to protect the optical element downstream of the slit and the main beamline device. There are two white light slits in the FEL-II beamline, located at 112 m and 319 m away from the light source point, respectively, which are used to define the receiving angle of the beamline and the receiving angle of the pink branch. The white light slit needs to be able to withstand the full FEL power. The insert material consists of B4C and tungsten metal, which are used to absorb FEL pulses and higher harmonics, respectively.

3.3.3 Offset mirrors

The offset mirror group is located at the very front of the beam delivery system and its main function is to separate the high-energy radiation coming out of the upstream accelerator and the X-ray free electron laser beam. In order to translate the position of the beam horizontally for a distance without changing the direction of beam transmission, the offset lens group is placed vertically. The mirror group consists of three (two) parallel deflection mirrors M1 and M2a/b. The M1/M2b mirror group is grazing at an angle of 5 mrad/3.7 mrad for the 2-3 keV photon energy range, and the M1/M2a mirror group is grazing at an angle of 10 mrad/8.7 mrad for the 0.2-2 keV photon energy range (Figure 3.3-4). In order to have enough space for the experimental station in the downstream test hall, the beam after passing through the M2 mirror is no longer parallel to the incident beam of the offset mirror group, and is emitted at an angle of 2.6 mrad.

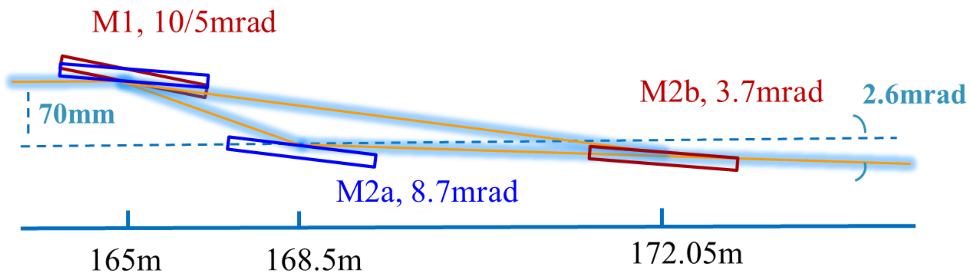

Figure 3.3-4 Offset mirrors in FEL-II beamline

The advantage of dividing the offset lens group into two groups according to the energy range is that it can effectively reduce the size of the optical element (as shown in Figure 3.3-5), increase the footprint of the photon beam on the optical element, and reduce the power density on the optical element. All optics used in the offset lens group are planar and positioned vertically. In order to reduce the sensitivity of the offset lens group to earth motion, the overall length of the lens group is within 5m, in which the M1 mirror is located at a distance of 165 meters from the light source point, and the grazing incidence angle of the beam can be changed to realize the common use of the two offset mirror groups. The M2a mirror is located at a distance of 168.5 m from the light source point and is grazing at 8.7 mrad. M2b is located at a distance of 172.05 meters from the light source point and grazing at 3.7 mrad. The offset between the M1 mirror and the M2a mirror is 70mm, and the offset between the M1 mirror and the M2b mirror is 70.5mm.

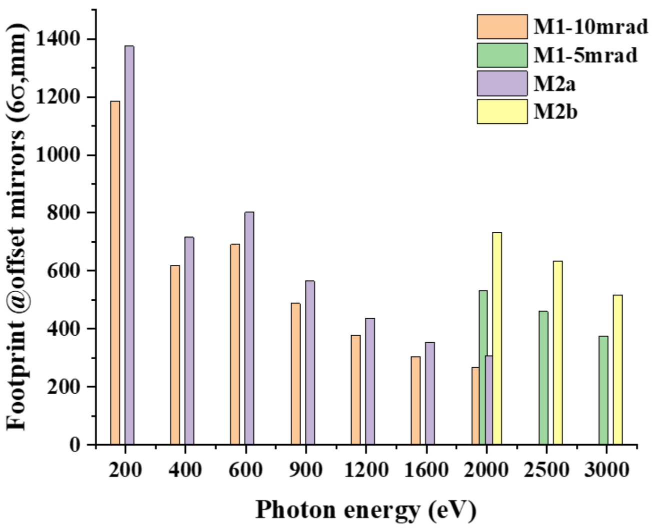

Figure 3.3-5 Footprint on the offset mirrors

Due to the limitation of the processing capacity of the optical components, it is difficult to achieve the receiving aperture of 6σ in the energy range covered by the beamline, considering the needs of the experimental station and the processing capacity of the existing ultra-smooth optical components, the effective length of the offset mirrors is selected as 700mm, and the receiving aperture of the offset mirrors is shown in Figure 3.3-6

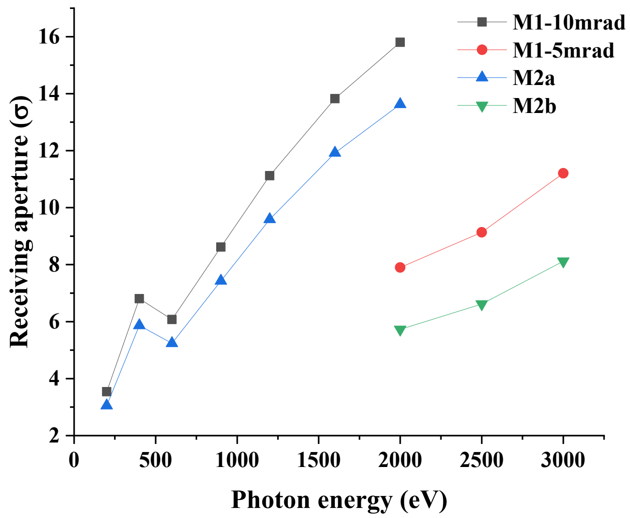

Figure 33-6 Receiving aperture of offset mirrors

As mentioned above, considering the reflection efficiency and radiation damage, all optical components in the offset mirrors are plated with B4C material, and the reflectance curve is shown in Figure 3.3-7. The reflectivity of the individual optical elements in the M1/M2b mirror group is more than 98%. In the M1/M2a mirror group, the reflectivity of a single optical element exceeds 90% except for the absorption edge of C, and the reflectance of the absorption edge of C can exceed 85%.

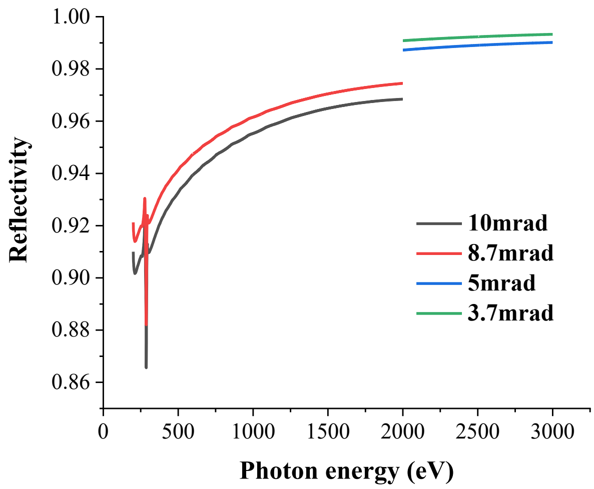

Figure 3.3-7 Reflectance curve of offset mirrors (B4C coating).

3.3.4 Grating monochromators

According to the light source parameters, the intrinsic spectral width of the FEL pulse in SASE mode is 0.1%-0.4%, which is much larger than the spectral width required by SSS and SES, two experimental stations with extremely high resolution of incident light energy. The monochromator has a coverage range of 0.2-2keV, where the optimized energy range is 0.4-17keV。 The monochromator selects a more mature variable-angle grating monochromator, which can cover a wide energy range, and the schematic diagram of the optical path of the grating monochromator is shown in Figure 3.3-8.

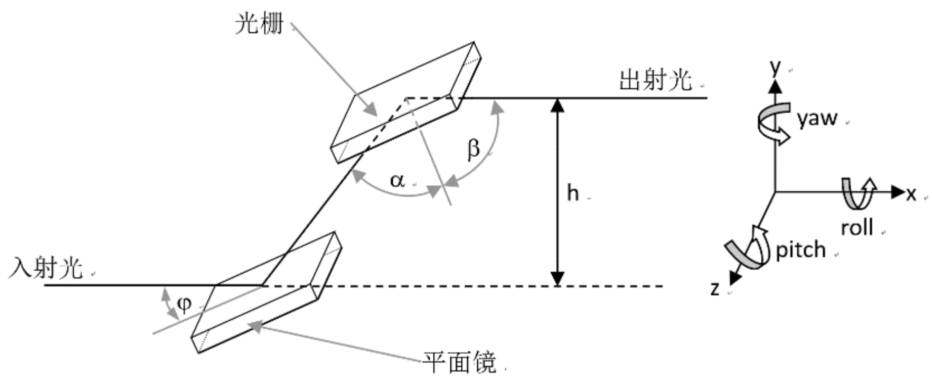

Figure 3.3-8 Schematic diagram of the optical path of the monochromator with an angle grating

The grating selects a variable line distance grating with aberration correction, which can be expressed as a power series of coordinates:

$$d(\omega) = d_0(1 + b_2\omega + b_3\omega^2 + b_4\omega^3 + \cdots)$$

where d0 is the spacing of the grating center, ω is the distance between any point on the grating and the grating from the center point in the dispersion direction, and the focusing equation of the plane variable line distance grating is in the meridian direction

$$\frac{\cos^2\alpha}{r_1} + \frac{\cos^2\beta}{r_2} - \frac{\cos\alpha + \cos\beta}{R} - b_2 m\lambda/d_0 = 0$$

Grating equations:

$$\sin\alpha - \sin\beta = Nm\lambda$$

Coma:

$$F_{30} = \frac{\cos^2\alpha\sin\alpha}{r_1} + \frac{\cos^2\beta\sin\beta}{r_2} - \frac{1}{R}\left(\frac{\sin\alpha\cos\alpha}{r_1} + \frac{\sin\beta\cos\beta}{r_2}\right) - \frac{2}{3}(b_2^2 - b_3)n\lambda/d_0$$

At specific energies, let F30=0, b3 can be obtained, and at other energies, F30≠0, but small, negligible, and the final grating resolution can be expressed as:

$$\Delta\lambda = \frac{1}{Nk}\Big(\omega F_{200} + \frac{3}{2}\omega^2 F_{300} + \frac{1}{2}l^2 F_{120} + \frac{1}{2}\omega^3 F_{400} + \frac{1}{2}\omega l^2 F_{220} + lF_{111} + \frac{1}{2}F_{102} + \frac{1}{2}\omega F_{202} + \omega l F_{211} + \cdots\Big)$$

The grating monochromator is located at 200 m away from the source point. For the ultra-high energy resolution requirements of the experimental station, the monochromator adopts three variable line spacing gratings, with line densities of 200l/mm, 500l/mm and 800l/mm, respectively, corresponding to different energy resolution capabilities. The Cff value is 1.5 for the 200l/mm grating, 3.0 for the 500 l/mm and 800 l/mm gratings. The image distance of the monochromator is 95 m. In order to ensure sufficient receiving aperture, the effective length of the three gratings is 300mm, and the receiving aperture of the three gratings is shown in Figure 3.3-9

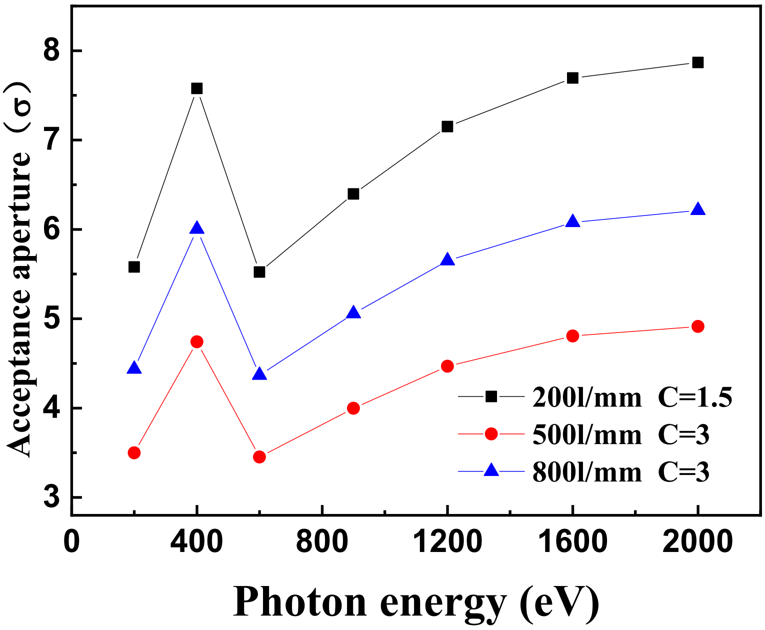

Figure 3.3-9 Receiving aperture of the grating

The energy resolution of the monochromator is calculated by taking into account the size of the light source, the size of the exit slit, the system aberration (out-of-focus aberration and coma), and the diffraction-limited capability of the grating. The contribution of the relative spectral widths to the energy resolution is as follows:

Light source size: $\Delta\lambda/\lambda_{so} = \frac{2.35d\Sigma_{yV}\cos\alpha}{m\lambda r_1}$

Exit slit size: $\Delta\lambda/\lambda_{ex} = \frac{sd\cos\alpha}{m\lambda r_2}$

Out-of-focus aberrations:$\Delta\lambda/\lambda_{de} = \frac{2dF_{20}W}{m\lambda}$

Coma: $\Delta\lambda/\lambda_{co} = \frac{3dF_{30}W^2}{2m\lambda}$

Grating diffraction limit: $\Delta\lambda/\lambda_{limit} = \frac{1}{mN}$

thereinto

$\Sigma\psi$ - RMS value of the light source size;

s – exit slit size;

W – half width of the grating scribing area;

N – the number of fringes within the beam irradiation range on the grating;

The energy resolution of the final grating monochromator is:

$$\Delta\lambda/\lambda_{total} = (\Delta\lambda/\lambda_{so} + \Delta\lambda/\lambda_{ex} + \Delta\lambda/\lambda_{de} + \Delta\lambda/\lambda_{co} + \Delta\lambda/\lambda_{limit})^{\frac{1}{2}}$$

After comprehensive consideration, the energy resolution of different gratings is shown in Figure 3.3-10

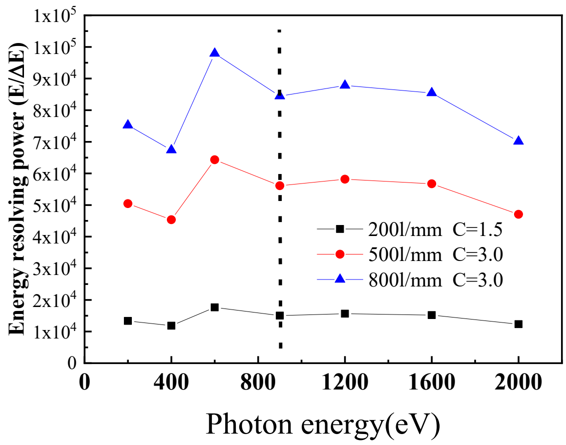

Figure 3.3-10 Monochromator energy resolution curve

The monochromator will use a combination of multiple gratings, which can meet the different needs of the experimental station. The experimental station can choose a grating with high energy resolution or high photon flux according to the scientific objectives, which is helpful for the experimental station to carry out diversified scientific experiments: when using an 800l/mm grating, the energy resolution corresponding to the grating monochromator can exceed 80000@900eV, which can meet the needs of the SSS experimental station; When using a 500l/mm grating, the energy resolution of the monochromator can exceed 50000@900eV to meet the needs of the SES experimental station. When using a 200L/mm grating, the energy resolution of the grating monochromator can reach 15000@900eV, which can meet the needs of low energy resolution and high throughput of the above two experimental stations. The tracing results are in good agreement with the theoretical calculations, as shown in Figure 3.3-11

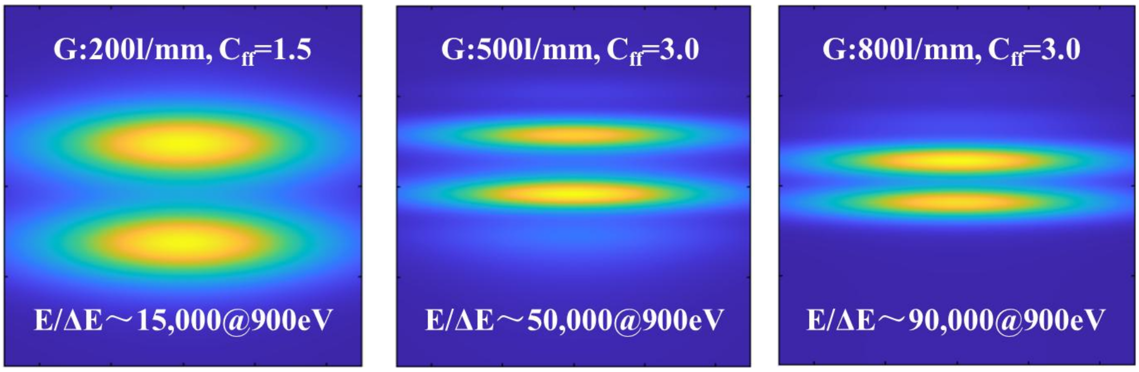

Figure 3.3-11 Energy resolution tracing results of monochromator (the height error of the plane mirror and the grating is 1 nm (rms))

Considering the characteristics of the SASE light source, the position of the saturation point of each pulse in the oscillator is not fixed, and there is a certain fluctuation, when the change range of the light source point is ±5m, the energy resolution of the grating monochromator is traced as shown in Figure 3.3-12, and it can be seen from the tracing results that the energy resolution ability of the grating monochromator is slightly worse than the ideal situation, but the design value can still be reached, which is mainly due to the very large object distance of the grating, and the change distance of the saturation point in the oscillator only accounts for a small proportion of the grating object distance.

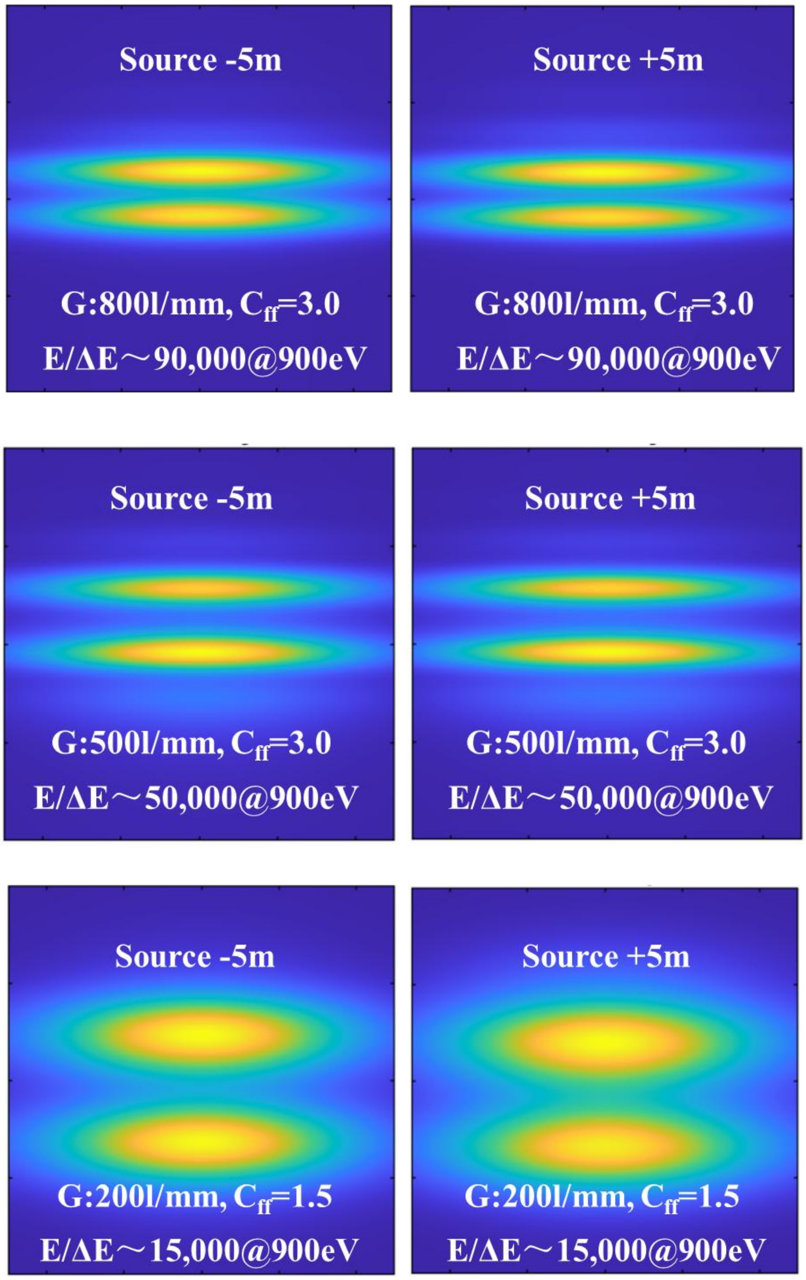

Figure 3.3-12 Energy resolution tracing result of grating monochromator when the source point changes by±5 m (the height error of the plane mirror and the grating is 1 nm (rms))

In order to obtain the highest energy resolution and take into account the efficiency of the monochromator, the opening of the exit slit in the vertical direction is determined by the spot size at the slit, as shown in Figure 3.3-13

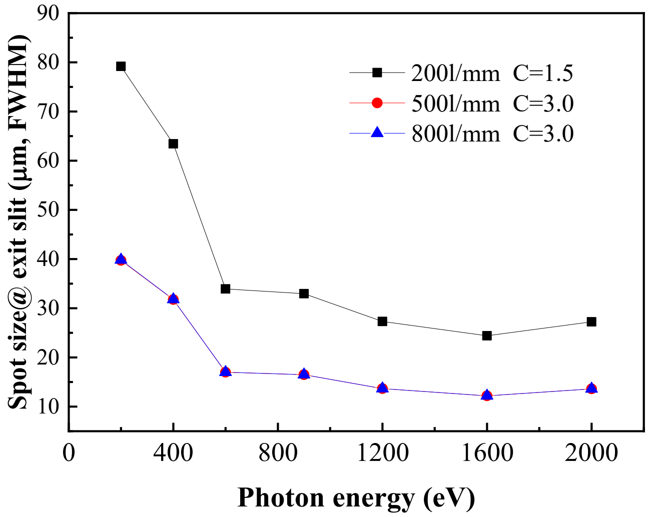

Figure 3.3-13 Spot size at the exit slit of the monochromator (vertical opening of the slit)

Figure 3.3-14 shows the spot size tracing results at the exit slit of the grating monochromator. In the horizontal direction, the beam reaches the exit slit without passing through any focusing element, so the horizontal spot size is 3 for all three gratings4mm （FWHM）。 The vertical spot size varies depending on the grating Cff value, with an optimized Cff value of 1.5 for a 200 l/mm grating and a tracer value of 35.0 µm for both 800 l/mm and 500 l/mm gratings. As a result, the vertical spot sizes are almost identical, with traces of 21.0 µm, 23.1 µm, and 36.6 µm, respectively.

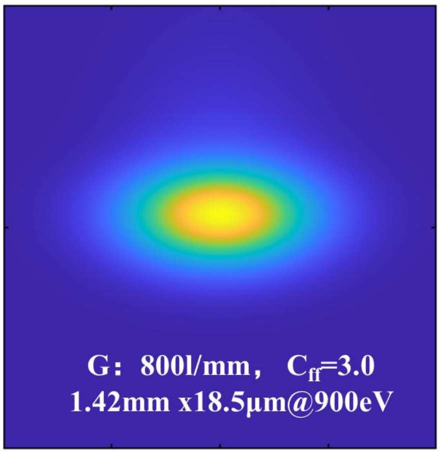

Figure 3.3-14 Spot size ray tracing result at the exit slit of the monochromator

The influence of different factors on the energy resolution of monochromators is shown in Figure 3.3-15. For the 200 L/mm and 800 L/mm gratings, the maximum contribution to the relative spectral width is the contribution of the light source size and the exit slit. Since the size of the opening of the exit slit is the same as the vertical size of the focused spot at the slit, the contribution of both is the same. The contribution of out-of-focus aberration and coma of the grating monochromator system is less than that of the diffraction limit of the grating, which shows that the aberration control of the system is excellent, and the influence on the overall energy resolution is small, which is an ideal monochromatic system, which also means that the smaller light source size can obtain higher power resolution. For the 500L/mm grating, the contribution of the light source size and the exit slit is close to the contribution of the grating diffraction limit, while the contribution of out-of-focus aberration and coma is much smaller than the above three, which means that when using a 500L/mm grating, the grating monochromator is also an ideal monochromatization system, but its energy resolution is mainly determined by the diffraction limit of the grating and the size of the light source.

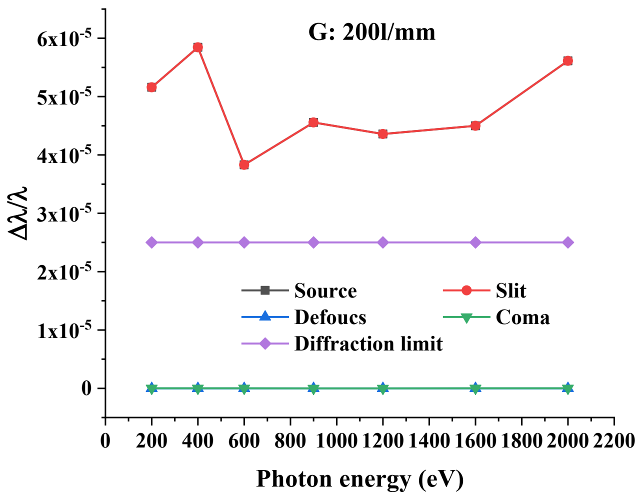
G: 200l/mm
Δλ/λ
6x10^-5
5x10^-5
4x10^-5
3x10^-5
2x10^-5
1x10^-5
0
Source
Slit
Defoucs
Coma
Diffraction limit
0 200 400 600 800 1000 1200 1400 1600 1800 2000 2200
Photon energy (eV)

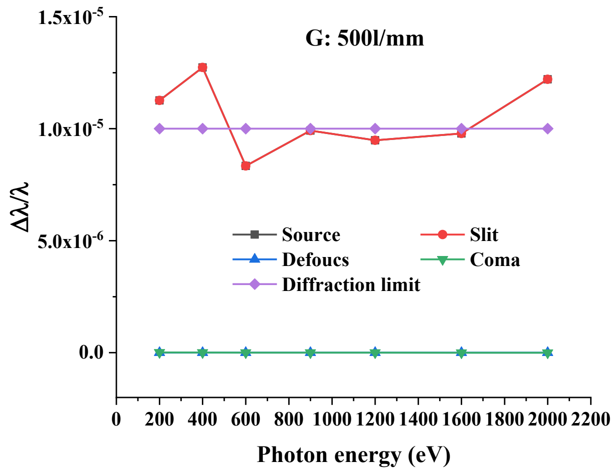
G: 500l/mm
Δλ/λ
1.5x10^-5
1.0x10^-5
5.0x10^-6
0.0
Source
Slit
Defoucs
Coma
Diffraction limit
0 200 400 600 800 1000 1200 1400 1600 1800 2000 2200
Photon energy (eV)

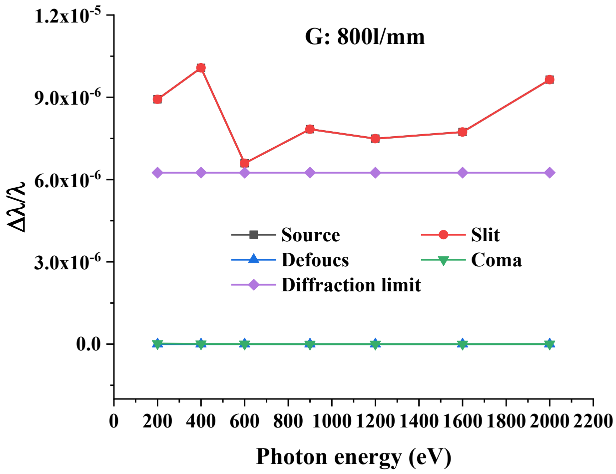

Figure 3.3-15 Contribution of various relative spectral widths to the energy resolution ability of monochromators

The surface quality of the grating will affect the performance of the grating, the energy resolution of the monochromator and the size of the focused spot, which in turn will affect the performance of the subsequent experimental station. In order to evaluate this effect, taking the highest requirement of 800 l/mm as an example, the spot size and the height of the side associated peak at the exit slit were analyzed under different combinations of height error and slope error, so as to determine the grating surface shape requirements, and each combination was simulated for 20 times to be averaged. Table 3.3-1 shows the size of the monochromatic spot at the exit slit under different combinations of height error and slope error. According to the slit, the size of the monochromatic spot changes almost unaffected by the grating surface shape.

Table 3.3-1 Spot size at the exit slit under different combinations of height error and slope error

Height error / Slope error	0.5nm	1.0nm	1.5nm	2.0nm
50nrad	16.805μm	17.2μm	16.92μm	17.05μm

100nrad	17.015μm	16.865μm	16.775μm	16.94μm
150nrad	16.94μm	17.13μm	17.095μm	17.1μm
200nrad	16.97μm	16.795μm	17.11μm	16.99μm

Under the influence of the thermal effect, the surface shape of the front plane mirror of the monochromator will change, from the plane surface shape to the curved surface type (which can be equivalent to the convex mirror), which will have a divergent effect on the incident beam, thereby affecting the object distance of the grating. Similarly, the surface shape of the grating will also change from a planar grating to a convex grating due to the thermal effect, and the focusing behavior of the grating will change. Therefore, the overall energy resolution of the monochromator will be reduced due to the thermal deformation of the optical components. This effect can be corrected by adjusting the Cff value of the grating appropriately. Assuming that the equivalent radius of curvature after the change of the front mirror is RM, and the equivalent radius of curvature after the change of the grating surface shape is RG, the object distance of the grating changes from the original r1 to r1', which is satisfied under the condition of ignoring the distance between the plane mirror and the grating

$$\frac{1}{r_1} + \frac{1}{r_1'} = \frac{1}{R_M \cos\theta}$$

where θ is the grazing incidence angle of the front mirror. In this case, the Cff value of the monochromator needs to be adjusted to Cff' accordingly, which needs to be satisfied:

$$C_{ff}' = \cos\beta' / \cos\alpha'$$

$$\frac{\cos^2\alpha'}{r_1'} + \frac{\cos^2\beta'}{r_2} - \frac{\cos\beta' + \cos\alpha'}{R_G} - b_2 m\lambda/d_0 = 0$$

The grazing incidence angles of the three gratings are shown in Figure 3.3-16, and the efficiency of +1 diffraction of the grating at different flare angles is shown in Figure 3.3-17, and the efficiency of VLS grating is calculated using the REFLEC program developed by VESSY. Only the case of S polarization is considered in the calculation, and the calculated structures are ideal, with an antiflare angle of 90 degrees. The calculated grating order is 1 order.

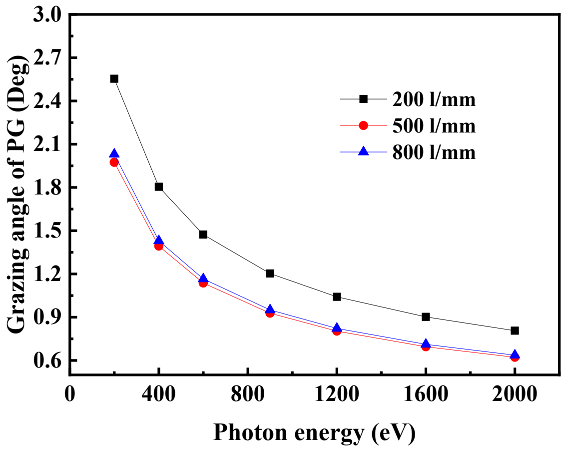

Figure 3.3-16 Grazing incidence angle of the grating in monochromator

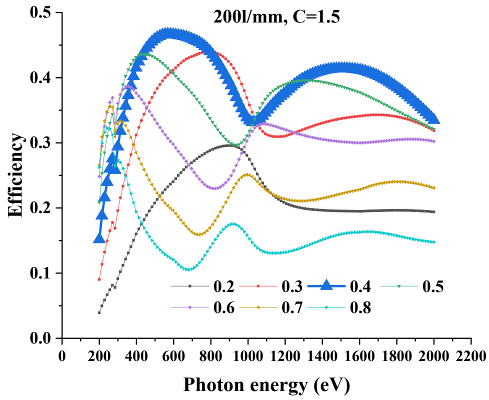

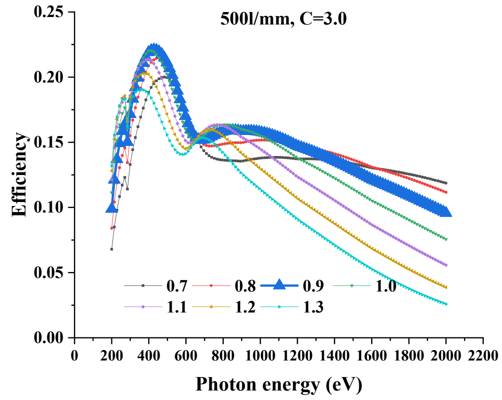

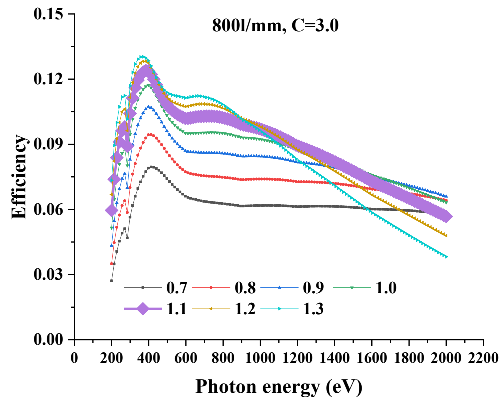

Figure 3.3-17 +1 order diffraction efficiency curves of different gratings at different blazed angles

For 200L/mm grating, select 0.4°, in the energy range of 400eV-2000eV, the diffraction efficiency of the grating +1 order is greater than 30%; For the 500l/mm grating, the flare angle is selected as 0.9° , and the diffraction efficiency of the grating +1 order is greater than 10% in the energy range of 400eV-1500eV. For 800L/mm gratings, the flare angle is selected as 11°, in the energy range of 400 eV-1500 eV, the diffraction efficiency of the grating +1 order is greater than 7%. Figure 3.3-18 shows that the grazing incidence angle of the plane mirror in the grating monochromator varies from 1.0° to 4.1° in the all-energy range. At this angle, the reflectance of different coatings commonly used in the soft X-ray wavelength range is shown in Figure 3.3-19.

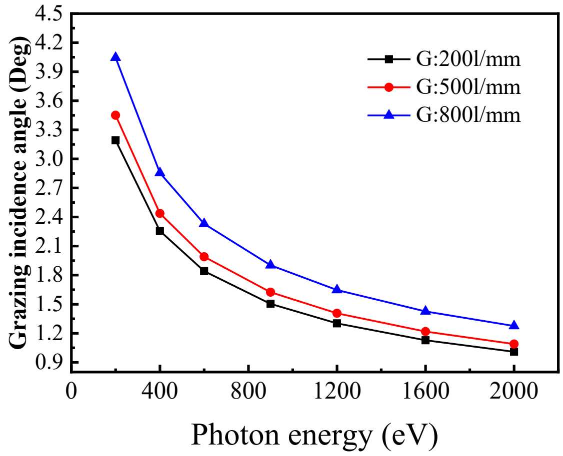

Figure 3.3-18 Grazing incidence angle of the plane mirror in the monochromator

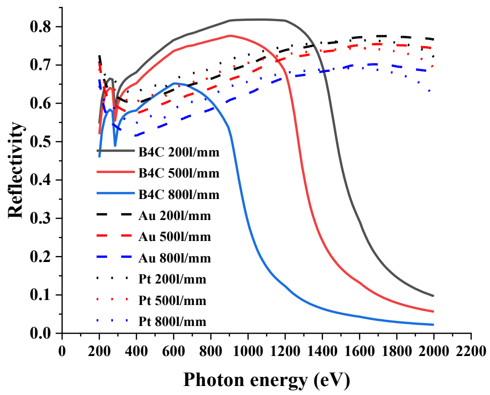

Figure 3.3-19 Reflectance of the plane mirror in the monochromator with different coatings

In consideration of the damage and contamination of the optical components at the C absorption edge, metal plating is used for the front mirror in the range of 200 eV to 400 eV. In the range of 400 eV-2000 eV, for 200 l/mm grating, the reflectivity of B4C is higher than that of Au and Pt when the photon energy is lower than 1400 eV, and the reflectance of Au and Pt is higher than that of B4C when the photon energy is higher than 1400 eV. For 500 l/mm grating, the reflectivity of B4C is higher than that of Au and Pt when the photon energy is lower than 1200 eV. For 800 l/mm gratings, the reflectivity of B4C is higher than that of Au and Pt at photon energies below 800 eV. Combined with the reflectivity and damage threshold of the material, the double coating of B4C and Pt was selected for the plane mirror, and the appropriate mirror coating was matched according to different gratings and the working energy section of the grating, as shown in Table 3.3-2.

Table 3.3-2 Working range of different coatings of the grating monochromator front mirror

	B4C	Pt
200l/mm	400eV - 1400eV	200eV - 400eV & 1400eV - 2000eV
500l/mm	400eV - 1200eV	200eV - 400eV & 1200eV - 2000eV
800l/mm	400eV - 800eV	200eV - 400eV & 800eV - 2000eV

The final efficiency of the grating monochromator is shown in Figure 3.3-20

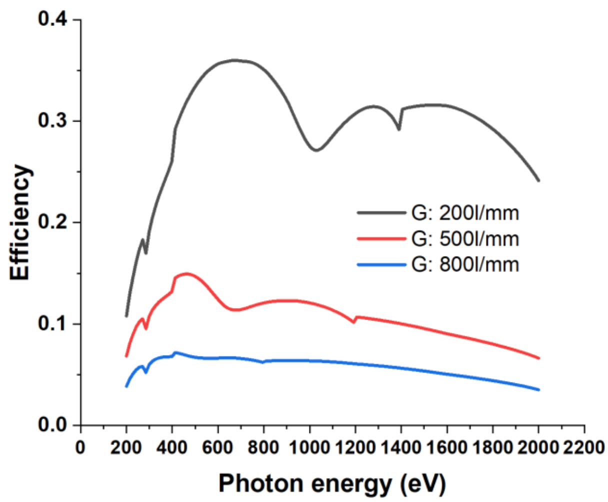

Figure 3.3-20 Efficiency curve of grating monochromator

Since the X-ray laser pulse passes through the grating, it will cause an additional optical path difference, which will cause a certain amount of broadening Δt to the pulse width, and since the XFEL will provide ultrashort pulses, the pulse-induced time broadening due to the high energy resolution must be taken into account, which can be estimated by:

$$\Delta t = \frac{Nm\lambda}{c}$$

where N is the number of grating strips illuminated by X-rays, m is the diffraction order, and is the wavelength of X-rays. For the grating used in the monochromator, the corresponding pulse broadening in different operating modes is shown in Figure 3.3-21, in which the pulse broadening is obvious at the low energy end, and the pulse can reach the PS level, while the high energy end remains at the order of several hundred fs.

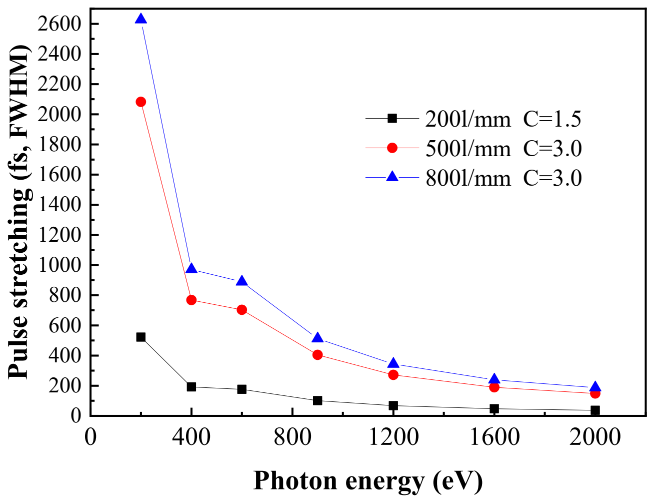

Figure 3.3-21 Pulse broadening after passing through the monochromator

For the variable line spacing grating, there will be certain processing errors in various parameters in the processing and preparation process of the grating, and the coefficient of the primary square term in the grating variable spacing equation has a great impact on the performance of the grating monochromator, that is, the B2 value, which directly affects the focusing performance of the variable line distance grating, and then affects the energy resolution ability of the grating monochromator. In the actual working process of the grating monochromator, the small error of the b2 value can be corrected by adjusting the Cff value of the grating, which will have two effects: on the one hand, the change of the Cff value will lead to the change of the compression capacity of the grating monochromator, which will directly affect the energy resolution of the grating monochromator; On the other hand, the change of the Cff value also means that the angle of incidence and diffraction angle of the grating will change, which will affect the projection length of the beam on the grating, and in the case of a certain grating length, this means that the receiving aperture of the grating will change. Taking the 800L/mm grating as an example, Figure 3.3-22 shows the change curve of the energy resolution ability of the grating monochromator at 900 eV and the corresponding beam projection length in the 6σ range of the grating when the processing error range of the grating b2 value is ±10%. Therefore, in order to ensure the ability to distinguish and keep the grating with a large enough receiving aperture as much as possible, the machining error of the b2 value of the grating is required to be within 2%.

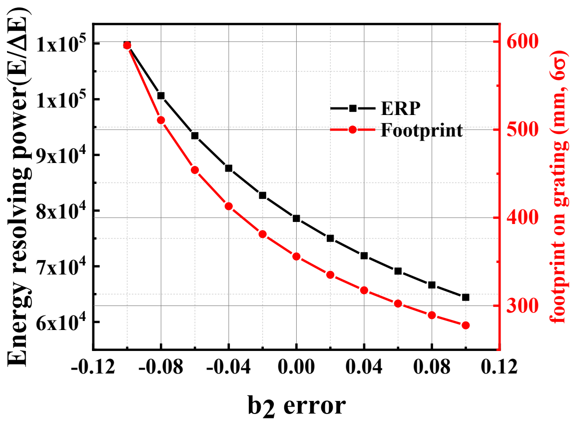

Figure 3.3-22 Effect of grating focal parameter (b2) error on the energy resolution of grating monochromator

The installation position of the grating monochromator is in the tunnel from the No. 3 to the No. 4 well, and the change of the ambient temperature in the tunnel will affect the relative height of the front and rear support legs of the monochromator, thereby causing the rotation of the entire monochromator, which will change the optical path, and finally cause the change of photon energy at the exit slit. Since the temperature changes slowly, it only causes a drift of the outgoing energy and does not affect the energy resolution of the grating monochromator. The beam incidence height of the grating monochromator is 1.3m, the image distance is 100m, and the base of the mirror box is 1m long, and its structure is shown in Figure 3.3-23

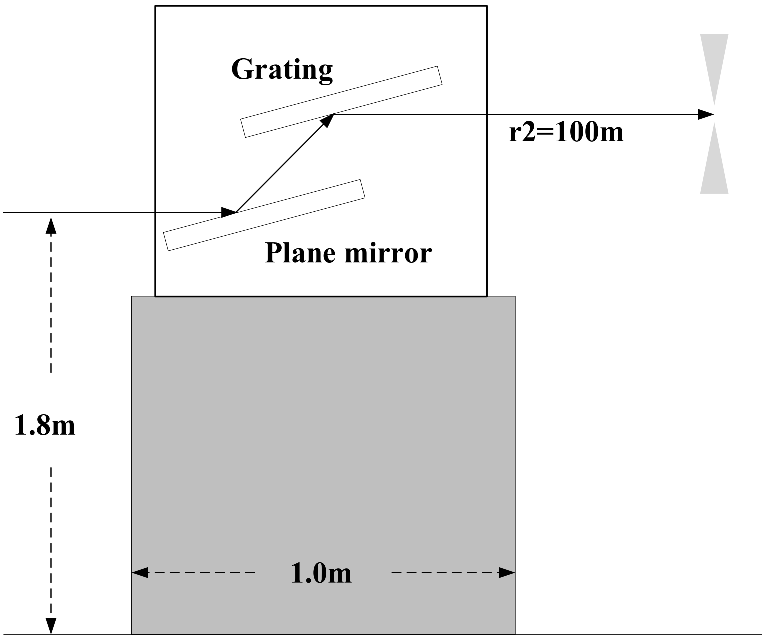

Figure 3.3-23 Schematic diagram of the structure of the grating monochromator

Suppose that when the ambient temperature changes, the grating monochromator rotates along the spot center of the plane mirrorδ, and the optical path before and after the rotation of the monochromator is shown in Figure 3.3-24, where Grc (X_{Gc}, YGc) is the center position of the grating when the monochromator is not rotated, Grc1 (XGc1, YGc1) is the center position of the grating after the monochromator is rotated, Ghit1 (XGhit1, YGhit1) is the incident position of the beam in the grating after the monochromator is rotated, and M2hit($X_{M2hit,0}$) is the illumination position of the beam in the plane mirror, and Mrc(XRM2,Y_{RM2}) is the rotating position of the plane mirror.

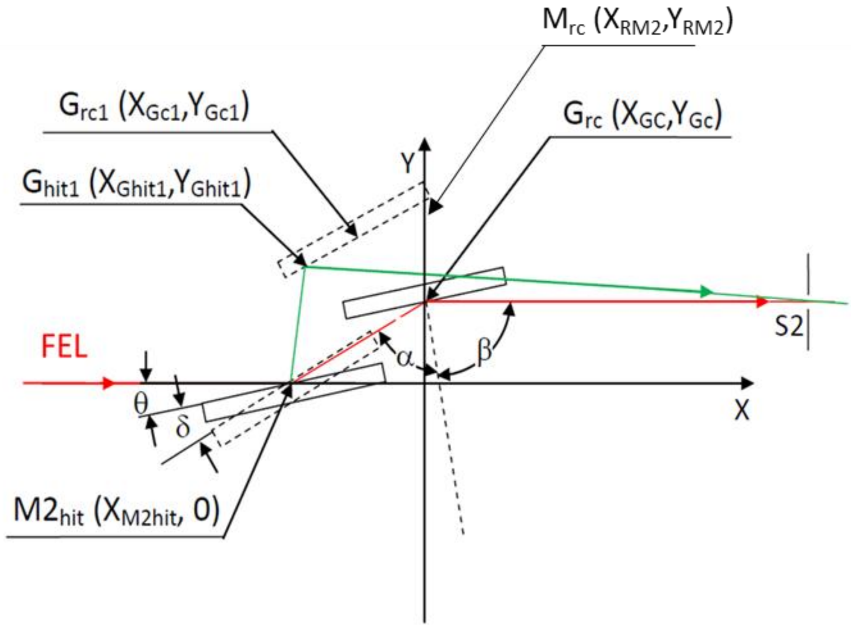

Figure 3.3-24 Schematic diagram of the optical path of the monochromator before and after rotation (red is the pre-rotation optical path and green is the rotated optical path).

The position of the FEL light on the plane mirror is:

$$X_{M2hit} = -\frac{Y_{RM2}\cos\theta - R}{\sin\theta}$$

Then, after the grating monochromator is rotated along the center of the plane mirror spot, the center position of the grating Grc1 becomes:

$$X_{Gc1} = X_{M2hit} + \sqrt{Y_{Gc}^2 + X_{M2hit}^2}\cos(2\theta + \delta)$$

$$Y_{Gc1} = \sqrt{Y_{Gc}^2 + X_{M2hit}^2}\sin(2\theta + \delta)$$

The equation for the projection of the grating surface in the XY plane is:

$$y - Y_{Gc1} = (x - X_{Gc1})\tan\left(\frac{\pi}{2} - \beta + \delta\right) = \frac{(x - X_{Gc1})}{\tan(\beta - \delta)}$$

The equation for the reflected beam of a plane mirror in the XY plane is:

$$y = \left(x - X_{M2hit}\right)\tan(2\theta + 2\delta)$$

Combining the above two equations, we can get the center of incidence position of the spot on the grating as:

$$X_{Ghit1} = \frac{\tan(\beta-\delta)\tan(2\theta+2\delta)\,X_{M2hit} + Y_{Gc1}\tan(\beta-\delta) - X_{Gc1}}{\tan(\beta-\delta)\tan(2\theta+2\delta)-1}$$

$$Y_{Ghit1} = \frac{\tan(2\theta+2\delta)\left(Y_{Gc1}\tan(\beta-\delta) - X_{Gc1} + X_{M2hit}\right)}{\tan(\beta-\delta)\tan(2\theta+2\delta)-1}$$

After the FEL beam is diffracted by the grating, the bandwidth of the outgoing light is defined by the outgoing slit, so after the monochromator is rotated, the outgoing slit defines the direction of the diffracted light, so the incident angle α 1 and diffraction angle β 1 of the beam on the grating after the monochromator is rotated can be obtained

$$\beta_1 = \beta - \delta + \tan^{-1}\left(\frac{Y_{S2} - Y_{Ghit1}}{X_{S2} - X_{Ghit1}}\right)$$

$$\alpha_1 = \pi - 2(\delta + \theta) - \beta_1$$

The distance s s between the incident position of the beam on the grating and the center of the grating after the monochromator is rotated is:

$$s = \sqrt{\left(X_{Gc} - Y_{Ghit1}\right)^2 + \left(Y_{Gc} - Y_{Ghit1}\right)^2}$$

From this, the grating line density at the incident position of the beam is obtained:

$$k(\omega) = k_0(1 + b_2\omega + b_3\omega^2 + b_4\omega^3 + \cdots)$$

Therefore, the energy drift of the grating monochromator due to temperature change is:

$$\Delta E = \frac{kmhc}{(\sin(\alpha_1) + \sin(\beta_1))e} \cdot 10^3 - E$$

For stainless steel materials, the coefficient of linear thermal expansion is 1.6x.10-5/K (Austenitic stainless steel) and 1.01x.10-5/K (Martensitic Stainless Steel), the coefficient of linear thermal expansion for marble is 4.6x.10-6/K, Figure 3.3- 25 is the amount of energy drift of the outgoing light when the grating monochromator holder is made of stainless steel.

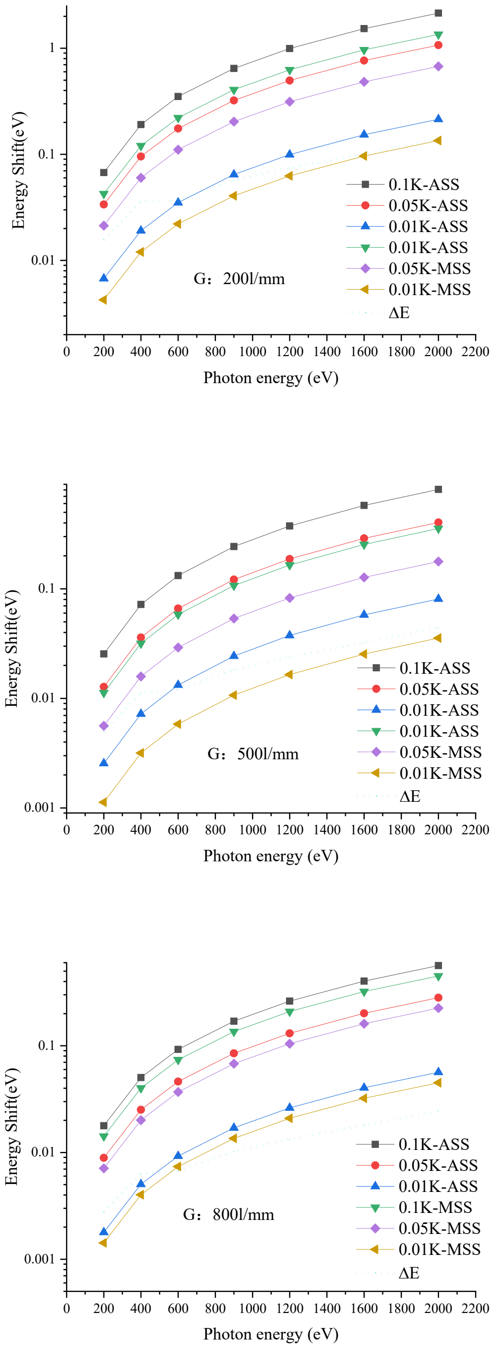

Figure 3.3-25 The energy drift of the outgoing beam when different types of stainless steel materials are used in the grating monochromator holder

Figure 3.3-26 shows the energy drift of the outgoing light when the grating monochromator holder is made of granite.

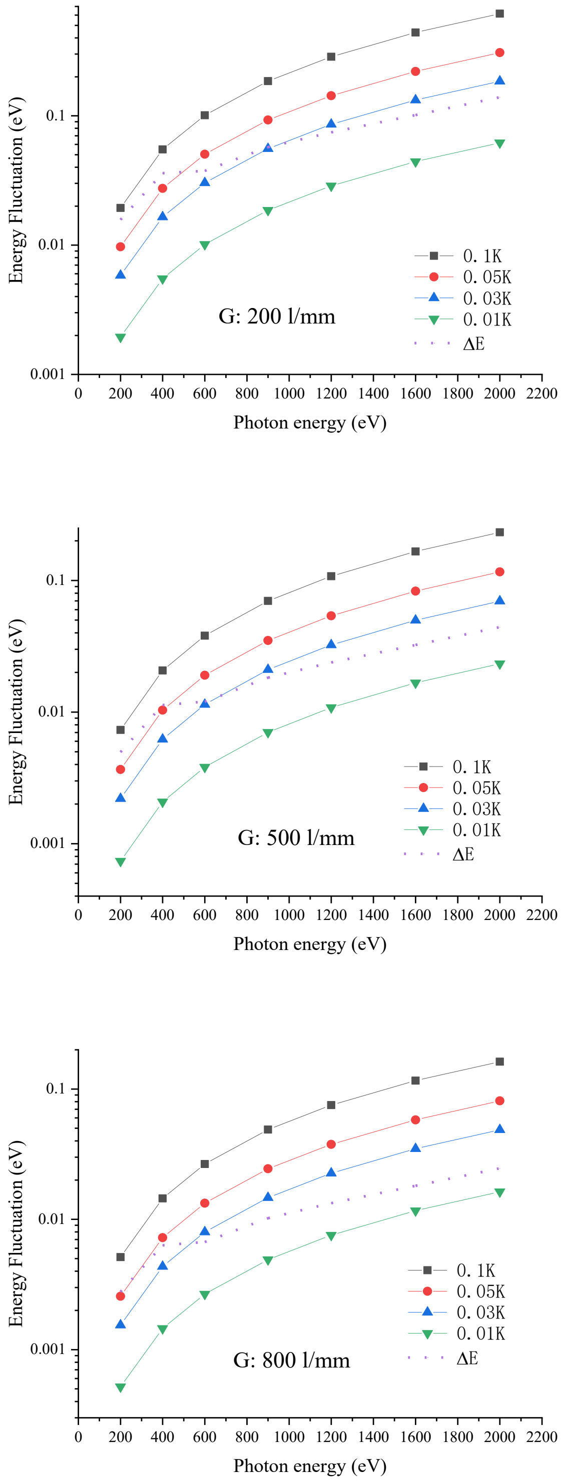

Figure 3.3-26 The energy drift of the outgoing beam when the grating monochromator holder is made of granite

Let's consider the effect of vibration on the change in photon energy at the exit slit of the grating monochromator. When the tunnel between the third and fourth wells vibrates, the vertical relative displacement between the front and rear legs of the monochromator will also cause the overall angle change of the monochromator, which is similar to the calculation of the influence of temperature on the energy drift, and it can be concluded that the relative energy drift of the outgoing light caused by vibration when using different gratings is shown in Figure 3.3-27

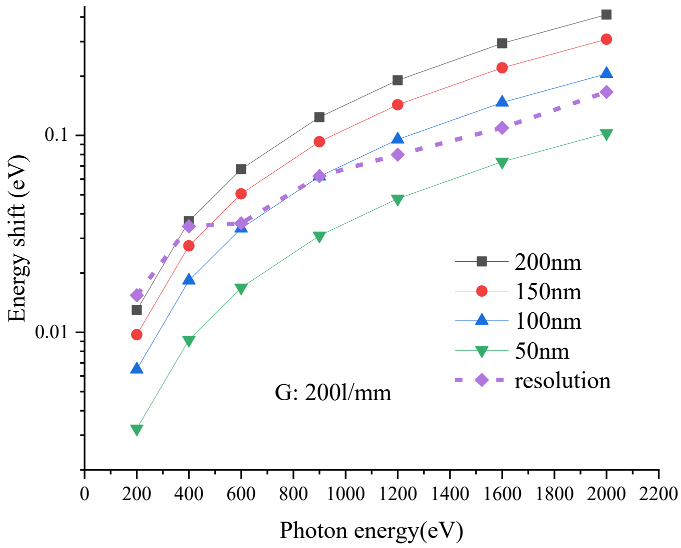

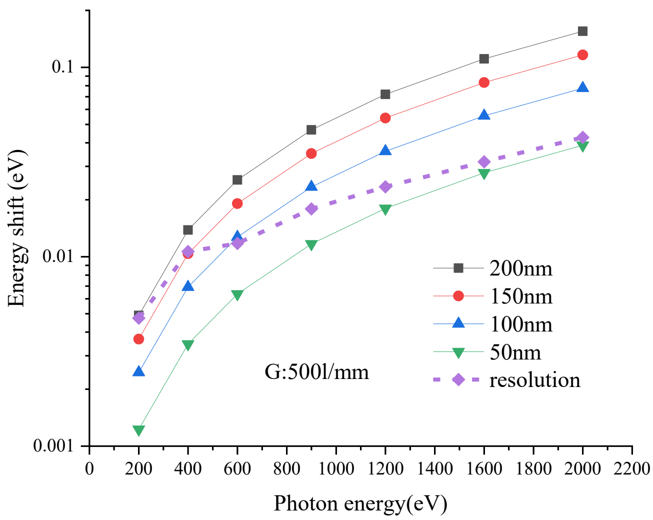

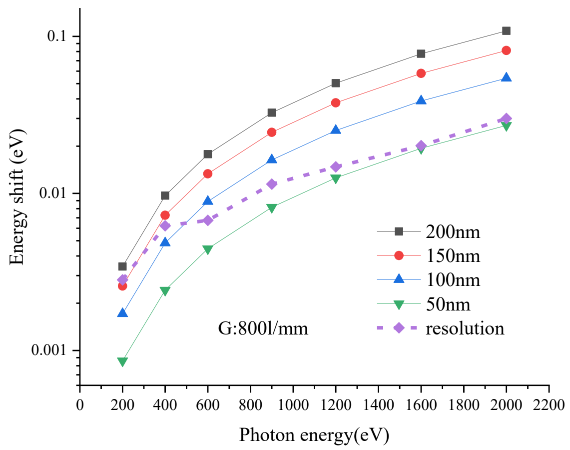

Figure 3.3-27 Relative energy drift of the outgoing light due to vibration when different gratings are used

As shown in the figure above, as the density of the grating line increases, the energy resolution of the monochromator also increases, and it is more sensitive to the vibration of the foundation. At the low energy end, for a 200 l/mm grating, the relative energy drift of the outgoing light is less than that of the grating monochromator when the vibration is less than 200 nm (rms), for the 500 l/mm grating, when the vibration is less than 150 nm (rms), the relative energy drift of the outgoing light is less than that of the grating monochromator, and for the 800 l/mm grating, when the vibration is less than 100 nm (rms), the relative energy drift of the outgoing light is less than the energy resolution of the grating monochromator. At the high energy end, the vibration requirements are similar for all gratings, and when the vibration is less than 50 nm (rms), the relative energy drift of the outgoing light is less than the energy resolution of the grating monochromator. After considering the ground vibration, the decrease in the energy resolution of the grating monochromator is shown in Figure 3.3-28

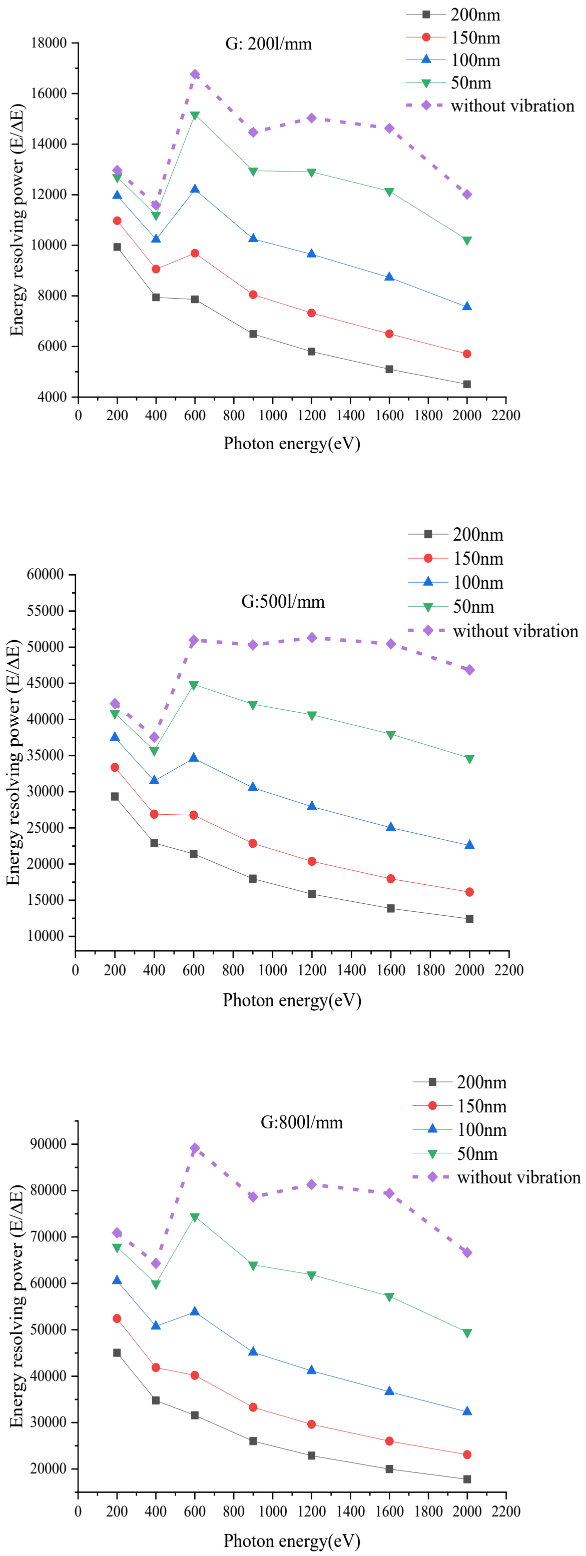

Figure 3.3-28 The influence of foundation vibration on the energy resolution of the grating monochromator when different gratings are used

Taking the energy at 900 eV as an example, the decrease in the energy resolution of the grating monochromator is shown in Table 3.3-2

Table 3.3-2 The energy resolution of the grating monochromator decreases due to ground vibration at 900 eV

Vibration (nm)	Energy resolving power degradation@900eV		
	200 l/mm	500 l/mm	800 l/mm
50	10%	16%	19%
100	29%	39%	43%
150	44%	55%	58%
200	55%	64%	67%

As can be seen from the above figure, for the 800L/mm grating, the energy resolution has decreased by about 20% when the ground vibration is 50 nrad, and about 40% when the ground vibration is 100 nrad, which is unacceptable, so for the full energy range covered by the grating monochromator, the ideal vibration level of the foundation should be below 50 nm (rms).

3.3.5 Stray-beam aperture

In order to ensure the energy resolution of the monochromator of the grating, a stray beam aperture need to be placed to block the stray light from entering the monochromator from the upstream. The stray diaphragm is located 4m upstream of the grating monochromator, and the aperture of the diaphragm is Φ25mm.

3.3.6 Exit aperture

An exit aperture should be placed behind the monochromator, located 3.5m downstream of the monochromator from the center of the grating, the function of the diaphragm is to completely block the 0-order diffraction light of the grating and let the +1-order diffraction light of the grating and the pink-through light that passes through after the grating is switched. Due to radiation damage, the material of the exit diaphragm is B4C. The maximum spot size of the incident light on the grating is 8.5 mm× 13.5 mm (H×V), and the maximum spot size of the +1 diffraction light is 8.5 mm×32 mm (H×V). The height difference of the monochromator is 20 mm, and in order to ensure that the +1 diffraction light of the grating and the straight-through pink light without the grating can pass through completely, the clear aperture of the exit diaphragm is selected as 30 mm × 48 mm (H×V). In order to completely block class 0 diffraction light, the exit diaphragm is a cylindrical structure, with a diameter of 260mm, and an eccentric design, and the clear aperture is not located in the center of the diaphragm.

In the energy range covered by the grating monochromator, the angle between the 0 diffraction and the +1 diffraction of the grating is 7 mrad to 71 mrad, in order to completely block the 0 diffraction light, the exit diaphragm must be able to cover the range of 7 mrad to 71 mrad, and the movement range of the 0 grade diffraction light on the exit diaphragm is 192 mm, as shown in Figure 3.3-29. A YAG:Ce crystal is placed in the irradiated area of the 0th order diffraction light above the exit diaphragm to observe the 0th grade diffraction of the grating.

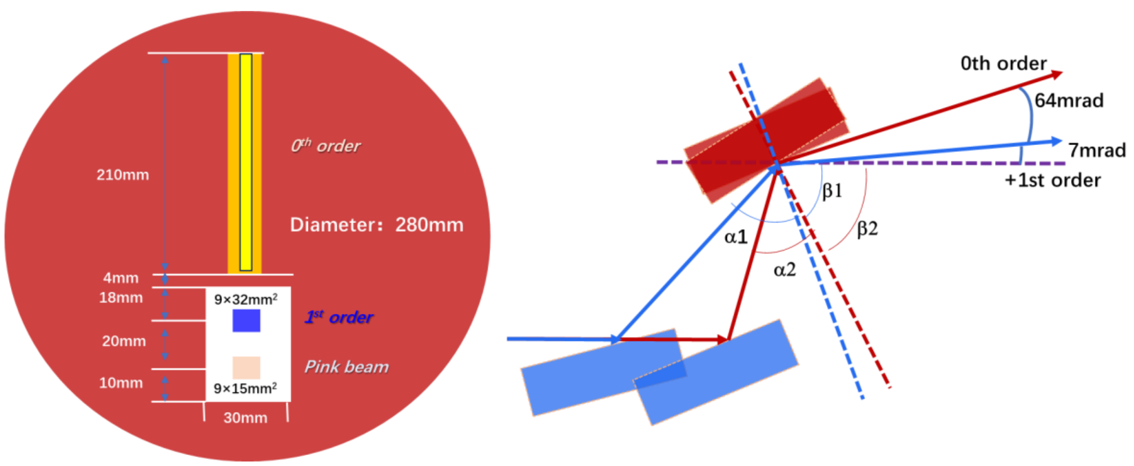

Figure 3.3-29 Schematic diagram of the exit aperture

The material of the aperture is selected as B4C, and a YAG:Ce crystal is placed in the 0-order diffraction region to observe the 0-order diffraction beam of the grating, so the YAG:Ce crystal will be strongly irradiated, and the damage problem needs to be considered. If the accelerator is operated in high charge mode, and the coating materials of the grating and the pre-mirror in the monochromator are materials with high reflectivity in the corresponding energy range, when the grating line density is 200 l/mm, the maximum absorbed dose of a single atom on the YAG:Ce crystal under a single pulse is shown in Figure 3.3-30, and the maximum absorbed dose of a single atom is almost an order of magnitude lower than the theoretical threshold of 0.14 eV/atom.

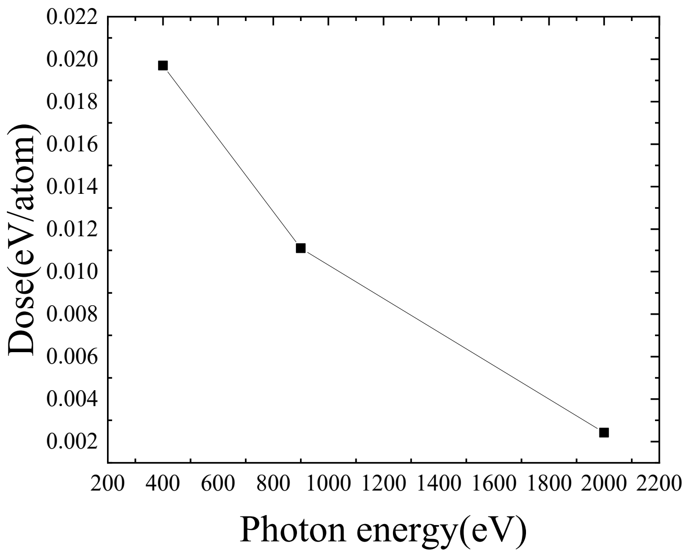

Figure 3.3-30 Maximum absorbed dose of YAG:Ce in the exit aperture

3.3.7 Exit slits

The exit slit of the grating monochromator is located 95 m downstream of the grating and is used to select the photons of the desired wavelength for the experimental station from the pink light of the FELT. There are two exit slits, one in the through line and one in the branch line. Since the beam is not focused in the horizontal direction and only in the vertical direction, the slit consists of two blades, upper and lower, and the beam is not restricted in the horizontal direction. Although the +1-order diffraction of the grating is relatively weak at the exit slit, the beam is focused in the dispersion direction in order to obtain higher energy resolution, so the exit slit is also subject to strong irradiation. In order to ensure the safety of the exit slit under strong irradiation, the blade material is also B4C, when the accelerator is running in high charge mode, and the coating materials of the grating and plane mirror in the monochromator are the materials with the highest diffraction efficiency and reflectivity under the corresponding photon energy, for the grating with different linear densities, the maximum absorbed dose at the slit is shown in Figure 3.3-31.

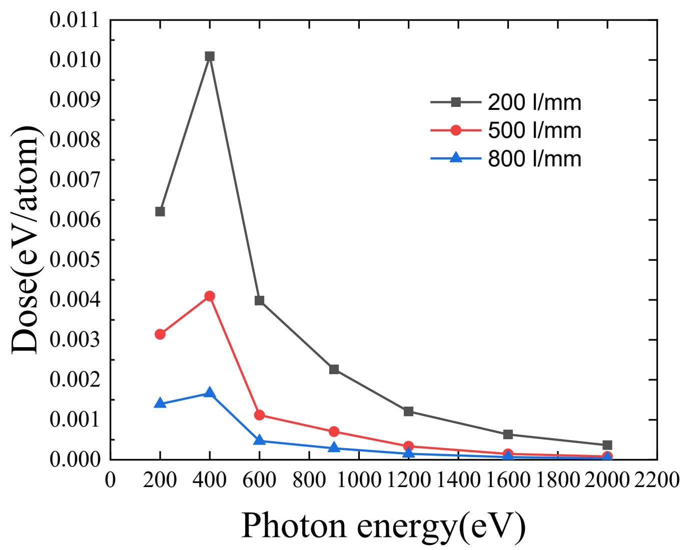

Figure 3.3-31 Maximum absorbed dose on the exit slit of the grating monochromator

3.3.9 Deflection mirrors

The deflection mirror is located at 267 m from the source point, and by moving the optics in or out of the optical path, the upstream FEL pulses can be distributed to different experimental stations located on the straight line and branch line. The deflector mirror consists of two mirrors that are horizontally switched, with a flat mirror deflecting the beam to the SES station and an elliptical cylindrical mirror deflecting the beam while focusing the beam horizontally to the SSS station. Considering the reflectance efficiency of the deflector, the working energy segment and the spatial layout in the experimental hall, the grazing incidence angle is selected as 17mrad, and the reflectance curve is shown in Figure 3.3-32. The maximum photon energy required for optimization for the two experimental stations on the branch line is 1700 eV, so the operating energy range of the deflection mirror is 200 eV-1700 eV.

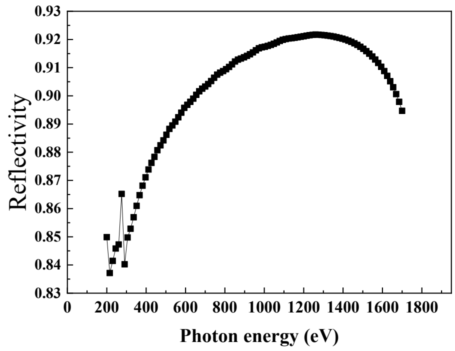

Figure 3.3-32 Reflectance curve of deflection mirror (B4C coating).

3.3.10 Attenuator

Because the single pulse energy of FEL can reach the millijoule level, it may cause damage to the equipment or detector on the beam line during the debugging stage of the beamline and the experimental station, so a flux attenuator needs to be added to the front end of the beamline, and a certain amount of attenuation of the beam is carried out in the debugging stage to ensure the safety of the beamline and various equipment and detectors on the experimental station. Flux attenuators not only attenuate the intensity of incoming light, reduce the thermal load on downstream optics, reduce the risk of damage to downstream equipment, but also prevent detector saturation.

The attenuation form of flux attenuator can be solid or gas, the obvious advantage of gas attenuator is that it has little impact on the wavefront, but because it needs to be filled with a large gas flow, compared with solid attenuator, the difficulty of gas attenuator is that it needs to design vacuum differential to realize the transition from inflated air pressure to ultra-high vacuum environment. According to the debugging requirements of the beamline and the experimental station, the physical design goal of the FEL-II beamline flux attenuator is to achieve a maximum attenuation of six orders of magnitude in the entire energy range.

X-rays will be absorbed as they pass through a gaseous medium, and the relationship between the number of photons absorbed and the gas pressure satisfies the Lambert-Beale law, which is how gas flux attenuators work.

$$I = I_0 e^{-\mu\rho d}$$

where I0 is the intensity of the incident beam, I is the intensity after photon absorption, μ is the mass absorption coefficient, ρ is the gas density, and d is the distance of photon transmission.

Considering that the instability of the free electron laser pulse light intensity is about 10%, the vacuum measurement accuracy of the gas flux attenuator is better than ±1%, and the pressure stability is also better than ±1%.

X-rays are absorbed when they pass through a gaseous medium, and can be used as working gases such as N2, Ar, Ne, Xe, etc. Since Ne and Xe require expensive gas recovery devices, only N2 and Ar are considered in the design of the FEL-II. The transmittance curves of different energies in N2 and Ar gas environments under different air pressures are shown in Figure 3.3-33, where the attenuation length of the gas is 15 m, without considering the ionization of the gas by X-rays and the heating of the gas by X-rays。 Due to the limitation of spot size, the differential aperture of the gas flux attenuator cannot be arbitrarily selected, which limits the maximum pressure of the working gas to 12 Torr. In this case, six orders of magnitude attenuation can be achieved for the incident beam below 2000 eV for N2 gas and six orders of magnitude for the incident beam below 2300 eV for Ar gas. Considering that the gas is ionized by X-rays and heated by X-rays will lead to the decrease of gas density, and the attenuation effect will be further weakened, in order to meet the attenuation requirements of the experimental station, it is necessary to add a solid attenuator to use together with a gas attenuator in the energy range of 2000 eV to 3000 eV.

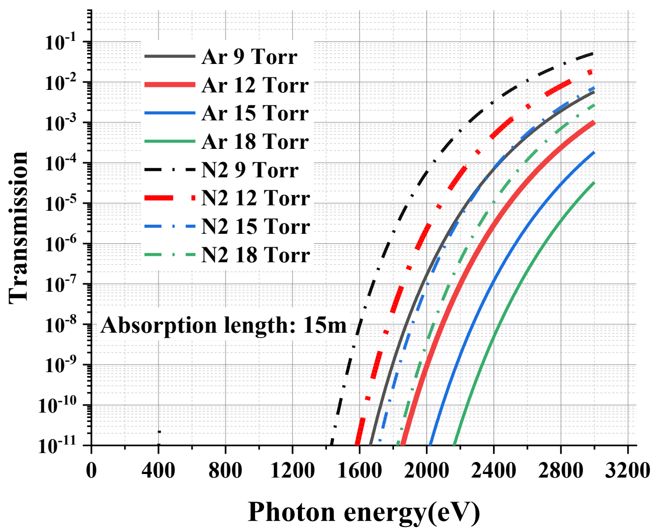

Figure 3.3-33 Transmittance curves of different energies in N2 and Ar gas environments at different air pressures

In the energy range covered by the FEL-II beamline, the spot size of the low-energy end is large, and the spot size of the high-energy end is small, so the limitation of differential aperture is mainly due to the size of the low-energy spot. Due to the limitation of the size of the optical element, the beamline cannot receive all the FEL light from the oscillator at the low energy end, and the receiving aperture of the beamline is mainly limited by the M1 mirror. The M1 mirror is located 165 meters from the light source point and has an effective cross-section of 7 mm, so the receiving aperture of the beamline is about 43 μ rad, and the differential system of the gas flux attenuator needs to be designed based on this aperture. Considering that gas molecules have a high absorption efficiency of low-energy photons and require low pressure, while high-energy photons are absorbed with low efficiency, the required pressure is high. Therefore, considering the spot size and gas absorption efficiency, the photon energy range can be divided into multiple segments, each corresponding to a different operating pressure and a matching clear aperture.

The layout of the vacuum differential system according to the gas load of the gas flux attenuator is shown in Figure 3.3-34. The vacuum differential system needs to provide a sufficiently large clear aperture within the photon energy range of the FEL-II beamline to ensure that the beam can pass through smoothly. This variable aperture design is mainly based on two considerations: one is to prevent the beam from hitting the pipe wall when passing through to ensure the safety of the equipment; Second, in order to provide the required level of attenuation, the effective gas pressure must be increased, and at the same time, the stability of the vacuum differential system must not be affected by excessive air flow. The static orifice is a short tube within the vacuum, which is the maximum clear aperture for the entire vacuum area, and the dynamic orifice is a standard vacuum valve with a hole.

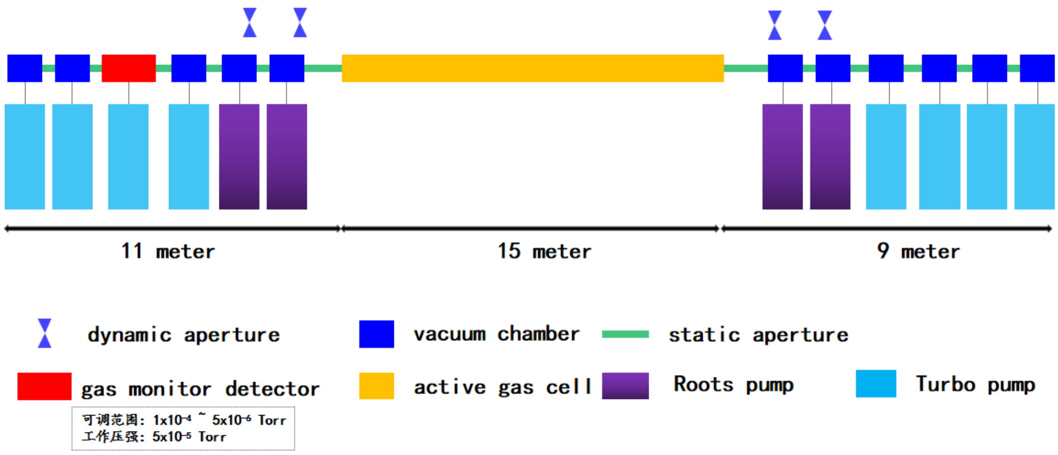

Figure 3.3-34 Schematic diagram of the vacuum differential of the FEL-II gas attenuator

The solid absorber is mainly used in the energy range of 2000eV-3000eV, supplemented by a gas attenuator to achieve the attenuation of six orders of magnitude of luminous flux. The materials used in the solid attenuator need to have good uniformity and thermal conductivity, on the one hand, the material has less damage to the wavefront, and on the other hand, it has strong damage resistance, and CVD diamond, Si, graphite, etc. can be selected. In the energy range of 2000 eV to 3000 eV, the transmittance curves of the beam under different material thicknesses are shown in Figure 3.3-35, where the density of CVD diamond is 3.52 g/cm3 and the density of graphite is 2.33 g/cm3.

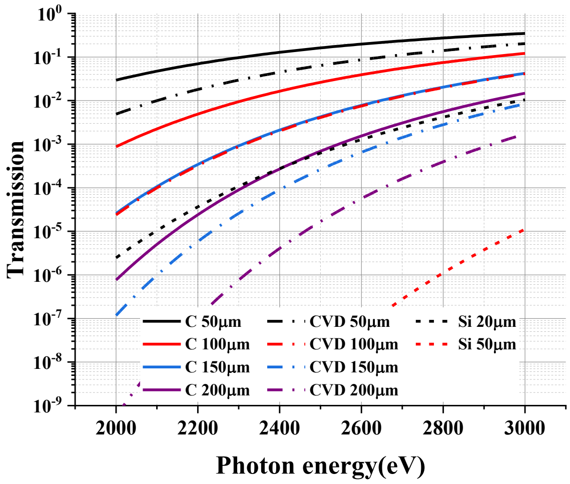

Figure 3.3-35 Transmittance curves of different energies at different material thicknesses

In the case where the upstream gas attenuator uses N2 gas, the solid attenuator needs to attenuate the beam by at least four orders of magnitude, and if the upstream gas attenuator uses Ar gas, then the solid attenuator also needs to attenuate the beam by at least three orders of magnitude. Considering the attenuation of the beam by the material and the thermal conductivity of the material itself, four pieces of CVD diamond with a thickness of 100 m were selected as the attenuation sheets of the solid attenuator, and the attenuation of the beam by six orders of magnitude was realized by combining with the upstream gas attenuator. The transmittance curves of the solid attenuator under different CVD diamond combinations are shown in Figure 3.3-36.

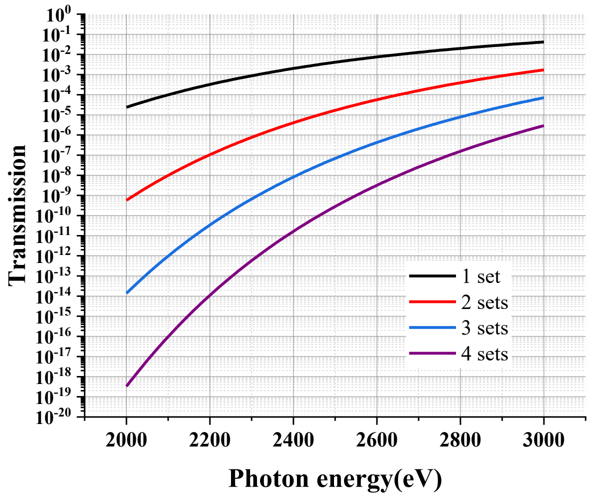

Figure 3.3-36 Transmittance curves with different CVD diamond combinations

3.3.11 Stability Analysis

Since the total length of the FEL-II beamline is nearly 350 meters, which is much longer than the usual synchrotron radiation beamline, the vibration of the optical elements in the beamline will have a greater impact on the final focused spot. If the optical element is equivalent to a thin lens, there are three main sources of focused spot jitter (as shown in Figure 3.3-37): the vibration M_S of the light source, the angular vibration M_a of the optical element, and the translational M_O of the optical element.

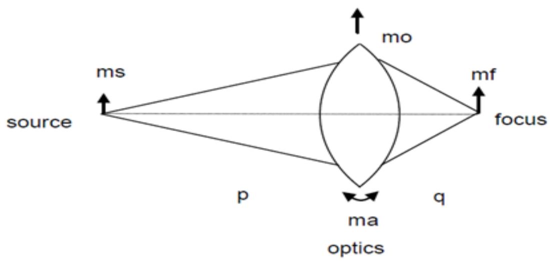

Figure 3.3-37 Schematic diagram of optical component vibration (from Eu-XFEL).

Assuming that the object distance of the optical element is p and the image distance is q, then the contribution of the light source vibration MS is:

$$\frac{q}{p}m_s$$

The translational MO contribution of the optics is:

$$\frac{p-q}{p}m_o$$

The contribution of the angular vibration MA of the optics is:

$$2qm_a$$

Then the vibration MF of the final focused spot is the convolution of the above three factors:

$$m_f=\sqrt{\left(\frac{q}{p}m_s\right)^2+\left(\frac{p-q}{p}m_o\right)^2+(2qm_a)^2}$$

For optics with different functions, the final effect on the focused spot is also different. Among them, the offset mirror group and the deflector mirror do not converge the beam, and the vibration of this type of optical element mainly deflects the beam, which is ultimately equivalent to the amplification of the vibration of the light source, as shown in Figure 3.3-38.

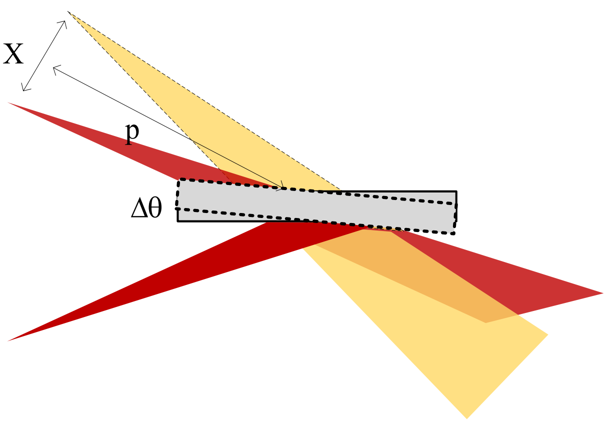

Figure 3.3-38 Schematic diagram of the influence of plane mirror vibration on the source point

If the distance between the optical element and the light source point is p, and the angular vibration of the optical element is Δθ, then the equivalent increase in light source vibration X is 2p*Δθ. The influence of the vibration of the offset lens group on the light source point of the subsequent optical element under different angular vibration conditions is shown in Figure 3.3-39

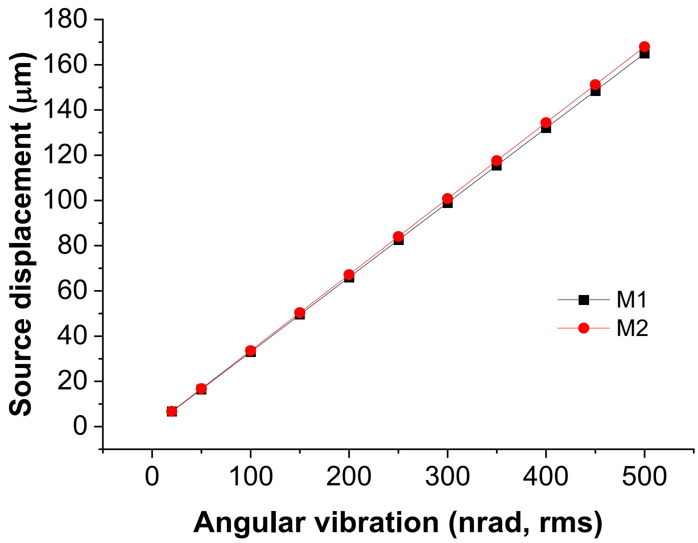

Figure 3.3-39 Effect of the vibration of the offset mirrors on the source point of the subsequent optical element

In the case of 2keV, the relative movement of the source point caused by the offset mirrors under the influence of different angular vibrations is shown in Figure 33-40

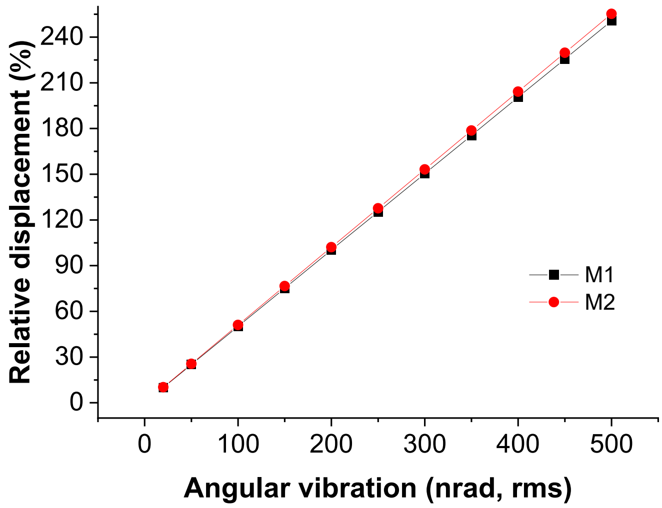

Figure 33-40 The relative movement of the source point caused by the offset mirrors under the influence of different angular vibrations

For focusing optical components, the influence of the light source point vibration and the translation of the optical element will eventually be suppressed because of the focusing of the optical element, and the degree of suppression is the same as the compression ratio of the element, while the influence of the angle vibration will not be suppressed, but amplified, and the magnification degree is proportional to the image distance of the element. Under the conditions of translational and angular vibration of different optical components, the vibration of the focused spot of each experimental station is shown in Figure 3.3-41, 42 and 43, where the vibration of the light source point is 10% of the size of the light source, and the vibration of the monochromator exit slit is 200nm.

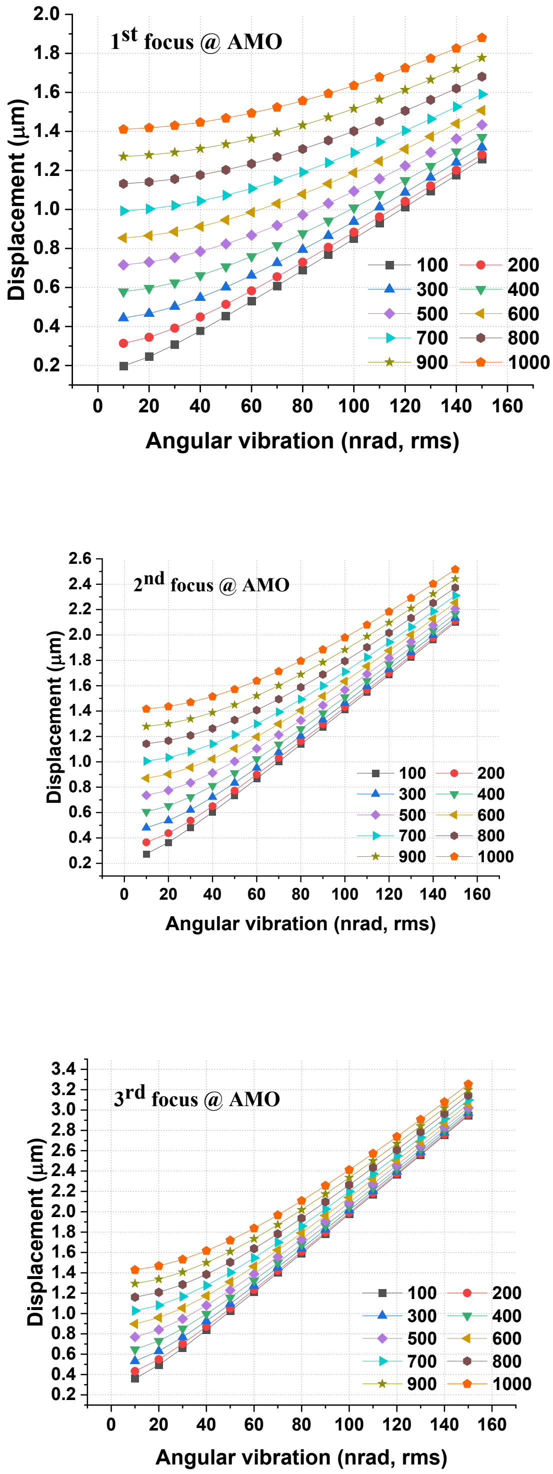

Figure 3.3-41 Vibration of the focal spot at the three focal positions of the AMO experimental station under the condition of translational and angular vibration of different optical components

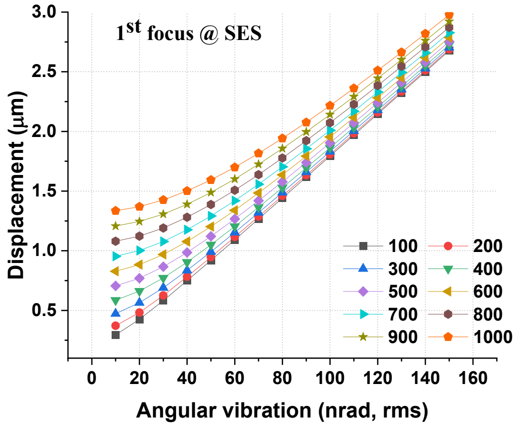

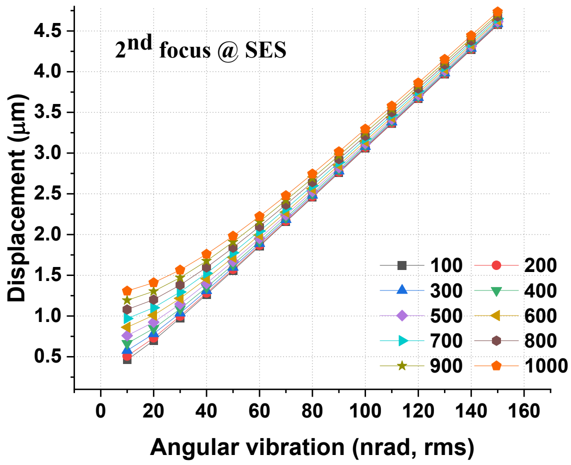

Figure 3.3-42 Vibration of the focusing spot at two focal positions of the SES experimental station under the conditions of translational and angular vibration of different optical components

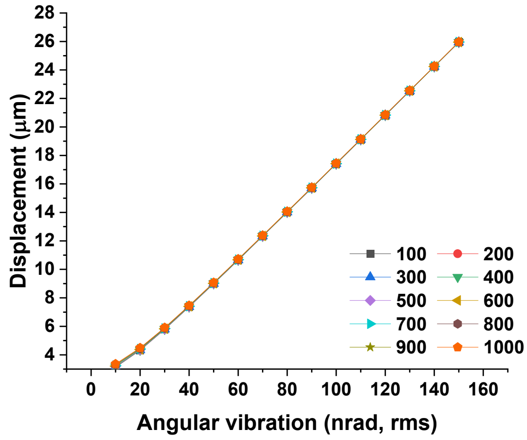

Figure 3.3-43 Vibration of the focused spot at the SSS experimental station under different translational and angular vibration conditions

Among the above three experimental stations, the SSS experimental station has the largest vibration at the sample point, which is mainly caused by the image distance of the horizontal focusing mirror. The SSS experimental station requires a large horizontal focusing spot, and its horizontal focusing mirror is located 261 meters away from the light source point and 64 meters away from the sample point, so the vibration of the horizontal spot is large, resulting in a large focus vibration after the final convolution. If the two directions are decomposed, the vibration in the horizontal direction is about tens of microns, while the vibration in the vertical direction is expected to be controlled below 1 micron, as shown in Figure 3.3-44 and 45

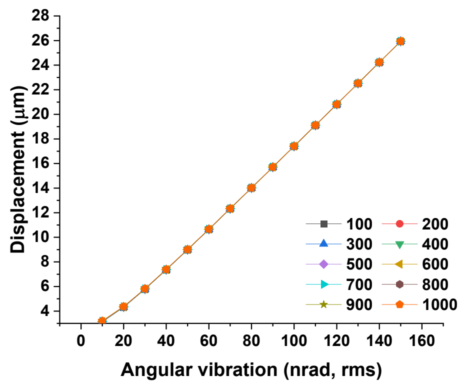

Figure 3.3-44 Vibration of the horizontally focused spot of the SSS experimental station under different translational and angular vibration conditions

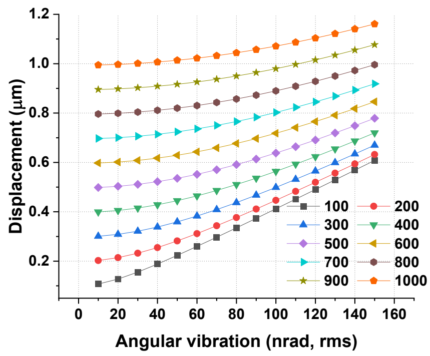

Figure 3.3-45 Vibration of the vertically focused spot of the SSS experimental station under the conditions of translational and angular vibration of different optical components

In summary, the stability of the focal point at the optimized energy point of each experimental station is shown in Table 3.3-3, and all experimental stations are calculated with the shortest image distance, in which the jitter of the light source point is calculated as 10% of the size of the light source (no signed document), the angular vibration of the optical element is 50 nrad (rms), and the translational motion is 200 nm。

Table 3.3-3 Focus stability at the energy optimization point of each experimental station

Experimental station	FISHHOOK	HIS	SSS	
Optimized Energy (eV)	900	900	900	
Stability (μm, rms).	0.51	0.95	H	V
			9.1	0.28

3.3.12 Optical Component Parameters

Table 3.3-4 Summary of parameters of FEL-II beamline plane mirrors

	M1	M2a	M2b
Substrate	Single Crystal Silicon (100)		
Maximum footprint (6σ, L×W, mm^2)	900×9	1018×10	694×3
Mirror length (L×W, mm^2)	750×50	900×50	900×50
Optical active length (L×W, mm^2)	700×30	700×30	700×30
Grazing incident angle (mrad)	5/10	8.7	3.7
Surface	Plane Mirror		
Bending (Yes/No)	No	Yes	Yes
Bending Mode	-	Dynamic bending	Dynamic bending
Mirror surface direction	Horizontal	Horizontal	Horizontal
Curvature radius (km)	＞800		
Sagittal Slope error (μrad, rms)	<1		
Tangential Slope error (μrad, rms)	<0.05		
Height error (nm， rms)	<0.5		
Coating material	B_4C		
Coating thickness (nm)	40		
Roughness (Å,rms)	<2		

Table 3.3-4 Summary of parameters of FEL-II beamline KB focusing mirror

	ECMV-AMO	ECMH-AMO	ECMV-SES(PEM)	ECMH-SES(PEM)	ECMV-SES(TAP)	ECMH-SES(TAP)	ECMV-SSS
Substrate	Single Crystal Silicon (100)						
Maximum footprint (6σ, L×W, mm^2)	1918×19	1918×19	500×10	690×8	500×10	690×8	494×1
Optical active length (L×W, mm^2)	850×30	850×30	650×30	800×30	650×30	800×30	450×10
Mirror length (L×W, mm^2)	1050×50	1050×50	700×90	850×90	700×90	850×90	500×30
Grazing incident angle (mrad)	10			15			
Surface	Elliptical cylinder						
Bending (Yes/No)	Yes			No			
Bending Mode	Reverse bending			-			
Profile Before bending	Elliptical cylinder			-			
a(mm)	172500	172500	21000	168500	23000	170500	15000
b(mm)	261.912	333.26	207.49	679.287	275.99	871.28	112.25
δ(mrad)	0.233	0.380	8.65	1.12	15.996	1.85	4.31
Object distance(m)	343	341.75	36.8	330.8	36.8	330.8	28.0
Image distance (m)	2.0-5.3	3.25-6.55	5.2	6.2	9.2	10.2	2.0
Curvature radius range (km)	0.40-1.10			0.64-1.35			
Height error（nm,rms）	<3.0	<1.5	<4.5	<1.5	<4.5	<1.5	<0.7
Tangential slope error (μrad,rms)	<0.1	<0.1	<0.1	<0.07	<0.1	<0.07	<0.07
Sagittal Slope error (μrad,rms）	<1						
Surface coating material	B_4C						
Coating thickness (nm)	40						
Surface roughness (Å rms)	<2						

Table 3.3-5 Summary of optical element parameters of FEL-II beamline offset mirrors

	M3/ ECMH-SSS	
Substrate	Single Crystal Silicon (100)	
Maximum footprint (6σ，L×W, mm^2)	590×15	
Optical active length (L×W, mm^2)	600×30	
Mirror length (L×W, mm^2)	650×90	
Grazing incident angle (mrad)	17	
Surface	Plane	Elliptical cylinder
a(mm)	-	162500
b(mm)	-	2115.425
δ(mrad)	-	15.50
Object distance(m)	-	267.0
Image distance (m)	-	58.0
Mirror surface direction	Horizontal	
Curvature radius (km)	＞1000	-
Height error（nm,rms）	1.5	
Tangential slope error (μrad,rms)	0.07	
Sagittal Slope error (μrad,rms）	<1	
Surface coating material	B_4C	
Coating thickness (nm)	40	
Surface roughness (Å rms)	<2	

Table 3.3-6 Summary of optical element parameters of FEL-II beamline grating monochromator

Name	PM-BM	PM-SSS	PG-BM			PG-SSS
Substrate	Single Crystal Silicon (100)					
Maximum footprint (6σ, L×W, mm^2)	376×20	185×5	470×21	750×21	590×21	280×5
Focal Spot moving range (mm^2)	530	380	-	-	-	
Optical active length (L×W, mm^2)	750×30	550×30	300×20	300×20	300×20	300×20
Mirror length (L×W, mm^2)	800×50	600×50	320×30	320×30	320×30	320×30
Optimized energy (eV)	-	-	900	900	900	900
C_{ff} Value	-	-	1.5	3.0	3.0	
Line density(l/mm)	-	-	200	500	800	800
b_2(l/mm^2)	-	-	4.58783e-5	2.49235e-5	2.4917e-5	1.133148 e-3
b_3(l/mm^3)	-	-	1.56696e-9	4.21339e-10	2.56986e-10	4.42378e-7
Grating mode	-	-	Blazed gratings			
Blazing angle (deg)	-	-	0.4	0.9	1.1	0.8
Surface	Plane					
Cooling mode	bottom-cooling					
Height error (nm, rms)	<0.7					
Tangential slope error (μrad, rms)	<0.07					
Sagittal Slope error (μrad, rms)	<1					
Surface coating material	B_4C /Pt	B_4C				
Coating thickness (nm)	40					
Surface roughness (Å, rms)	<2					

4. Beamline performance simulation

4.1 Focus

All experimental stations after FEL-II were focused using KB mirrors. KB focusing mirrors consist of two independent elliptical cylindrical mirrors that focus in both directions of the beam. Ellipsoidal mirrors and elliptical cylindrical focusing mirrors are defined as follows:

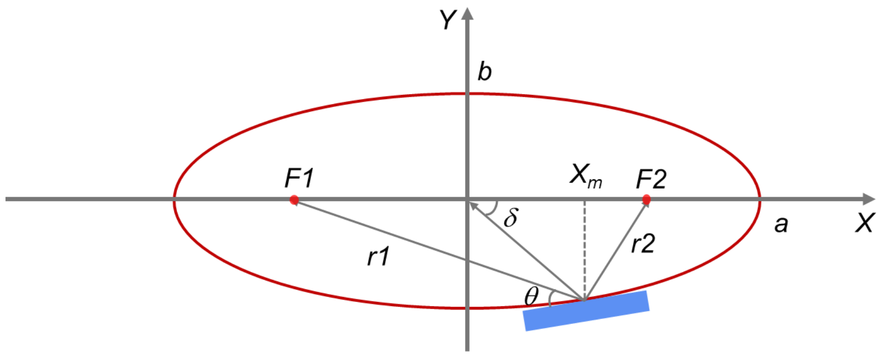

Figure 4.1-1 Ellipsoidal mirror and elliptical cylindrical focusing mirror

a, b are the semi-major axis and semi-minor axis, xm is the abscissa value of the mirror tangent point in the elliptical coordinate system, r1 and r2 are the object distance and image distance, the ellipsoidal focusing mirror is a and b, the slight incidence angle is θ, and the delta angle is defined as the major axis a(+x direction) and the polar axis rotated counterclockwise from the +x direction to the angle of the center of the mirror.

Calculate the parameters of an elliptical cylindrical mirror in *m*

$$c = \sqrt{a^2 - b^2}$$

$$y = -b\sqrt{1 - \frac{x^2}{a^2}}$$

$$r_1 = \sqrt{\left(x + \sqrt{a^2 - b^2}\right)^2 + b^2\left(1 - \frac{x^2}{a^2}\right)}$$

$$r_2 = \sqrt{\left(x - \sqrt{a^2 - b^2}\right)^2 + b^2\left(1 - \frac{x^2}{a^2}\right)}$$

$$\alpha = \arctan\left(\frac{bx}{a^2\sqrt{1 - \frac{x^2}{a^2}}}\right)$$

$$\beta = \arctan\left(\frac{b\sqrt{1 - \frac{x^2}{a^2}}}{x + \sqrt{a^2 - b^2}}\right)$$

$$\theta = \alpha + \beta$$

$$delta = \arctan\frac{y}{x}$$

Solving the above simultaneous equations, a*, b, x and delta* can be obtained, when the arc is rotated around the major axis a, it is an ellipsoidal focusing mirror, otherwise it is an elliptical cylindrical focusing mirror.

4.1.1 AMO Experimental Station Focusing System

The sample point of the AMO experimental station is located 345 m away from the light source point on the straight line, and the pink light is directly focused to the sample point without the need for a monochromator. The AMO station consists of three subsystems, 2.0 m, 3.8 m and 5.6 m from the center of the last KB mirror. The focusing system will use the reverse dynamic bending technology to achieve free switching of the focus at the different sample points, the focusing mirror type will be prepared as the first focus point as the standard, and then the focus point will be adjusted to the last two sample points by changing the surface shape through the bending mechanism. The focused optical path of the AMO experimental station is shown in Figure 4.1-2.

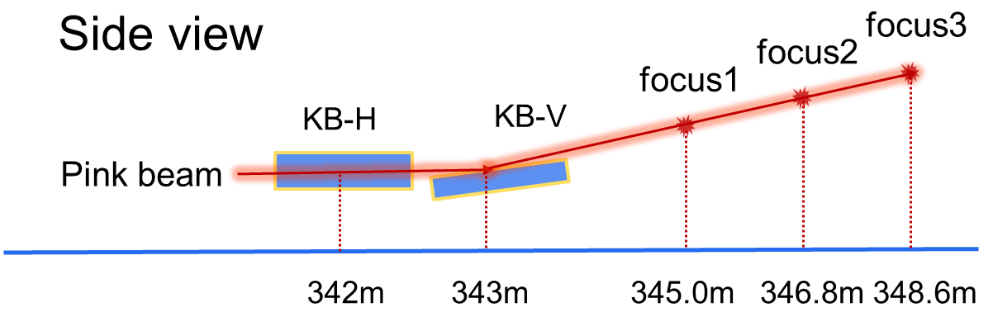

Figure 4.1-2 Schematic diagram of the focused optical path of the AMO experimental station

Taking the 900 eV energy point as an example, the spot size settlement results and tracking results at each sample point of the experimental station are shown in Figure 4.1-3, 4, 5, 6, and 7, and the height error of the optical element is not considered during the tracking.

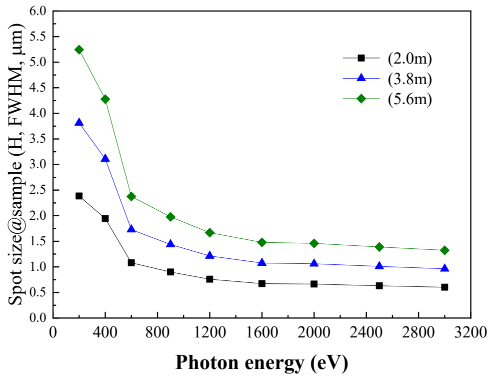

Figure 4.1-3 Horizontal focal points at different sample points at the AMO experimental station

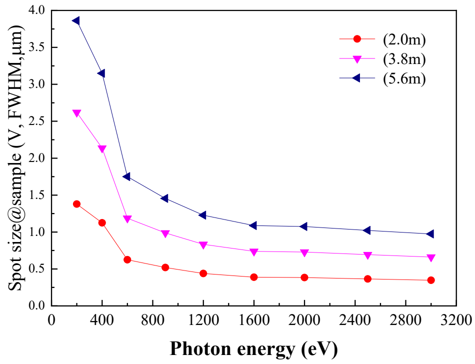

Figure 4.1-4 Vertical focal points at different sample points at the AMO experimental station

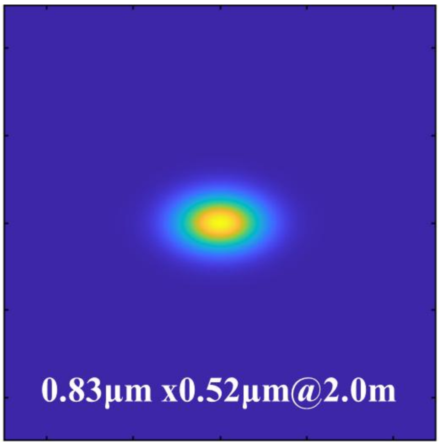

Fig. 4.1-5 Simulation results of the focal point at the 2.0 m sample point of the AMO experimental station

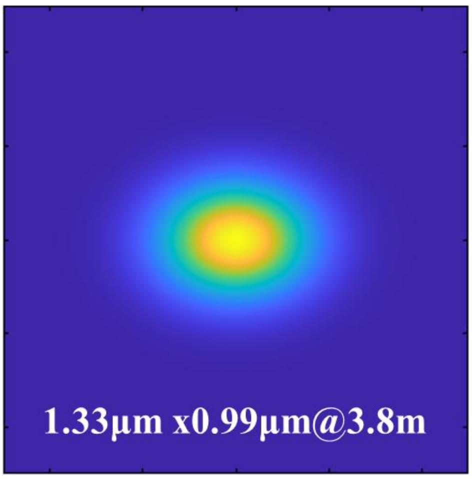

Fig. 4.1-6 Simulation results of the focal point at the 3.8 m sample point of the

AMO experimental station

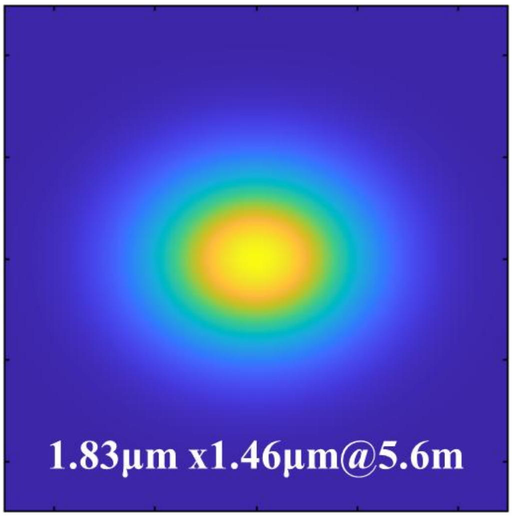

Figure 4.1-7 Simulation results of the focal point at the 5.6 m sample point of the AMO experimental station

For the AMO experimental station, the beam passes through the offset mirror group and the KB focusing mirror to reach the experimental station, because the AMO experimental station covers a large energy range, so in the range of 200eV-2000eV, the offset lens group adopts a combination of M1 (10mrad)/M2a (8.7mrad), In the range of 2000eV-3000eV, the offset lens group adopts the combination of M1 (5mrad)/M2b (3.7mrad), and the transmission efficiency of the beam line is shown in Figure 4.1-8. The effect of the height error of the optical element in the beamline at a typical energy point on the beam transmission efficiency is analyzed in Section 4.2.2.

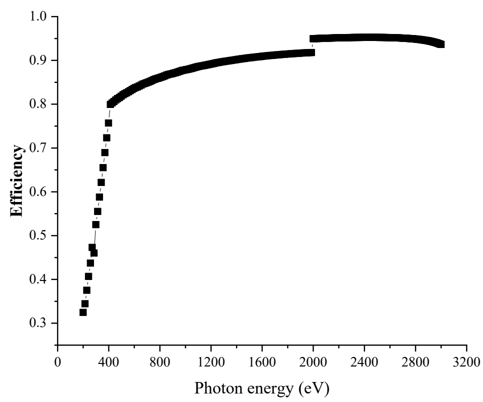

Figure 4.1-8 Beamline transmission efficiency of AMO experimental station

The focused spot of the three stations can be less than 10×10 μm2 in the full energy range. The power density at the three sample points is shown in Figure 4.1-9, which is calculated based on the fundamental wave of the light source, and only considers the transmission efficiency of the beam line and the spot size under the ideal focusing condition, and does not calculate the receiving aperture and height error of the optical element.

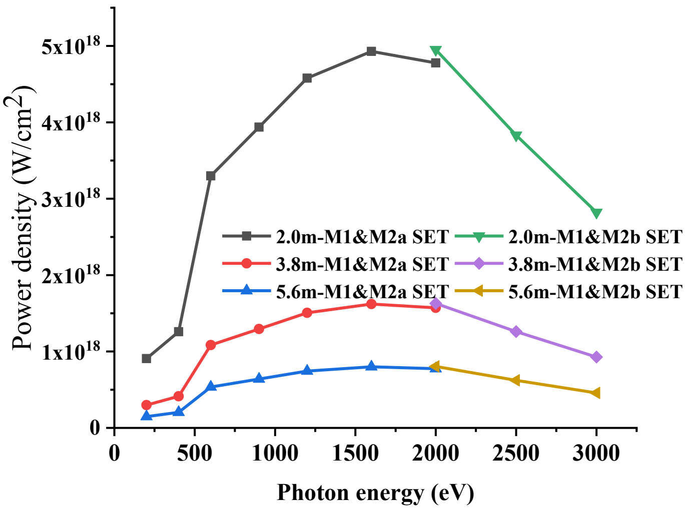

Figure 4.1-9 Power density at three sample points at the AMO experimental station

The transmission efficiency of FEL pulses to the AMO station and the harmonic content at the sample points of the station are shown in Figure 4.1-10. Depending on the needs of the experimental station, the energy coverage of the beamline ranges from 200 eV to 3000 eV, and the reflection characteristics of B4C materials are also different in such a wide energy range. When the photon energy is greater than 3000eV, its reflectivity decreases sharply, so its cut-off ability of higher harmonics is very strong, but for the 200eV-1000eV range of the low energy end, its third harmonic all falls within the optimized range of the beamline, especially the energy range of 200eV-600eVThe third harmonic and fifth harmonics fall completely within the optimized range of the beamline and are difficult to filter out through the transmission system, so the higher harmonic content at the sample point is less than 1% when the photon energy is greater than 1000 eV, and the higher harmonic content at the sample point is less than 10% when the photon energy is less than 1000 eV.

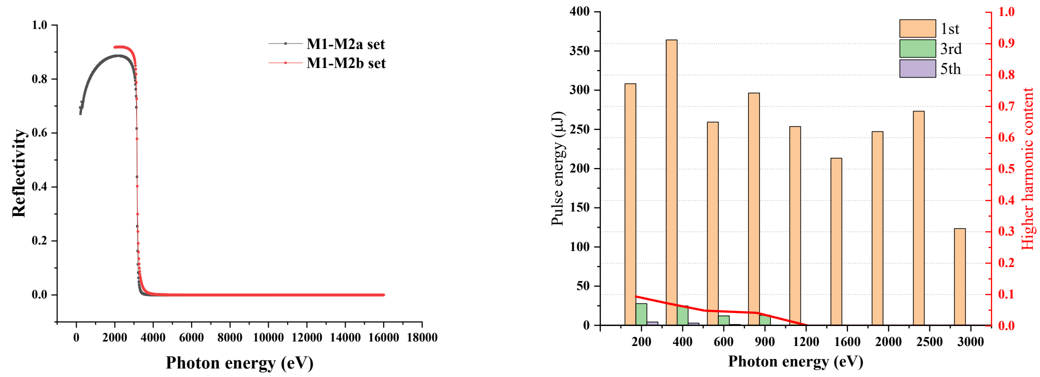

Fig. 4.1-10 The transmission efficiency of FEL pulses to the AMO station and the harmonic content at the sample points of the station

4.1.2 SSS Experimental Station Focusing System

The sample point of the SSS experimental station is located 325 m away from the light source point on the branch line, and the experiment requires a high-energy resolution monochromatic light incidence, and the vertical spot is required to be less than 1.8 μm

@900eV, greater than 30 μ m@900eV horizontally. The small spot in the vertical direction is mainly to ensure the energy resolution of the RIX spectrometer of the experimental station. The purpose of the large horizontal spot is to increase the spot area at the sample point to reduce the flux density and avoid radiation damage to the sample under multi-pulse irradiation. To achieve this, the vertical focusing mirror is located 2 m in front of the sample, while the horizontal focusing mirror is located at the beamline deflector mirror, on the same substrate as the deflection mirror. The focused optical path of the SSS experimental station is shown in Figure 4.1-11.

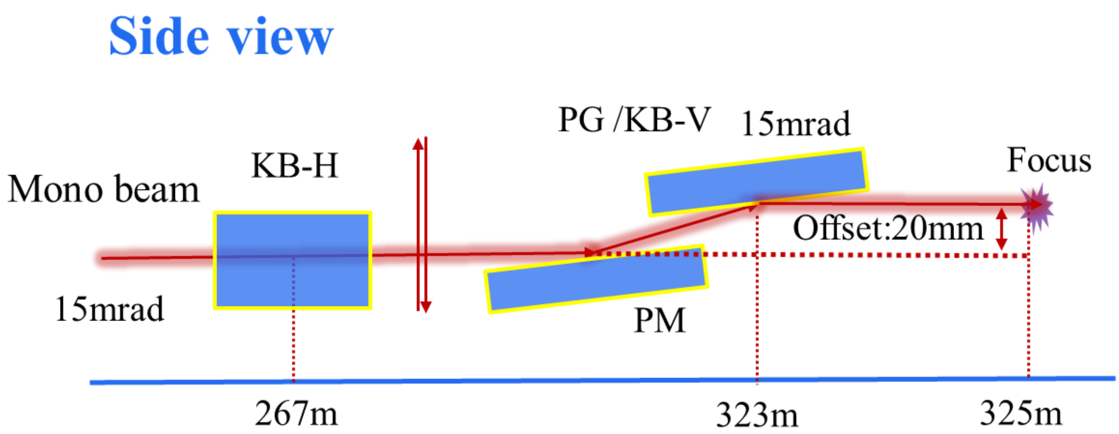

Figure 4.1-11 Schematic diagram of the focusing optical path of the SSS experimental station

When the vertical focusing mirror is grazing at 15mrad, taking the 900eV energy point as an example, when the grating monochromator uses gratings with different linear densities, the spot size settlement results and tracing results at the sample point are shown in Figure 4.1-12 and 13, and the height error of the optical element is not considered.

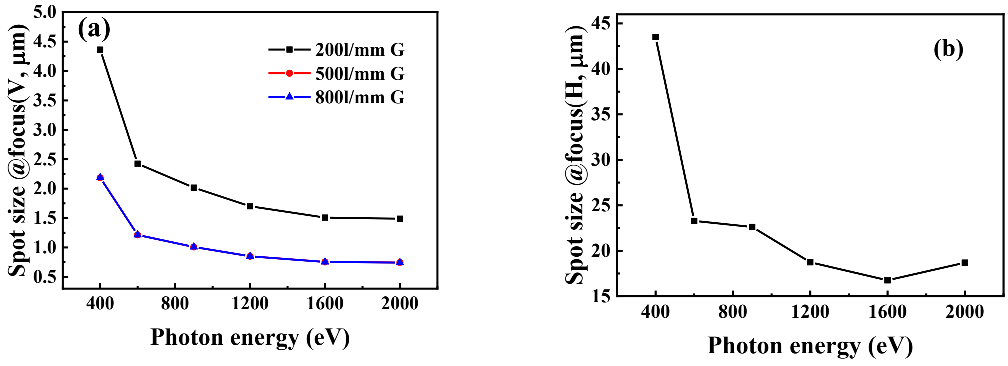

Fig. 4.1-12 The focal point at the sample point of the SSS experimental station is (a) in the vertical and (b) in the horizontal

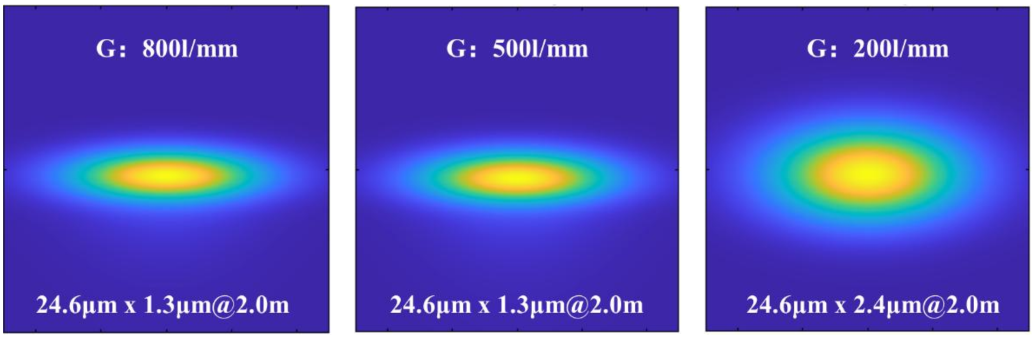

Figure 4.1-13 Simulation results of focal point at the sample point of SSS experimental station (ECM mirror focus).

For the SSS experimental station, when the KB focusing mirror is used, the beam passes through the offset mirror group, the grating monochromator, the deflection mirror and the KB focusing mirror, and the transmission efficiency of the beam line is shown in Figure 4.1-14, the curve does not consider the influence of the height error of the optical element in the beam transmission, and the influence of the height error of the optical element in the beam line at the typical energy point on the beam transmission efficiency is analyzed in Section 4.2.3.

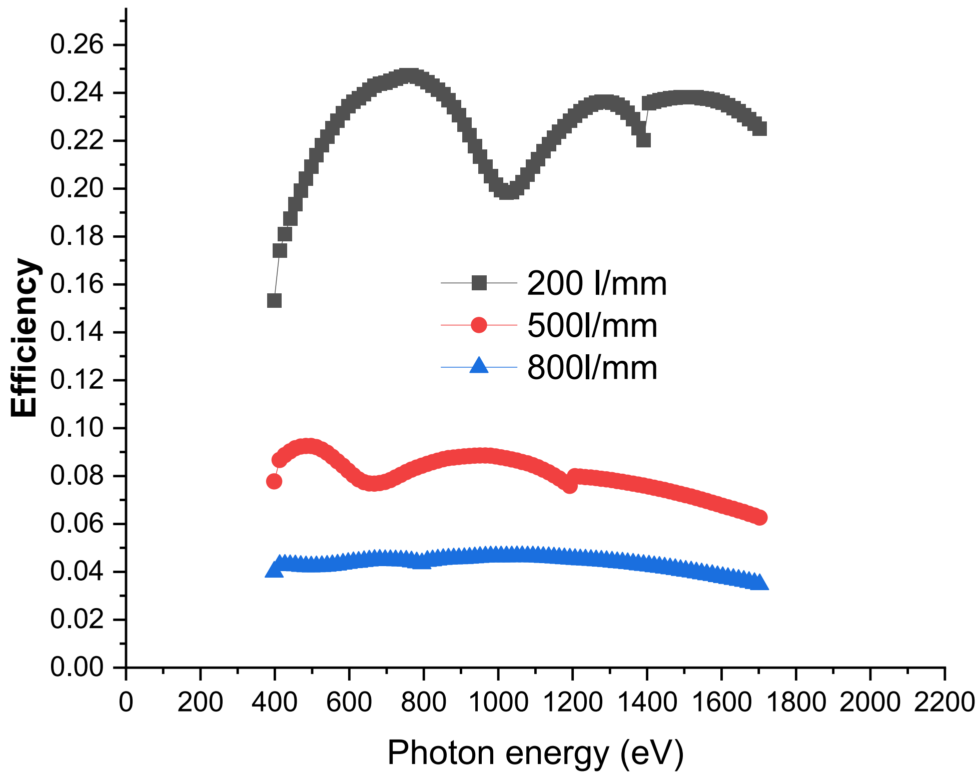

Figure 4.1-14 Beamline transmission efficiency of the SSS experimental station when the KB focusing mirrors are used

In order to compress the pulse broadening after passing through the monochromator, a set of pulse compression device needs to be added in front of the SSS experimental station, which is similar in structure to the grating monochromator, and the angle rotation of the front plane mirror changes the angle of incidence of the beam on the grating, and the wavelength of the outgoing light is changed by the angle rotation of the grating. The focusing mirror of the SSS station and the grating of the pulse compression device are installed at the same position for switching: if pulse compression is required, the grating is used to focus the upstream beam to the sample point; In the absence of pulse compression, a focusing mirror is used to focus the upstream beam to the sample point to ensure that the beam is incident horizontally at the sample.

For the pulse length compression device, its structure is similar to that of the grating monochromator, and the variable inclusion angle design is adopted, and the inclusion angle is changed by changing the angle of the front mirror. There are two options for the design of the optical path of the pulse compression device: one is the optical path symmetrical with the upstream monochromator, which uses -1 order diffraction of the grating; The other is an asymmetrical optical path with an upstream monochromator, using +1 order diffraction of the grating. Considering the difference in the diffraction efficiency of the grating, the asymmetric optical path is selected, and the optical schematic diagram is shown in Figure 4.1-15

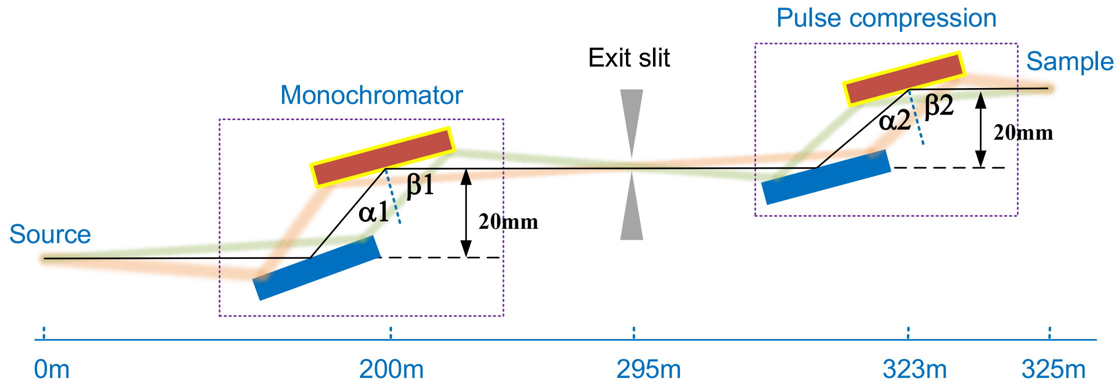

Figure 4.1-15 Optical schematic diagram of pulse length compensation device of SSS experimental station

The degree of compensation of the pulse length after passing through the pulse length compression device depends on the irradiation area of the spot on the compensation grating and the selected diffraction order of the outgoing light. When the grating line density is the same, the spot area on the grating is the same, and the diffraction order is also selected, it is theoretically possible to completely compensate for the pulse broadening caused by the upstream monochromator. Because the image distance of the grating monochromator is larger than that of the compensation grating in the pulse compression device, the spot area on the compensation grating is smaller than that on the grating monochromator with the same grating line density and outgoing light diffraction order, so the pulse broadening cannot be fully compensated. In the grating monochromator, the FEL beam pulse width is up to 800 l/mm, taking the grating as an example, when the compensation grating in the pulse compression device adopts a combination of different line densities and Cff values, the FEL pulse width reaching the experimental station is shown in Figure 4.1-16

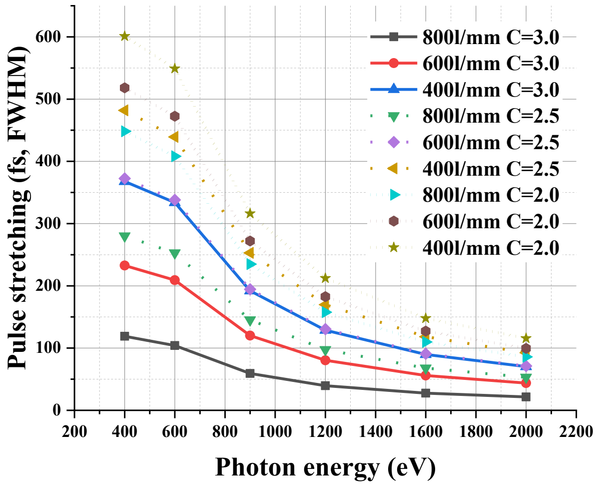

Figure 4.1-16 Broadening of FEL pulses arriving at the experimental station when the compensation grating adopts a combination of different line densities and Cff values

The duration of the incident light pulse is less than 200 fs, which includes both the intrinsic length of the FEL pulse and the contribution of the grating monochromator. The intrinsic length of the FEL pulse is about 30fs, so when the Cff value of the compensation grating is 3.0, the 800l/mm and 600l/mm gratings can meet the needs of the experimental station, and when the Cff value of the compensation grating is 2.5, only the 800l/mm grating can meet the needs of the experimental station. In this case, the diffraction efficiency of the grating at different flare angles is shown in Figure 4.1-17, and the grating coating is Au.

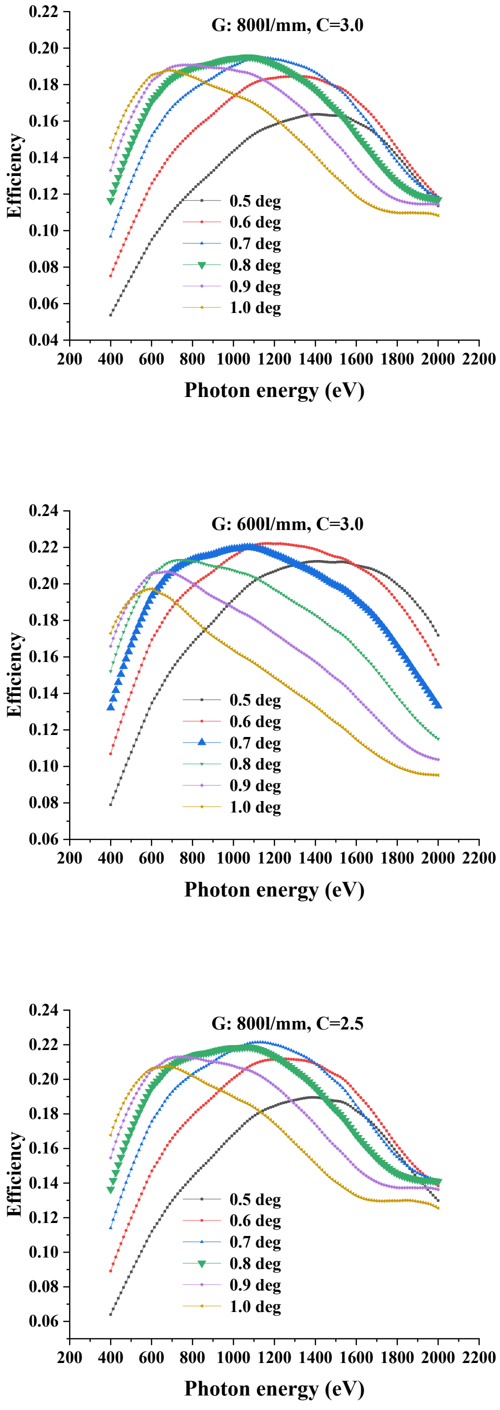

Figure 4.1-17 Diffraction efficiency of the compensation grating at different blazed angles

As can be seen from the above figure, the diffraction efficiency of 800l/mm grating (C=2.5) and 600l/mm grating (C=3.0) is almost the same, slightly higher than that of

800l/mm grating (C=3.0). Pulse spreading of less than 150 fs at the sample point can be achieved within the optimized energy range of the SSS station. At this point, when the grating monochromator uses a grating with different line densities, the pulse broadening to the SSS experimental station is shown in Figure 4.1-18

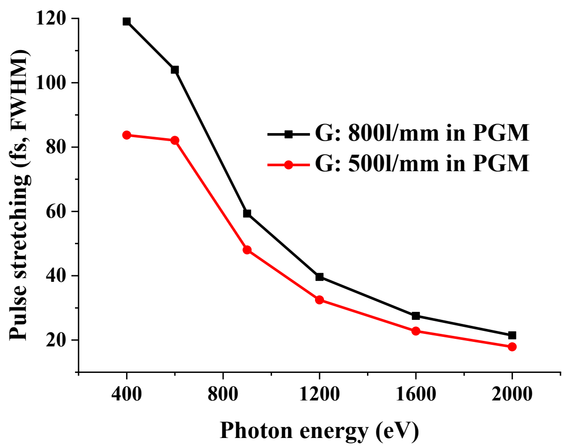

Figure 4.1-18 Simulation results of focal point at the sample point of SSS experimental station (ECM mirror focusing).

When using a pulse length compression device, the focusing of the beam is ultimately done by the grating instead of the focusing mirror, and its focusing ability is stronger than that of the KB focusing mirror due to the influence of the Cff value of the grating, so the spot size at the sample point is smaller when focusing with the grating than when focusing with the KB focusing mirror. Figure 4.1-19 shows the spot tracing results at the sample point after using the pulse length compression device, where the height error between the grating monochromator and the optical element in the pulse length compression device is 1 nm (rms), and the height error of the offset mirror group is 2 nm (rms).

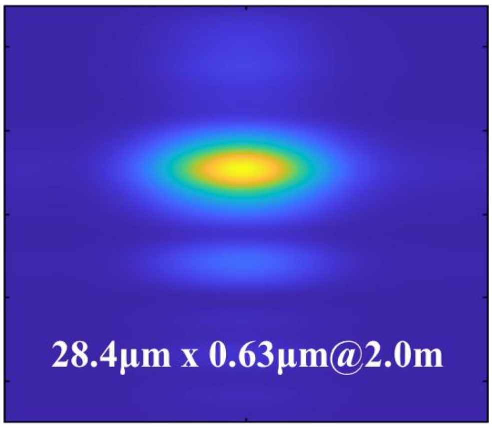

Figure 4.1-19 Simulation results of focal point at the sample point of SSS experimental station (grating focusing).

Due to the very large horizontal focusing KB mirror distance of the SSS experimental station, the angular vibration of the optical element will cause a large lateral jitter of the horizontal spot, which is equivalent to the increase of the horizontal spot size in the case of multi-pulse accumulation. Since the spot produces a projection in the vertical direction in the case of non-strictly horizontal incidence, this has a simultaneous effect on the size of the vertical spot, which is exacerbated when the focused spot grazing over the sample. Taking the 900 eV energy point as an example, the equivalent horizontal spot at the sample point is shown in Figure 4.1-20 when multiple pulses accumulate when only the horizontal KB mirror is shaken

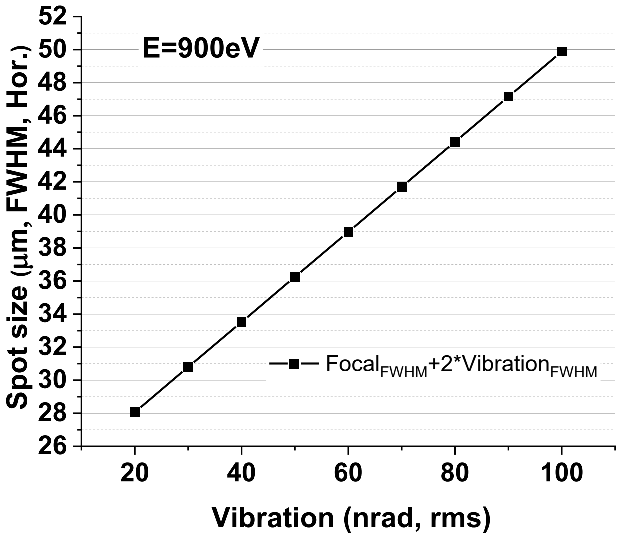

Figure 4.1-20 Equivalent horizontally focal point at the sample point of the SSS experimental station under the condition of multi-pulse accumulation considering only the vibration of the horizontal focusing mirror

If the spot is not incident horizontally, and the focused spot is grazing on the sample, the increment of the equivalent horizontal spot in the vertical direction is shown in Figure 4.1-21, where the vibration of the horizontal KB mirror is considered to be 50 nrad (rms), 80 nrad (rms), 100 nrad (rms), and 150 nrad (RMS) for the four cases, the angle of incidence on the sample varies from 2° to 5°, and the spot tilt angle ranges from 0.01° to 0.1°.

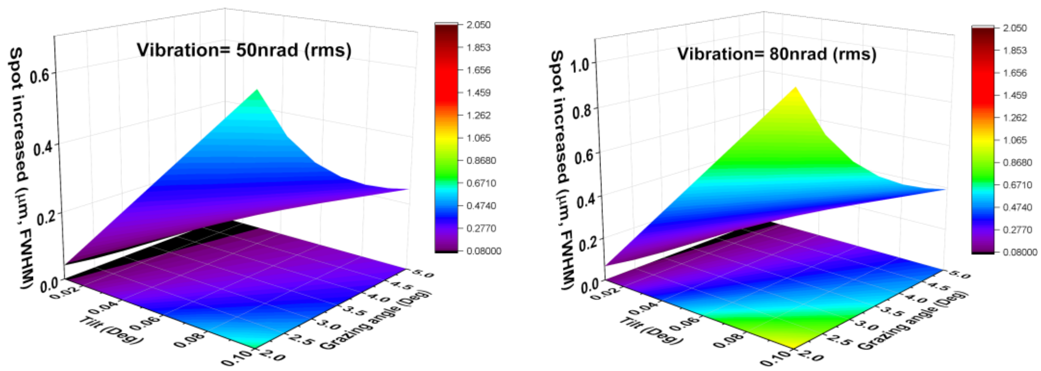

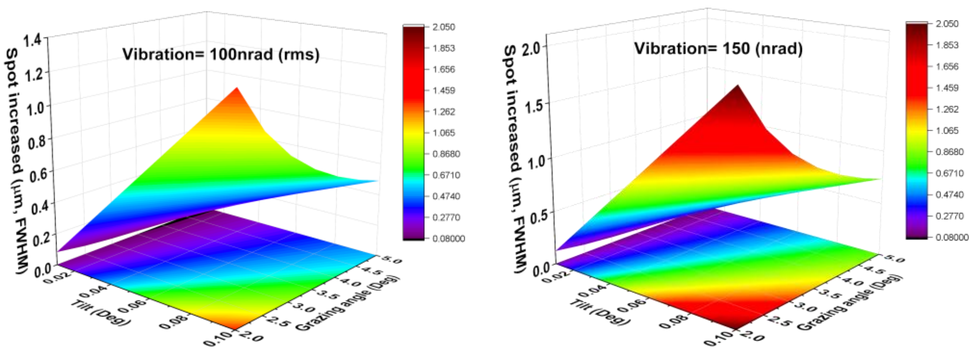

Figure 4.1-21 The vertical spot size increment caused by the horizontal spot when the beam is slightly incident at different grazing angles and different tilt angles on the sample with different horizontal KB mirrors vibration

If the grazing incidence angle of the focused spot on the sample is 2° and the tilt angle is 0.1°, then the vertical spot increment caused by the horizontal spot with the angle of the horizontal KB focusing mirror at the 900 eV energy pointis shown in Figure 4.1-22.

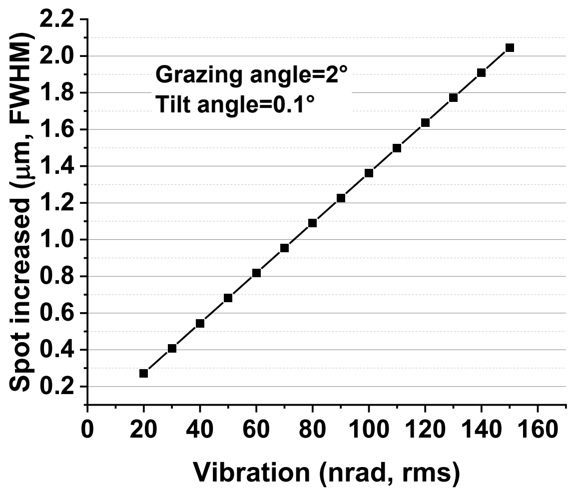

Figure 4.1-22 The relationship between the vertical spot increment caused by the horizontal spot and the grazing angle of the horizontal KB focusing mirror (the grazing incidence angle is 2°, and the tilt angle is 0.1°).

The requirement of the vertical focusing spot of the RIX spectrometer of the experimental station is less than 2 μm, and when the KB focusing mirror is used, the theoretical focusing spot is 1.2 μm, so in this extreme case, the angular vibration of the horizontal KB mirror and the vertical KB mirror needs to be controlled below 40nrad (rms). Of course, when the tilt angle of the spot is much less than 0.1° by adjusting the attitude of the optical element, the angle vibration requirements for the two KB mirrors can be reduced.

4.1.3 SES Experimental Station Focusing System

The sample point of the SES experimental station is located 337 m from the light source point on the branch line, and the experimental station requires monochromatic light incidence. The SES experimental station consists of two subsystems, namely the Electron Microscope System (PEM) and the Ultrafast Electron Dynamics System (TAP), which are 337m and 342m away from the light source point respectively, and the focused spot is required to be less than 20×20μm2. The focusing system uses two sets of focusing mirrors with different curvatures to focus the FEL pulses to the non-sample point, and the two experimental systems are 5 meters and 9 meters away from the KB mirrors respectively. The focused optical path of the SES experimental station is shown in Figure 4.1-23

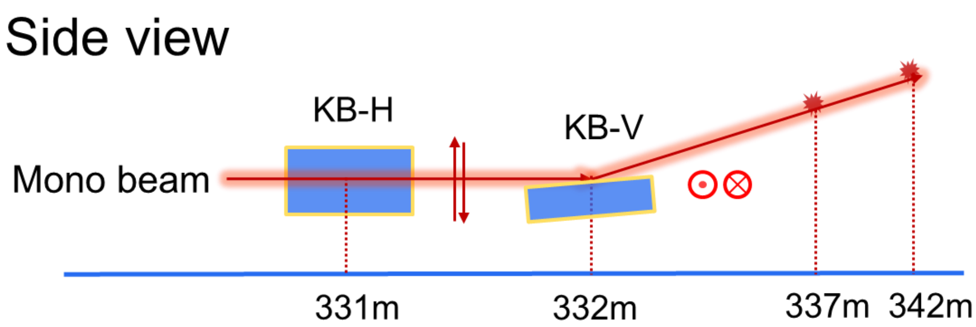

Figure 4.1-23 Schematic diagram of the focused optical path of the SES experimental station

The KB focusing mirrors are all incident at 15mrd, and the spot size settlement results and tracking results at the sample point are shown in Figure 4.1-24, 25, and 26, in which the tracking results use an 800 l/mm grating, and the height error of the optical element is not considered (see the next section for the consideration of height error).

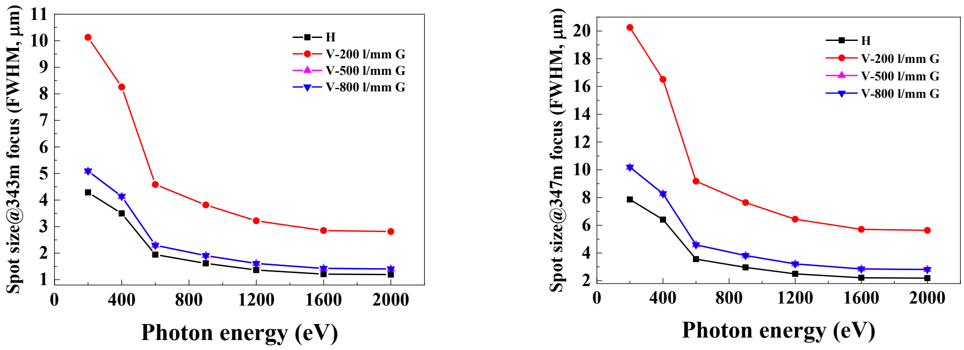

Figure 4.1-24 Focal point curves at two sample points of the SES experimental station

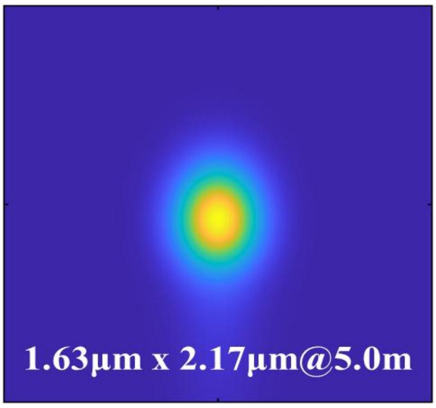

Fig. 4.1-25 Simulation results of the focal point at the 5.0 m sample point at the SES experimental station at 900 eV

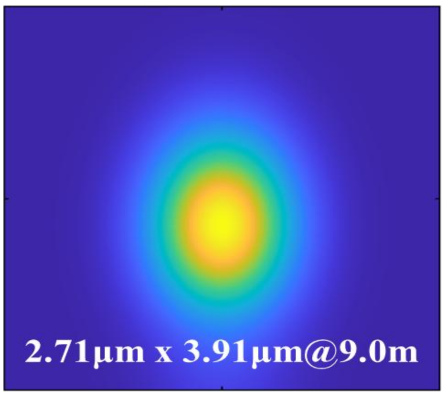

Figure 4.1-26 Simulation results of the focal point at the 9.0 m sample point at the SES experimental station at 900 eV

Both experimental systems can achieve focused spot sizes of less than 20×20 μm^2 in both directions.

For the SES experimental station, the beam passes through the offset mirror group, the grating monochromator, the deflection mirror and the KB focusing mirror to the experimental station, and the transmission efficiency of the beam line is shown in Figure 4.1-27, the curve does not consider the influence of the height error of the optical element in the beam transmission, and the effect of the height error of the optical element in the beam line on the beam transmission efficiency at the typical energy point is analyzed in Section 4.2.5.

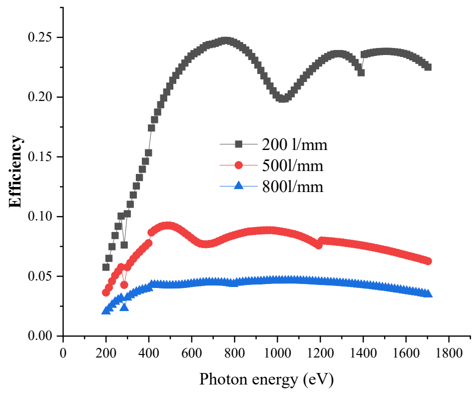

Figure 4.1-27 Beamline transmission efficiency of SES experimental station

4.2 Height error of optical components

According to the characteristics of high pulse energy, high repetition rate and high coherence of SHINE free electron laser, the beamline is one of the principles of maintaining wavefront integrity in the optical design according to the requirements of the FEL-II experimental station. In order to maintain wavefront integrity, reasonable requirements need to be placed on the height error of the optical components. According to the Marechal criterion, the wavefront error of the beam needs to be less than λ /14(RMS) (in this case, the Strel ratio SR=0.8). According to this standard, the height error of each optical element is:

$$h_{rms} = \frac{\lambda}{14} \cdot \frac{1}{2\sqrt{N \cdot \alpha^2}}$$

where λ is the operating wavelength, N is the number of optical elements, and α is the grazing incidence angle of the incident beam on the optical element. Figure 4.2-1 shows the requirements for the height error of optical components at different photon energies, in which the beam reaching the SSS experimental station and the SES experimental station on the branch line needs to pass through 7 mirrors (including the grating monochromator), and the beam reaching the AMO experimental station on the straight line needs to pass through 4 mirrors.

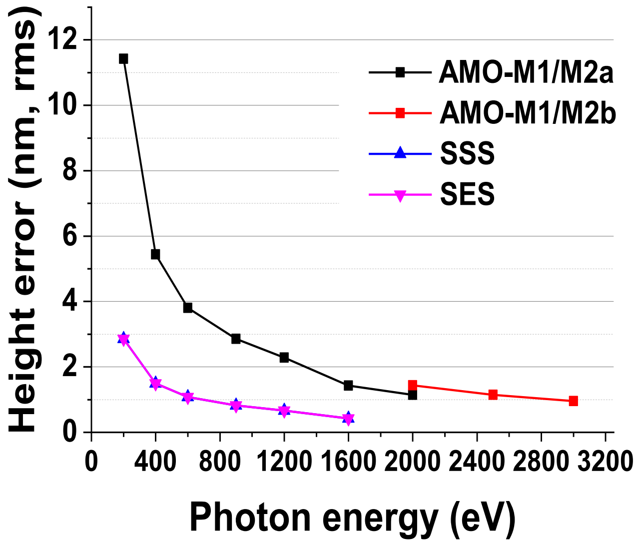

Figure 4.2-1 Requirements for the height error of optical components at each experimental station

For different experimental stations, according to the different experimental properties, the requirements for the focused spot are also different: most of the experiments carried out by the AMO experimental station are single-pulse experiments, which have high requirements for the peak intensity of the focused spot; However, most of the experiments carried out by the SSS and SES stations are multi-pulse accumulation experiments, which require sufficient photon count, but do not have high requirements for the peak brightness of the focused spot. On the other hand, in addition to the last focusing mirror for the focusing element exclusive to each experimental station, the beam line offset mirror group, the grating monochromator and the deflection mirror are all common elements of all experimental stations or part of the experimental stations, so in order to ensure the peak intensity of the focused spot of each experimental station, It is necessary to put forward the requirements for the optics on the beam line as a whole.

4.2.1 Grating monochromator height error requirements

Because the SSS experimental station and the SES experimental station have extremely high requirements for the relative spectral width of the incident light, this puts forward higher requirements for the surface shape of the optical elements in the grating monochromator, the spot size that reaches the slit of the monochromatic light after passing through the grating monochromator cannot be increased, and the intensity of the side-associated peak of the focused spot also needs to be within a reasonable range, because the size of the focused spot and the intensity of the side-accompanied peak of the monochromatic light will affect the relative spectral width of the incident light of the subsequent experimental station. Taking the 800L/mm grating with the highest energy resolution as an example, the surface shape requirements of the grating monochromator optical components can be determined by analyzing the spot size and the height of the side associated peaks at the exit slit under different combinations of height error and slope error. Table 4.2-1 lists the spot sizes at the exit slit under different combinations of height error and slope error, and the average results are averaged 20 times for each combination.

Table 4.2-1 Spot size (μm, FWHM) at the exit slit under different combinations of height error and slope error

Height error / Slope error	0.5nm	1.0nm	1.5nm	2.0nm
50nrad	16.805	17.2	16.92	17.05
100nrad	17.015	16.865	16.775	16.94
150nrad	16.94	17.13	17.095	17.1

200nrad	16.97	16.795	17.11	16.99

From the above table, it can be seen that under the combination of different height error and slope error, the spot size at the exit slit hardly changes, which can meet the needs of use. The relative intensities of the companion peaks of the focused spot for each of these combinations are shown in Table 4.2-2.

Table 4.2-2 Relative intensity of the companion peak of the spot at the exit slit (%) under different combinations of height error and slope error

Height error / Slope error	0.5nm	1.0nm	1.5nm	2.0nm
50nrad	-	6.47	11.08	19.43
100nrad	-	5.63	12.73	16.5
150nrad	-	5.15	11.63	18.29
200nrad	-	5.13	15.06	22.43

From the above table, the slope error has little effect on the relative strength of the para-peaks, but with the increase of the height error, the relative strength of the para-peaks increases. When the height error is 0.5 nm, the relative intensity of the side companion peak is almost negligible, and when the height error is 1.0 nm, the relative intensity of the side companion peak is about 5% of the focused spot, which can meet the needs of subsequent experimental stations. Therefore, the final height error of the optical element in the grating monochromator is better than 1.0 nm (rms) and the slope error is better than 100 nrad (rms).

Therefore, the height error requirements of the offset mirror group will be considered in conjunction with the height error requirements of the focusing lens of the experimental station, and the height error of the beamline offset lens group in the calculation is considered 1.0 nm (rms) and 2.0 nm(RMS). Due to the different optimized energy bands of each experimental station, considering that the influence of the height error of the optical element is obviously greater at the high energy end than at the low energy end, the upper limit of the optimized energy range is selected for the analysis of the influence of the height error of the optical element at each experimental station.

4.2.2 AMO Experimental Station

The optimized energy range of the AMO experimental station is 400eV-2000eV, taking the upper limit of the optimized energy range at 2000eV energy as an example, the relative photon flux of the focused spot at the first focal point of the experimental station, the relative peak intensity, horizontal and vertical spot size with the height error of the KB focusing lens are shown in Fig. 4.2, 3, 4, and 5

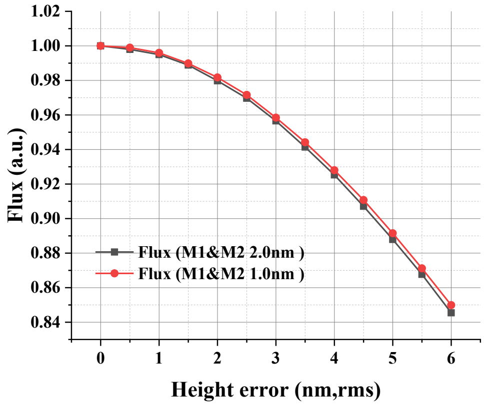

Fig. 4.2-2 Relative photon flux of the focused spot at the AMO experimental station at 2keV as a function of the height error of the optical element

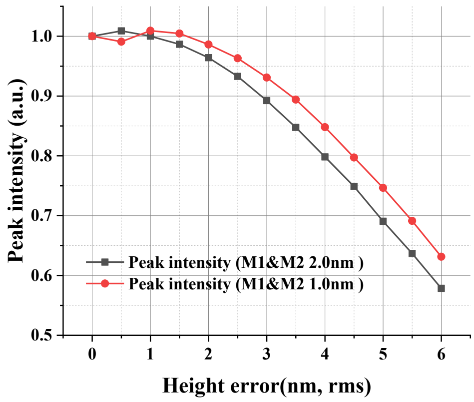

Fig. 4.2-3 The relationship between the relative peak intensity of the focused spot at the AMO experimental station at 2keV and the height error of the optical element

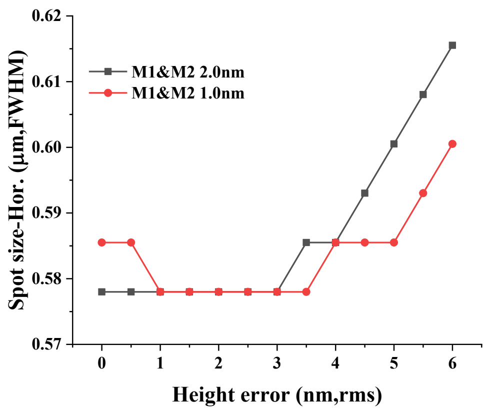

Figure 4.2-4 Relationship curve of the horizontal spot size of the focused spot at the AMO experimental station at 2keV as a function of the height error of the optical element

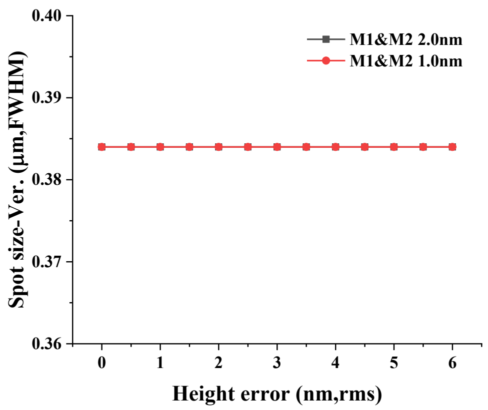

Fig. 4.2-5 The relationship between the vertical spot size of the focused spot at the AMO experimental station at 2keV and the height error of the optical element

With the increase of the height error of the KB mirror at the AMO experimental station, the photon flux and peak intensity at the sample point decreased, the horizontal spot size increased slightly, and the vertical spot size barely changed. This is mainly due to the fact that the beam passes through three mirrors in the horizontal direction and only the last KB focusing mirror in the vertical direction, so the horizontal direction is more sensitive to the influence of the height error of the optical element. The effect of the change in the height error of the beamline offset mirror group on the photon flux at the focal point is not very obvious, and the effect on the peak intensity is not more than 10%. Since the AMO station requires the incident FEL pulse to have a high peak intensity, the height error of the horizontal KB focusing mirror of the AMO experimental station should be better than 3.0 nm (rms) and the height error of the vertical KB focusing mirror should be better than 5.0 nm (rms), and the peak intensity at the focal point can reach 90% of the ideal state when the height error of the offset mirror group is 2.0 nm (rms).

4.2.3 SSS Experimental Station

The optimized energy range of the SSS experimental station is 400eV-2000eV, taking the upper limit of the optimized energy range at 2000eV energy as an example, the relative photon flux of the focused spot at the first focal point of the experimental station, the relative peak intensity, horizontal and vertical spot size with the height error of the KB focusing lens are shown in Fig. 4.2-6, 7, 8, and 9. The height error of the optical element in the grating monochromator is 1.0 nm (rms).

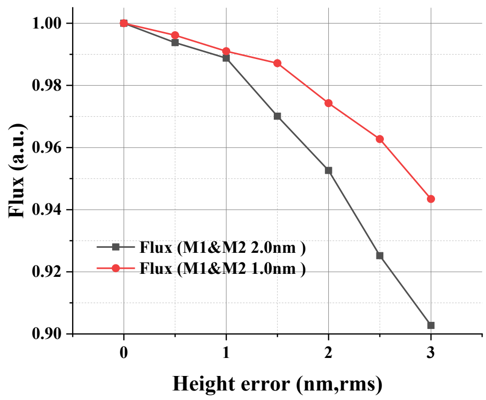

Fig. 4.2-6 Relationship between the relative photon flux of the focused spot at 2keV and the height error of the optical element

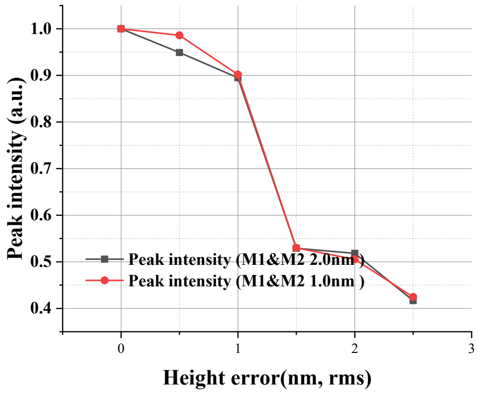

Fig. 4.2-7 The relationship between the relative peak intensity of the focused spot at 2keV and the height error of the optical element

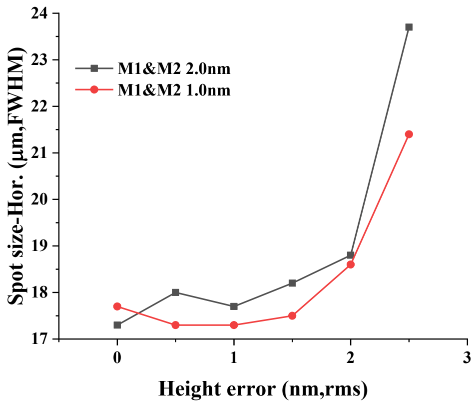

Fig. 4.2-8 Relationship curve of the horizontal spot size of the focused spot at the SSS experimental station at 2keV with the height error of the optical element

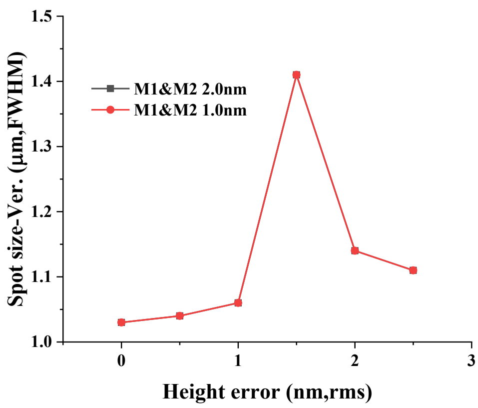

Fig. 4.2-9 Relationship between the vertical spot size of the focused spot at the AMO experimental station at 2keV and the height error of the optical element

With the increase of the height error of the KB mirror at the SSS experimental station, the photon flux and peak intensity at the sample point decreased, and the spot size in both directions increased greatly. It is evident that the decrease in peak intensity at the focal point is much greater than the decrease in photon flux, mainly due to the increase in the size of the focal spot. As the height error of the optics increases, the size of the vertical spot at the focal point nearly doubles, and then splits, so that even though the photon flux at the focal point remains above 90% compared to the ideal state, the peak intensity still decreases dramatically. Although the SSS experimental station mainly performs multi-pulse accumulation experiments and does not require the peak intensity of a single pulse, the vertical spot size will affect the energy resolution of the RIX spectrometer of the experimental station, so the spot size is required. Therefore, the height error of the vertical KB focusing mirror of the SSS experimental station should be better than 1.0 nm (rms), and the height error of the horizontal KB focusing mirror should be better than 2.0 nm (rms).

4.2.4 SES Experimental Station

The optimized energy range of the SES experimental station is 400 eV-2000 eV, taking the upper limit of the optimized energy range of 2000 eV as an example, the relative photon flux of the focused spot at the first focal point of the experimental station, the relative peak intensity, the horizontal and vertical spot size with the height error of the KB focusing lens are shown in Figure 4.2-10, 11, 12, and 13. The height error of the optical element in the grating monochromator is 1.0 nm (rms), and the effect of the height error of the beam reaching the SES experimental station is also taken into account by passing through the deflection mirror M3.

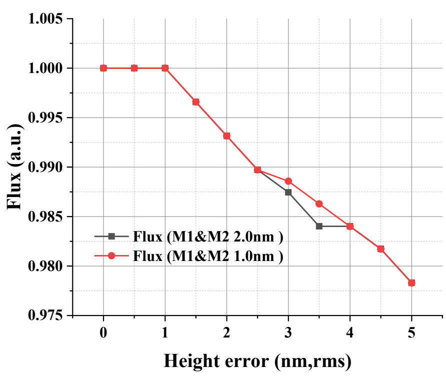

Fig. 4.2-10 Relative photon flux of the focused spot at SES at 2keV as a function of the height error of the optical element

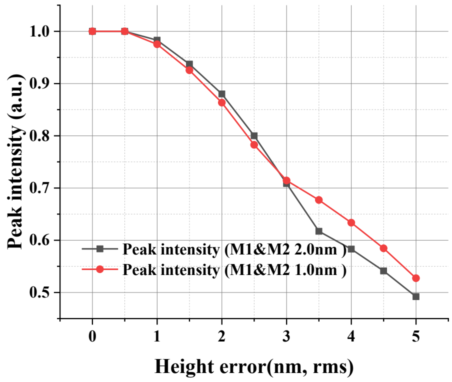

Fig. 4.2-11 Relationship curve of the relative peak intensity of the focused spot at the SES experimental station at 2keV as a function of the height error of the optical element

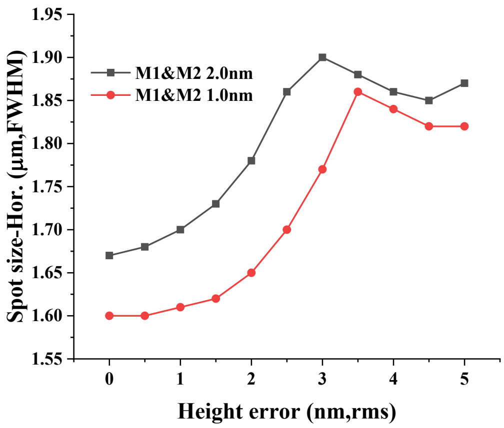

Figure 4.2-12 Relationship between the horizontal spot size of the focused spot at 2keV and the height error of the optical element

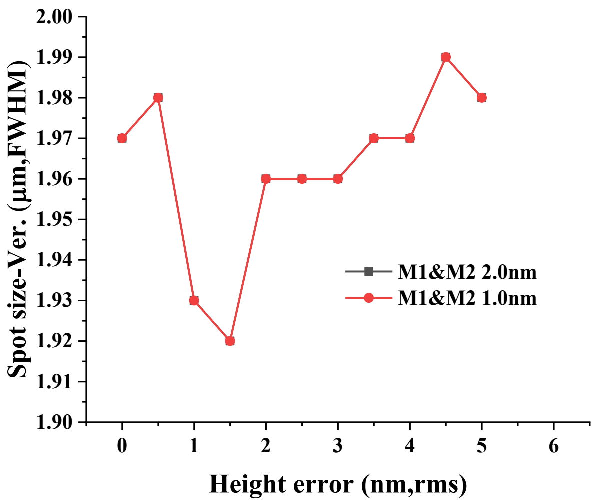

Figure 4.2-13 The relationship between the vertical spot size of the focused spot at 2keV and the height error of the optical element

With the increase of the height error of the KB mirror (including the horizontal deflection mirror M3) at the SES experimental station, the photon flux at the sample point remained almost constant, the peak intensity decreased, and the horizontal spot size increased greatly, and then there was a split, and the vertical spot size did not change significantly, so the decrease in peak intensity was mainly caused by the increase of the horizontal spot size. Therefore, the height error of the horizontal KB focusing mirror should be better than 2.0 nm (rms), the height error of the vertical KB focusing mirror should be better than 5.0 nm (rms), and the height error of the deflection mirror M3 should be better than 2.0 nm (rms).

For the offset lens group, it can be seen from the above calculation results that the height error of the beamline offset lens group mainly has a great impact on the focused spot of the experiment in the horizontal direction, which is mainly because the offset lens group is placed horizontally. When its height error is 2.0nm (rms), the focused spot performance of the experimental station (including spot size, photon flux, peak intensity, etc.) is not much lower than that when the height error is 1.0nm (rms), which can already meet the needs of the experimental stationConsidering the nature of the Gaussian spot, the photons are mainly concentrated in the half-height and width range of the spot, and the height error of the optical element in this range is much greater than that of the edge part, considering the processing difficulty of the ultra-smooth optical element, the influence of clamping, bending and the influence of thermal effect, etc., the height error of the offset lens group can be sub-regionally required: the height error is better than 1.0nm in the range of the half-height and width of the spot, which is better than 3.0nm in the full mirror length range.

In summary, the final height error requirements of each optical element on the FEL-II beam line are shown in Table 4.2-3.

Table 4.2-3 Final height error requirements for each optical component on the FEL-II beamline

Optics		Height error (nm, rms/PV)	Whether to bend or not
Offset mirrors	M1	3.0nm/12.0@full range 1.0nm/4.0@300mm central part	not
	M2a	3.0nm3.0nm/12.0@full range 1.0nm/4.0@350mm central part	be
	M2b	3.0nm3.0nm/12.0@full range 1.0nm/4.0@320mm central part	be
PGM	PM	1.0/4.0	not
	PG	1.0/4.0	not
DM	M3	2.0/8.0	not
KB-AMO	KB-H	3.0/12.0	be
	KB-V	5.0/20.0	be
KB-SSS	KB-H	2.0/8.0	not
	KB-V	1.0/4.0	not
KB-SES	KB-H	2.0/8.0	not
	KB-V	5.0/20.0	not

The height error requirement is the minimum height error requirement in the working state of the optical component, which includes the manufacturing error of the optical component, the sum of various errors caused by mechanical clamping, bending, and thermal effects.

Heat Loading and Radiation Damage

4.1Heat load

When considering the effect of thermal load on the optics in the beamline, the data of the FEL-II light source at 1MHz repetition rate, high charge mode and no taper are used. The effects of heat loads on the optics in the beamline at different repetition rates are assumed to be linear for the high charge and taper modes, low charge modes, and different repetition rates.

4.1.1 Offset mirrors

For X-ray lasers with high repetition rate and high brightness, the beamline will be subjected to great heat load pressure and radiation damage pressure. Considering the FEL laser fundamental, the oscillator background synchrotron radiation, and the FEL higher harmonics, the thermal power distribution of FEL laser over the offset mirror group is shown in Figure 4.1-1, 2, and 3.

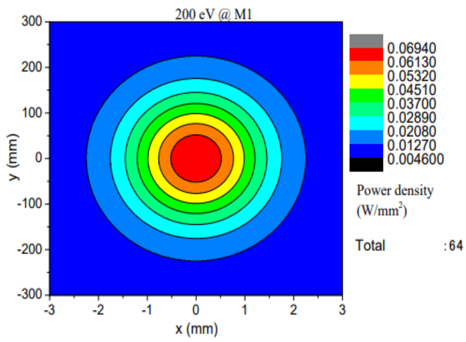

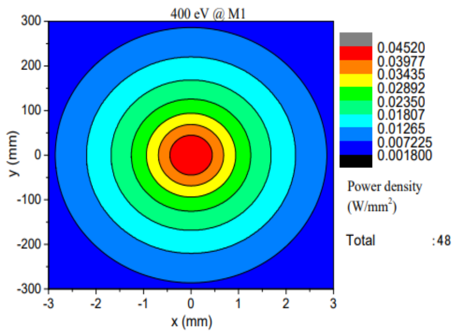

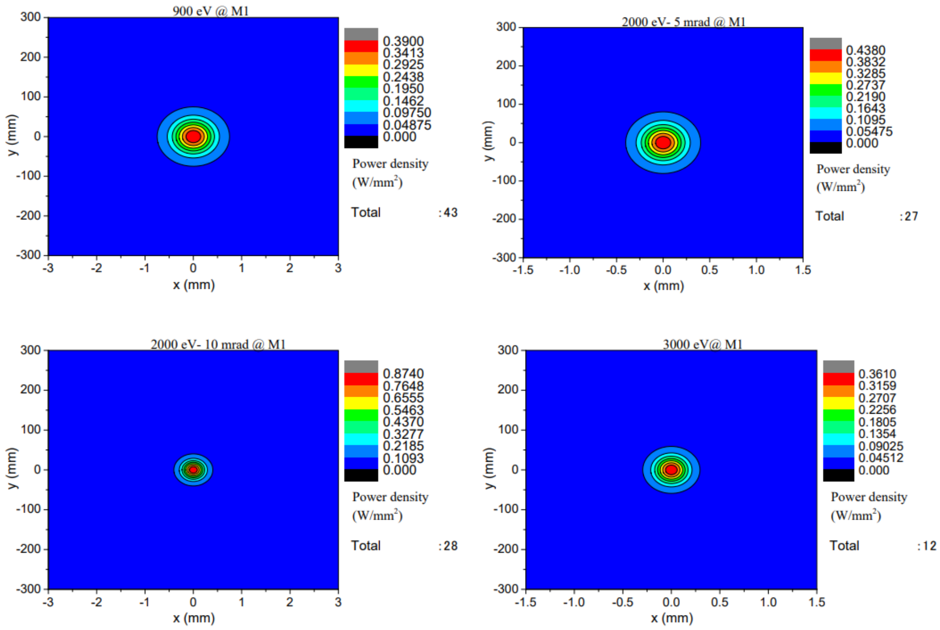

Fig. 4.1-1Thermal load distribution on offset mirror group M 1

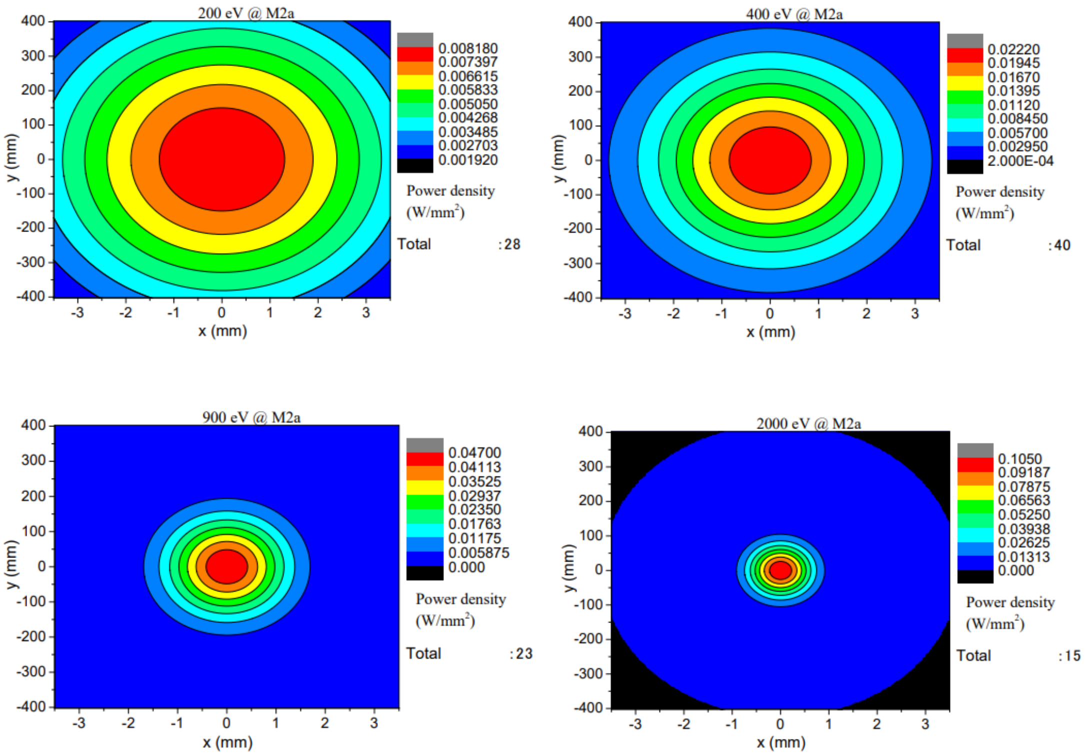

Figure 4.1-2 Thermal load distribution on the offset mirror group M2a

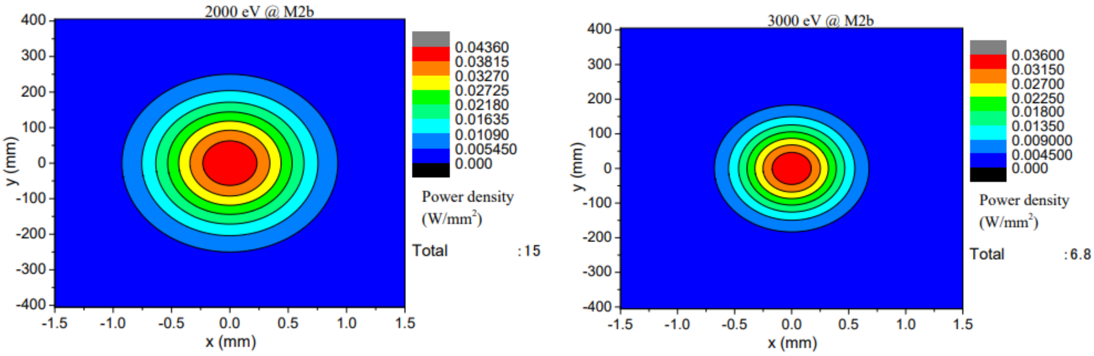

Figure 4.1-3 Thermal load distribution on M2b of the offset mirror group

For the offset lens group, the cooling method of "indium-water cooling" was adopted, the cooling water temperature was 30 ° C, the flow rate was 1.5 L/min, the film coefficient of the inner wall of the water pipe was 3177 W/m2/° C, and the film coefficient of the contact surface between the copper tube and indium iron, and indium iron and monocrystalline silicon was 150000 W/m2/° C. When the accelerator is running at 1 MHz repetition rate, in high charge mode, the temperature distribution on the optics is shown in Figures 4.1-4, 5, and 6 according to the results of finite element analysis

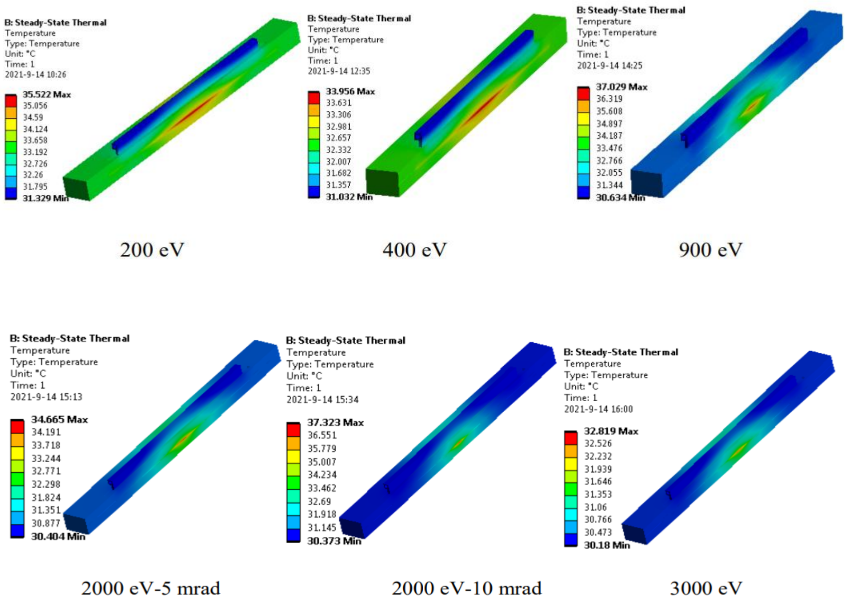

Figure 4.1-4 Temperature distribution on offset mirror group M1

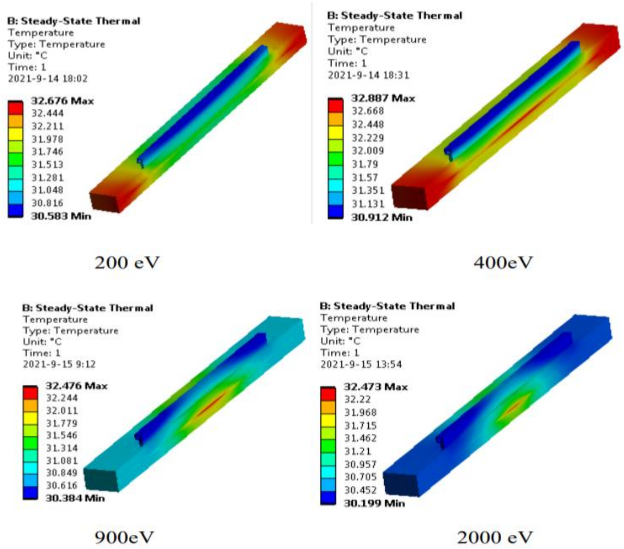

Figure 4.1-5 Temperature distribution on the offset mirror group M2a

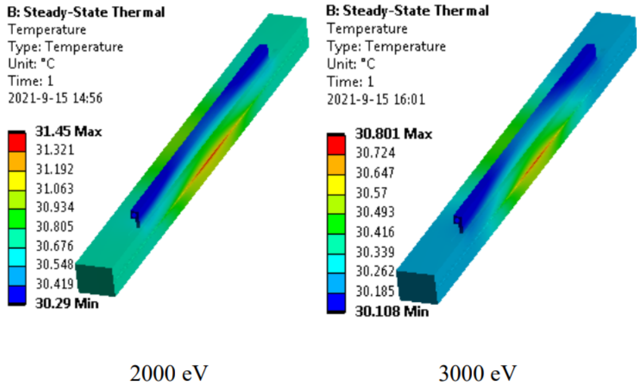

Figure 4.1-6 Temperature distribution on M2b of the offset mirror set

The deformation of the offset lens group is shown in Figures 4.1-7, 8, and 9

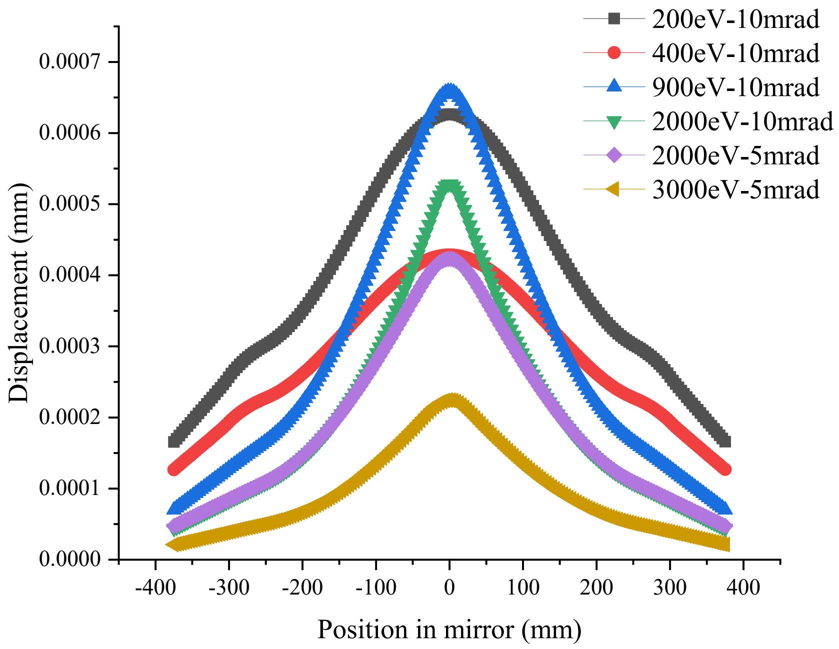

Fig. 4.1-7 Deformation of M1 mirror at different energy points at 1MHz repetition rate and high charge mode

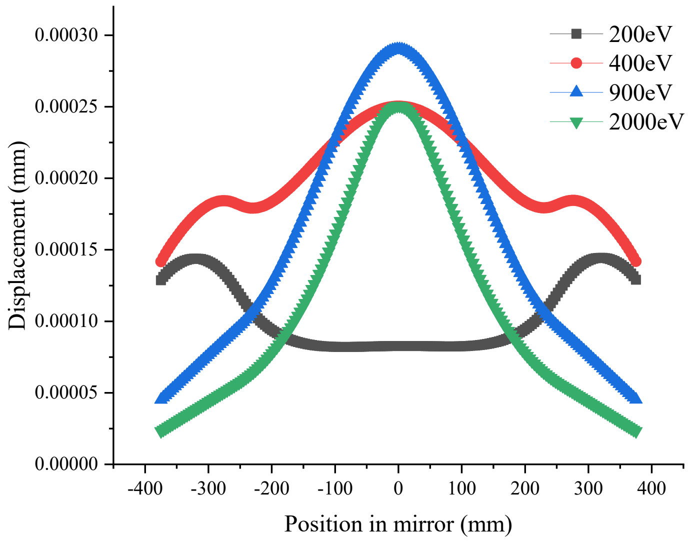

Fig. 4.1-8 Deformation of M2a mirror at different energy points at 1MHz repetition rate and high charge mode

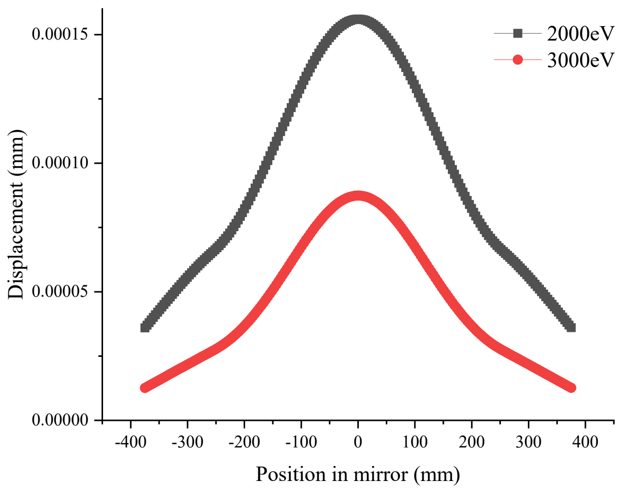

Fig. 4.1-9 Deformation of M2b mirror at different energy points at 1MHz repetition rate and high charge mode

Table 4.1-1 shows the error of the equivalent radius of curvature of each optical element of the offset lens group and the residual height after deducting the surface shape when the accelerator is operated at different FEL repetition frequencies

Table 4.1-1 The equivalent radius of curvature of each optical element of the offset lens group and the residual height error after deducting the surface shape of the surface under different FEL repetition frequencies

	M1						M2a				M2b	
Photon energy (keV).	200	400	900	2000 (10mrad)	2000 (5mrad)	3000	200	400	900	2000	2000	3000
Absorbed power (W).	64.5	48.6	43.3	28.2	27.3	12.5	28.2	40.5	23.3	15.2	15.2	6.8
Equivalent radius (km).	51.27	141.22	20.62	6.89	36.45	41.8	-	228.17	82.93	42.86	217.2	252.5

Residual height error (nm, rms).	2.87	12.66	12.79	1.93	9.45	3.83	-	0.87	1.3	0.74	1.04	0.35

The above results are 1MHz repetition rate, and the results in High charge mode can meet the requirement of less than 2.0nm (rms) when the repetition rate is reduced to 100kHz, according to the height error requirement of the optical element. Considering that the thermal load of the optics increases by a factor of 3-4 in taper mode, the maximum permissible repetition rate is 30kHz when the accelerator is running in High charge+taper mode.

4.1.2 Grating monochromator

In the working state, the thermal power distribution between the plane mirror and the planar grating in the grating monochromator is shown in Figure 4.1-10 and 11

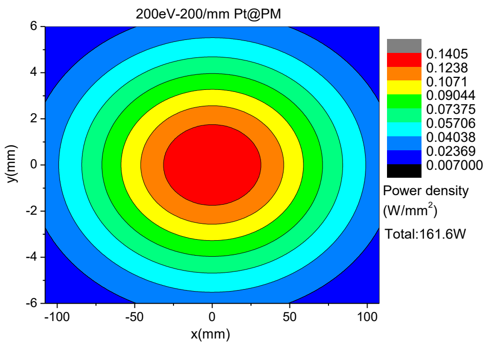

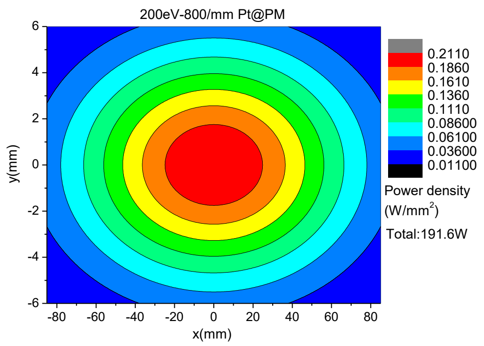

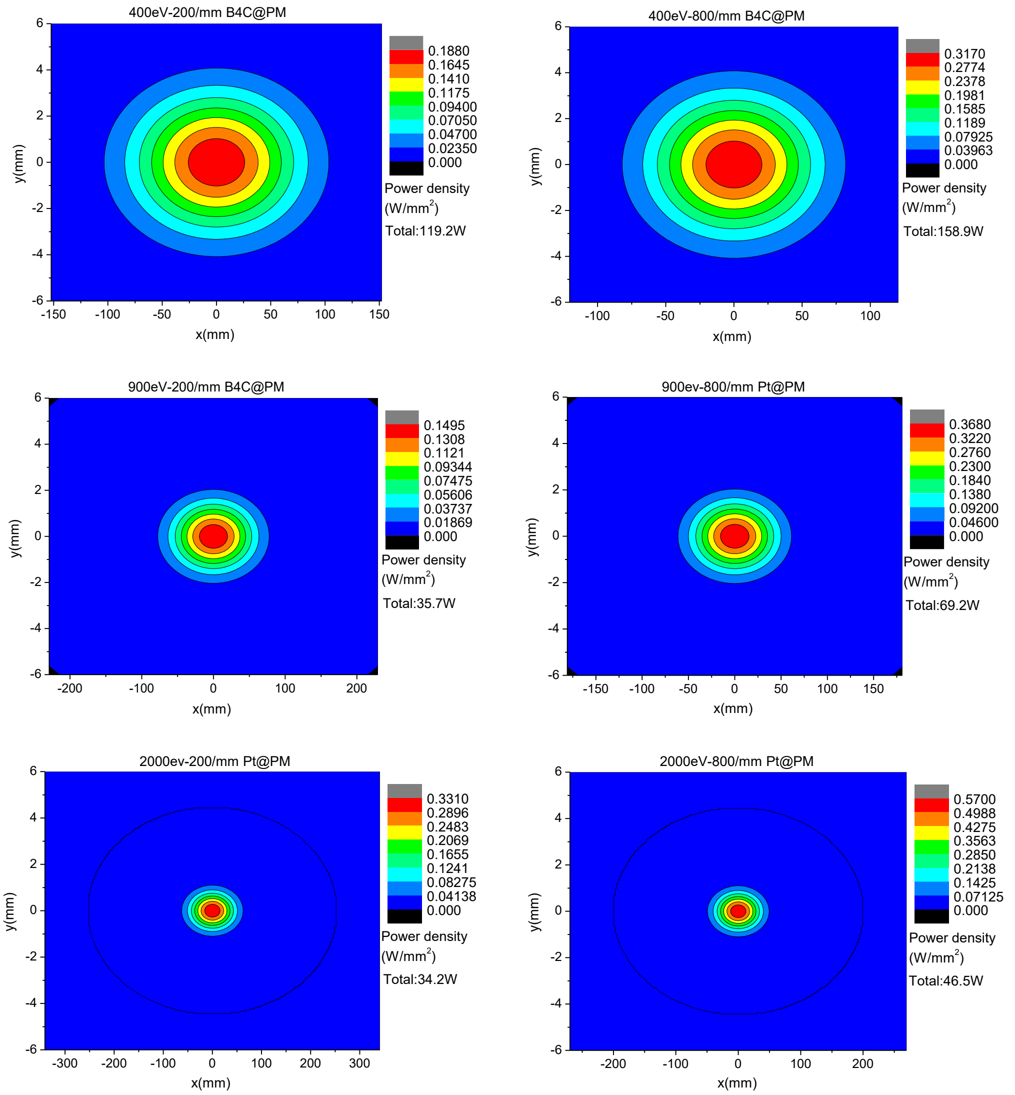

Figure 4.1-10 Thermal load distribution on the grating monochromator plane mirror PM

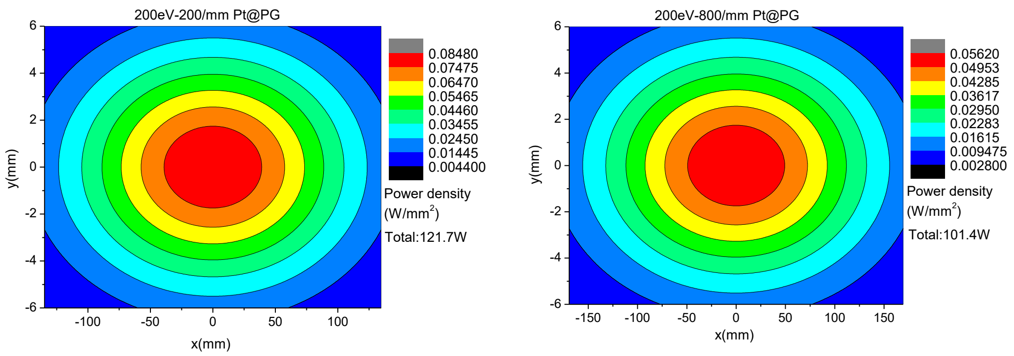

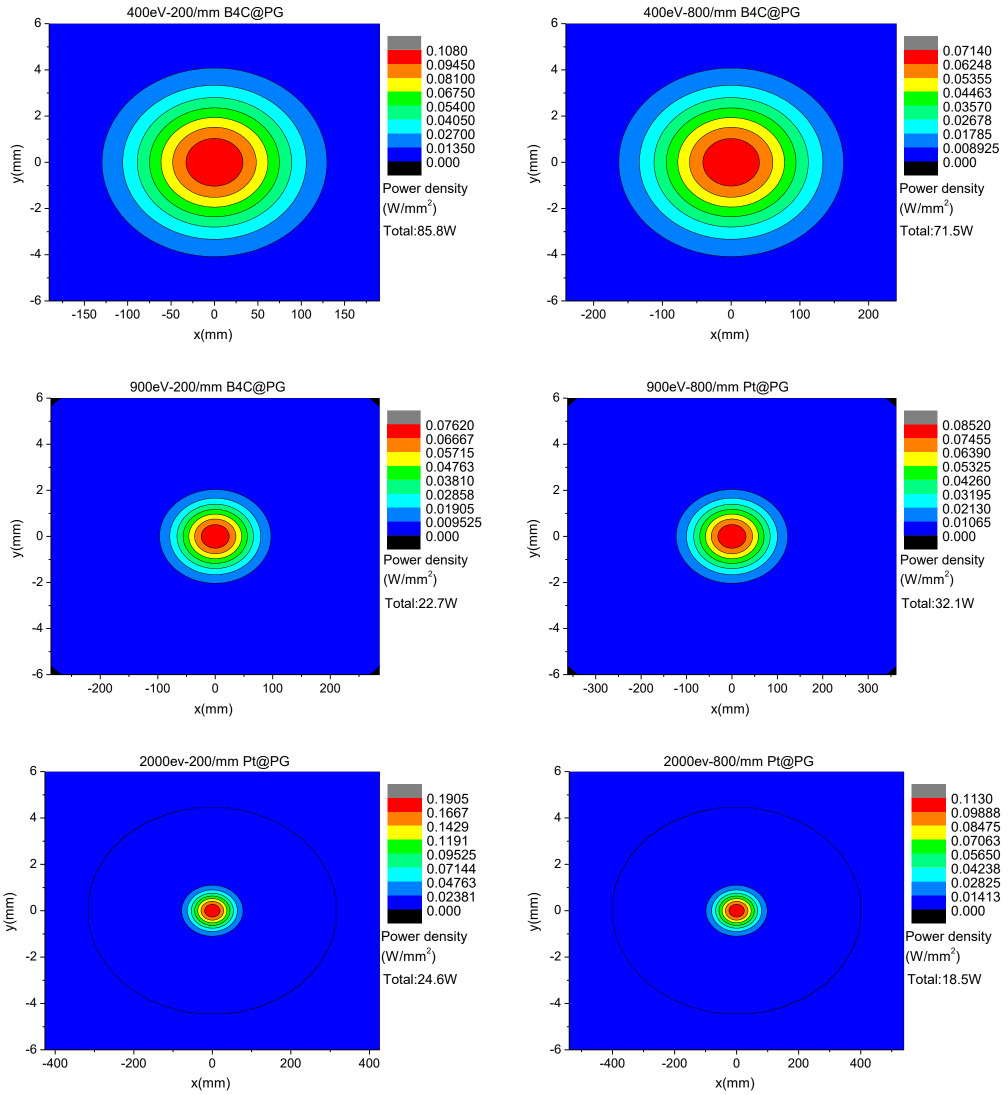

Figure 4.1-11 Thermal load distribution on the PG of the planar grating of the monochromator grating

For the grating monochromator, the cooling method of "water-side cooling" is adopted, and the length of the cooling tube is about 80% of the spot length (based on 900 eV), the cooling water temperature is 30 °C, the flow rate is 1.5 L/min, and the membrane coefficient of the inner wall of the water pipe is 3177 W/m2/°C. When the accelerator is running at 1 MHz repetition rate and high charge mode, the temperature distribution on the optical element is shown in Figure 4.1-12 and 13 according to the results of finite element analysis

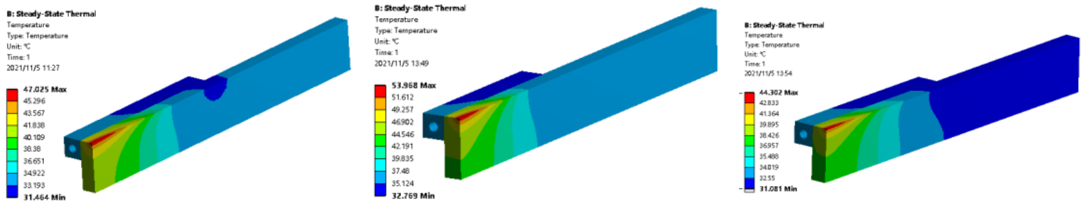

200 eV, 200/mm 200 eV, 800/mm 400 eV, 200/mm

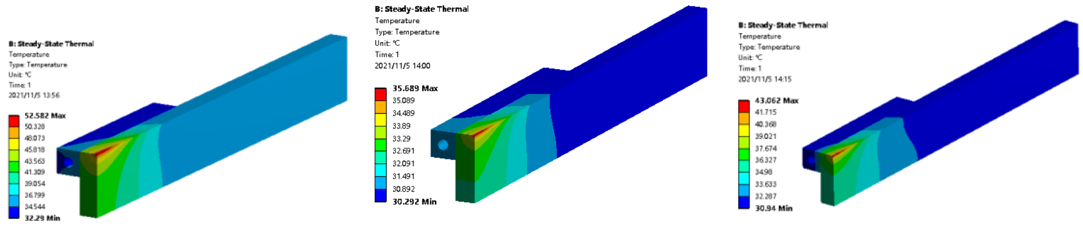

400 eV, 800/mm 900 eV, 200/mm 900 eV, 800/mm

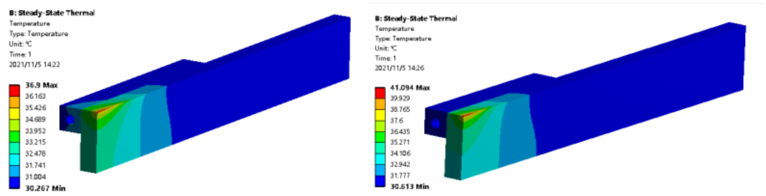

2000 eV, 200/mm 2000 eV, 800/mm

Figure 4.1-12 Temperature distribution on the grating monochromator plane mirror PM

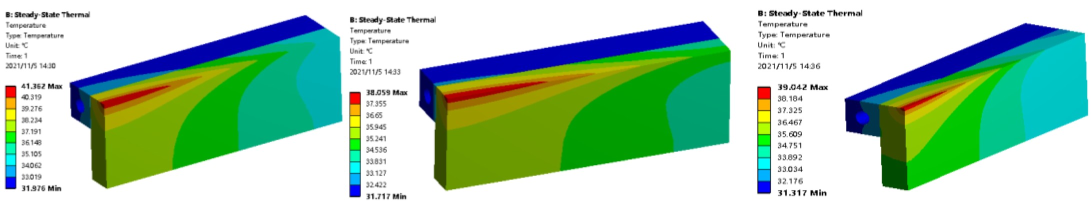

200 eV, 200/mm 200 eV, 800/mm 400 eV, 200/mm

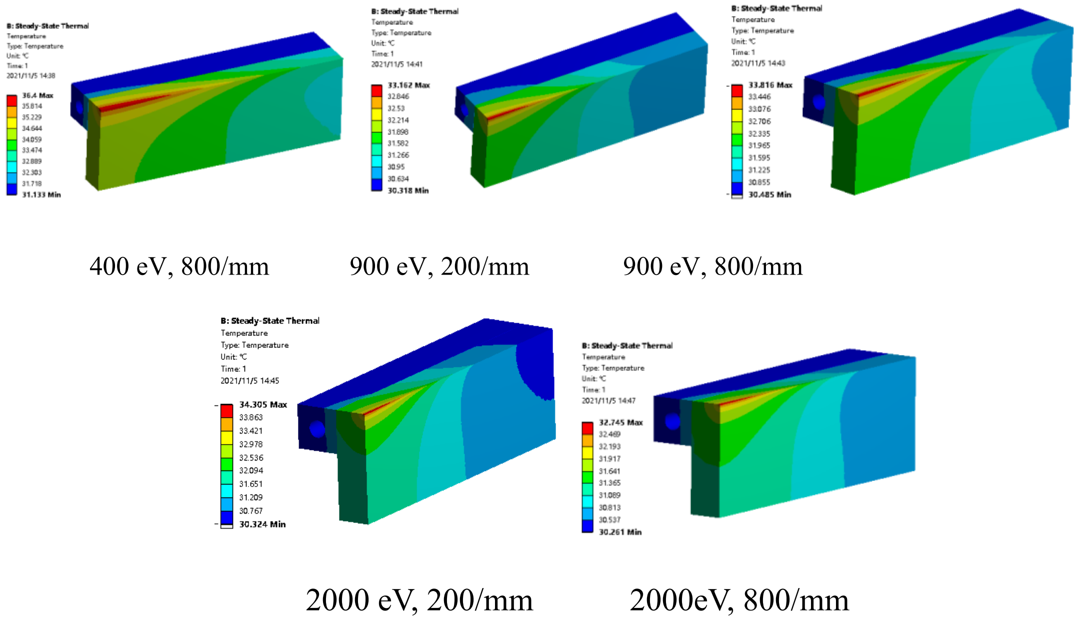

Figure 4.1-13: Temperature distribution on the PG of the monochromator planar grating of the grating

The deformation of the grating monochromator is shown in Figure 4.1-14 and 15

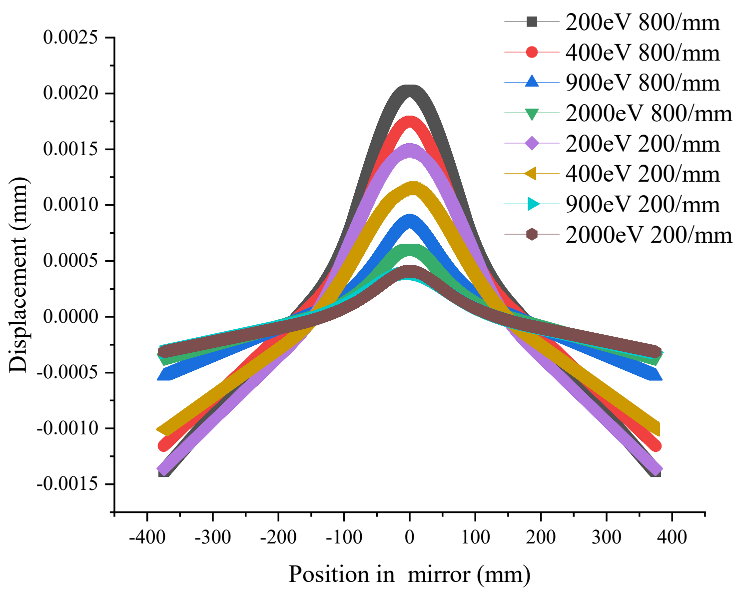

Figure 4.1-14 Deformation of the grating monochromator plane mirror PM at 1MHz repetition rate at different energy points in high charge mode

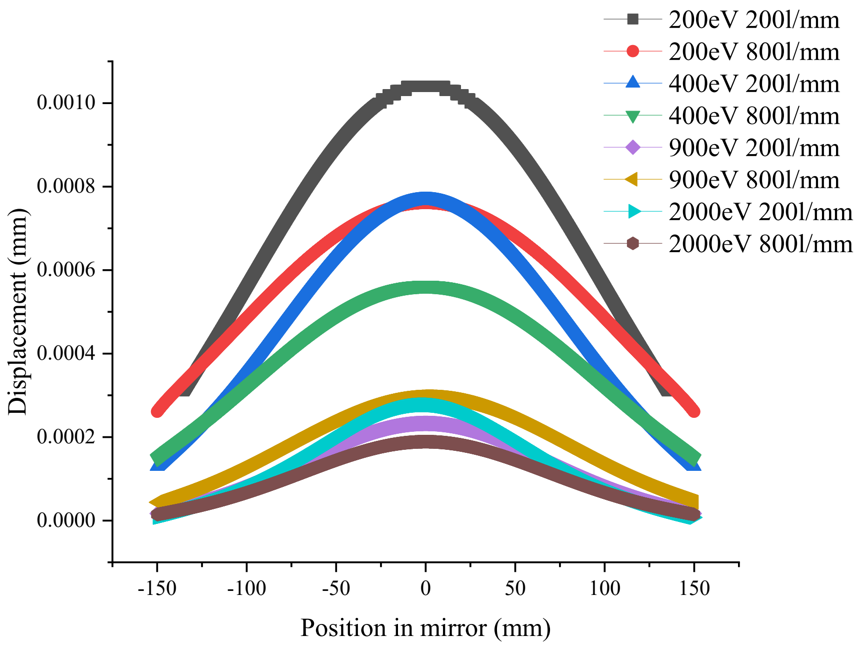

Figure 4.1-15 Deformation of the planar grating PG of the monochromator at 1MHz repetition rate at different energy points in high-charge mode

As mentioned above, the monochromator front mirror will change the surface shape due to the thermal effect, which can be equivalent to a convex mirror with a radius of curvature RM. Similarly, a grating can be equivalent to a convex grating with a radius of curvature RG. According to the results of finite element analysis, taking the 800l/mm grating and 900eV energy point as an example, the equivalent curvature radius of the thermal deformation of the front mirror under different FEL repetition frequencies, the equivalent object distance caused by the curved surface shape, and the residual height error of the optical element after deducting the curved surface shape are shown in Table 4As shown in 1-2, the equivalent radius of curvature of the thermal deformation of the monochromator grating, the error between the equivalent radius of curvature and the residual height after deducting the surface shape of the surface produced by the thermal deformation, is shown in Table 41-3.

Table 4.1-2 Equivalent radius of curvature, equivalent object distance, and

residual height error of monochromator pre-mirror at different repetition rates

	400eV				900eV			
Repetition rate (Hz)	1M	100k	50k	10k	1M	100k	50k	10k
Equivalent radius of curvature (km)	2.24	22.43	44.86	224.28	3.42	34.21	68.42	342.1
Equivalent distance (m)	43.7	147.3	169.4	193.1	44.2	147.9	170.0	193.2
Residual Height Error (nm)	1.26	0.13	0.06	0.01	2.76	0.28	0.14	0.03

Table 4.1-3 Equivalent radius of curvature and residual height error of monochromator grating at different repetition rates

	400eV				900eV			
Repetition rate (Hz).	1M	100k	50k	10k	1M	100k	50k	10k
Equivalent radius of curvature (km).	17.31	173.1	346.2	1730.98	25.16	251.64	503.27	2516.4
Residual height error (nm).	0.77	0.08	0.04	0.08	1.68	0.17	0.08	0.3

After bringing the equivalent distance and radius of curvature of the grating into the focusing equation of the grating, the α of incidence angle and diffraction angle of the grating satisfying the focusing condition can be obtained by obtaining the β of the incidence angle and diffraction angle of the grating, so that the corrected Cff value can be calculated. The corrected Cff values at the 400 eV and 900 eV energy points are shown in Figure 61-16.

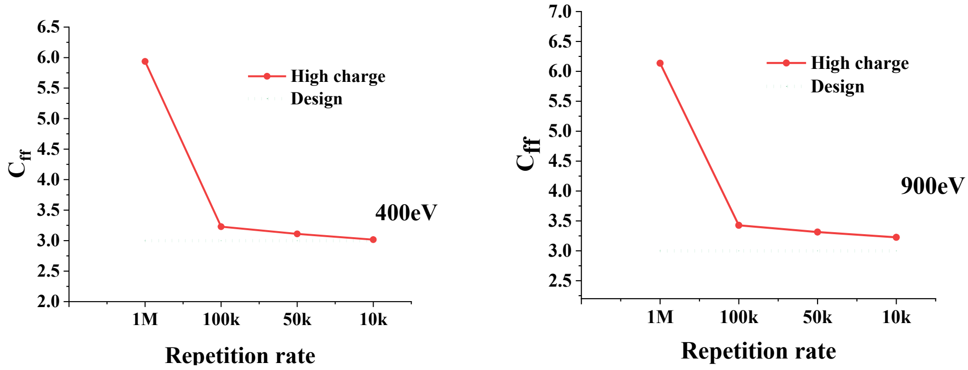

Figure 41-16 Modified Cff values of monochromators at different repetition rates at 400 eV and 900 eV energy points

Take the 900 eV energy point as an example, as shown in Table 4As listed in 1-2 and 3, when the accelerator is operated at 1 MHz and in high charge mode, the residual height error of the grating front mirror is 2.76 nm, and if the height error is required to be less than 1.0 nm, the maximum repetition frequency allowed for the accelerator to operate is about 350 kHz. It should be noted that the above thermal analysis calculations are analyzed using the data in the high charge mode of the accelerator, and it can be seen from the light source parameters that the energy of a single pulse in high charge and tapper mode is about 3 times that of high charge and non-tapper mode, and about 20 times that of low charge mode, which means that if the accelerator is running in high In charge and tapper mode, the monochromator allows a repetition rate of 100kHz, and if the accelerator is running in low charge mode, the monochromator can run at 1Mhz repetition rate.

4.1.3 Deflection mirrors

In the operating state, the thermal power distribution on the deflector mirror is shown in Figure 4.1-17:

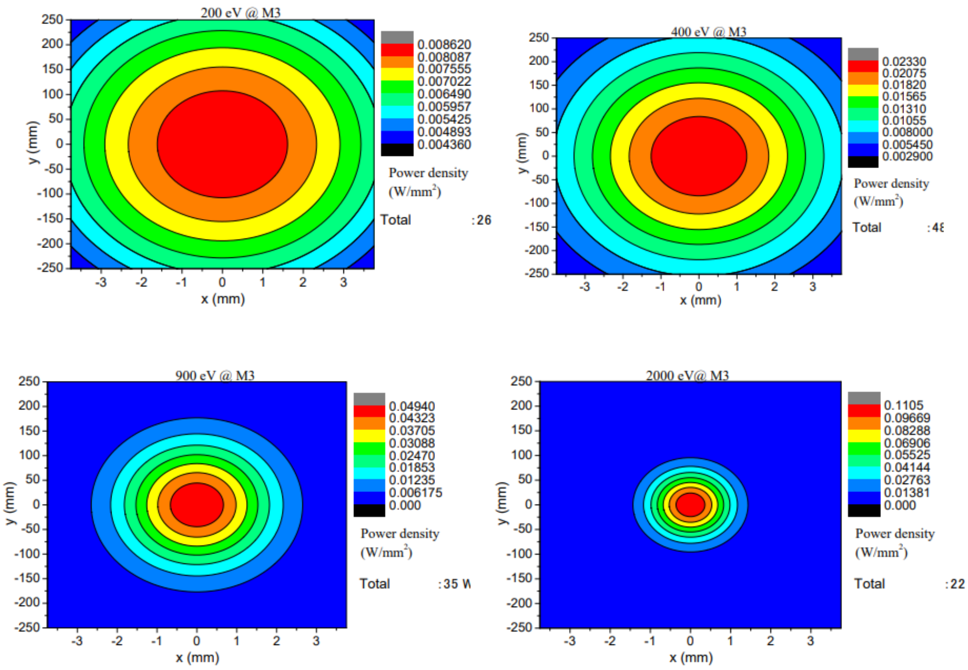

Figure 4.1-17 Thermal load distribution on a deflector mirror

The cooling method of "indium-water cooling" is the same as that of the offset mirror group, the cooling water temperature is 30 ° C, the flow rate is 1.5 L/min, the film coefficient of the inner wall of the water pipe is 3177 W/m2/° C, and the film coefficient of the contact surface between the copper tube and indium iron, and indium iron and monocrystalline silicon is 150000 W/m2/° C. When the accelerator is running at 1 MHz repetition rate and in high charge mode, the temperature distribution on the optics is shown in Figure 4.1-18 according to the results of finite element analysis

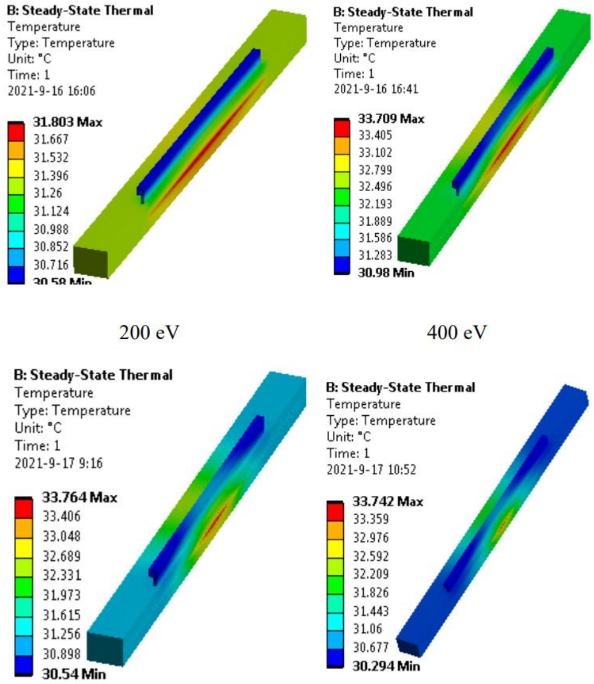

Figure 4.1-18 Temperature distribution on the deflector mirror

The deformation of the offset lens group is shown in Figure 4.1-19

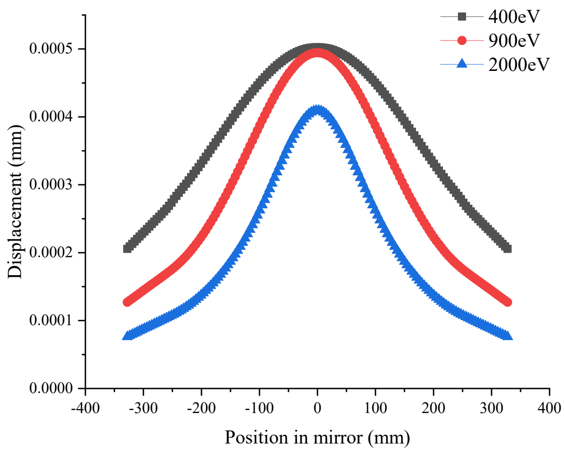

Figure 4.1-19 Deformation of the deflector at different energy points at 1MHz repetition rate and high charge mode

When the accelerator is operated at different FEL repetition frequencies, the error between the equivalent radius of curvature of the deflector and the residual height after deducting the surface shape of the surface is shown in Table 4.1-4

Table 4.1-4 Equivalent radius of curvature and residual height error of deflection focusing mirror at different repetition rates

	400eV		900eV	
Repetition rate (Hz).	1M	100k	1M	100k
Equivalent radius (km).	2070	20703	897.78	8977.83
Residual height error (nm, rms).	0.11	0.17	0.1	0.15

From the above table, it can be seen that the residual height error of the M3 mirror can meet the requirements at the full repetition frequency, but the radius of curvature cannot meet the requirements of more than 1000km at the energy point of 900eV, so the maximum working repetition rate of the M3 mirror is 800kHz in high charge mode, and the maximum working repetition frequency in taper mode is 200kHz considering the increase of power in taper mode.

4.1.4 KB focusing lens

In the working state, the thermal power distribution on KB at different grazing angles is shown in Figure 4.1-20 and 21

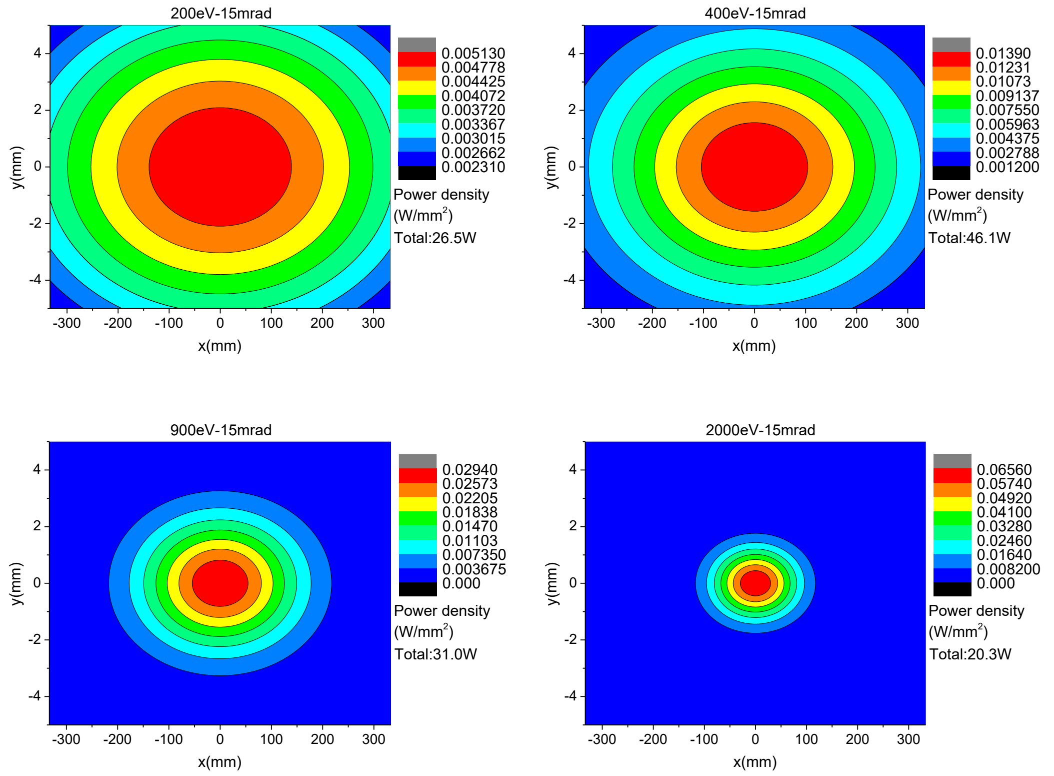

Figure 4.1-20 Thermal load distribution on the KB focusing mirror with a grazing incidence angle of 15 mrad

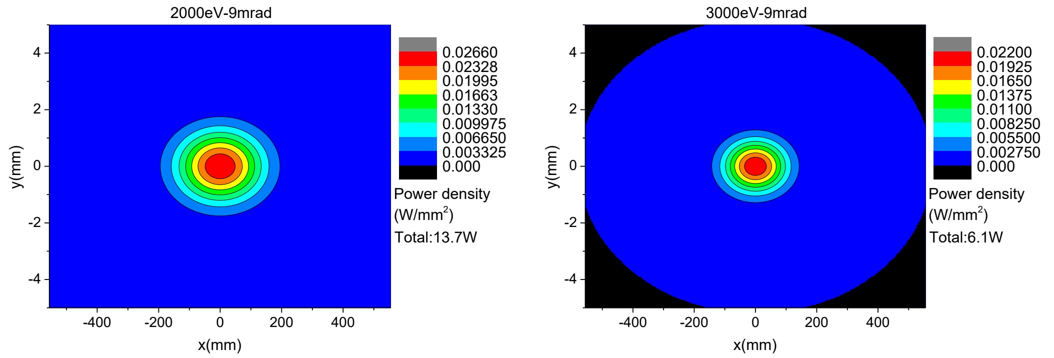

Figure 4.1-21 Thermal load distribution on the KB focusing mirror with grazing incidence angle of 20 mrad

For KB focusing lenses, the cooling method is the same as that of the offset lens group, and the cooling method of "indium-water-cooling" is adopted. The cooling water temperature is 30 °C, the flow rate is 1.5 L/min, and the membrane coefficient of the inner wall of the water pipe is 3177 W/m 2/°C calculated by equations (1)-(5). In addition, the film coefficient of the contact surface between copper tube and indium iron, and indium iron and monocrystalline silicon is 150,000 W/m2/°C. Unlike offset lenses, KB mirrors reflect the beam in the vertical direction and have two attitudes: face-up and face-down. For the horizontally deflected KB mirror, the single cooling channel model is used, and for the vertically deflected KB mirror, the double cooling channel model is used to place the two models upside down. When the accelerator is running at 1 MHz repetition rate, in high charge mode, the temperature distribution on the optics is shown in Figure 4.1-22, 23, 24, 25, and 26 according to the results of finite element analysis

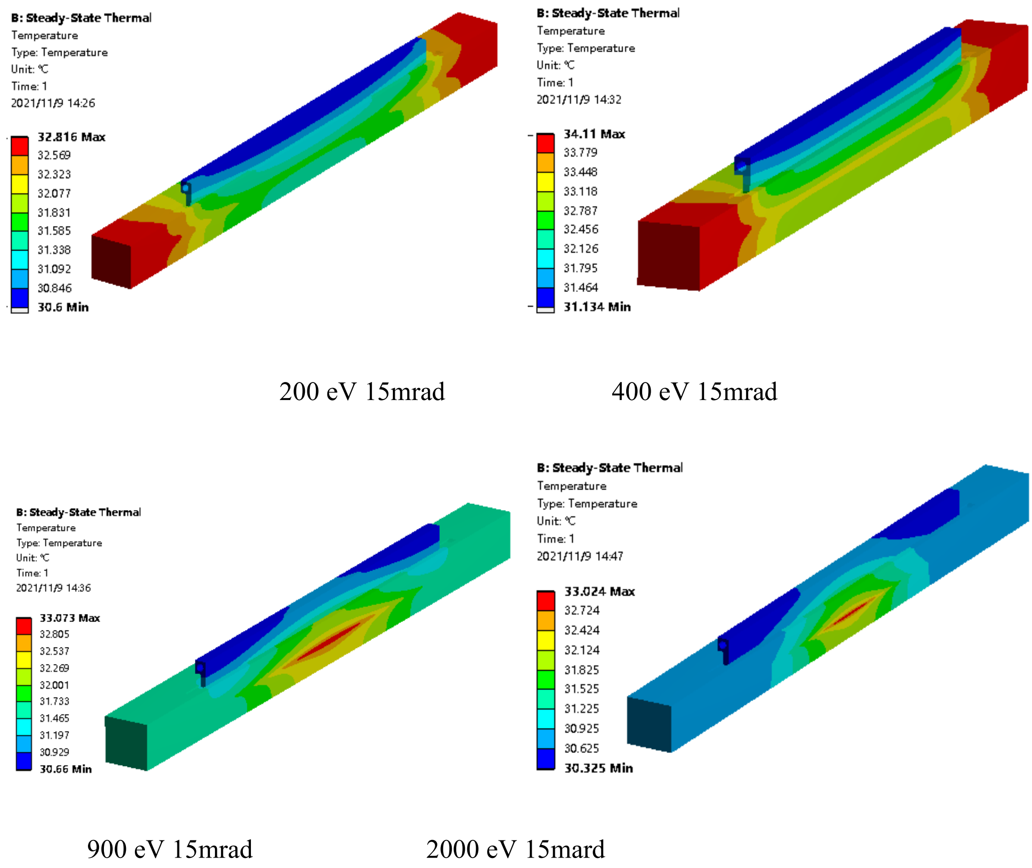

Figure 4.1-22 Temperature distribution of a KB focusing mirror at 15 mrad grazing incidence and single-tube lateral placement

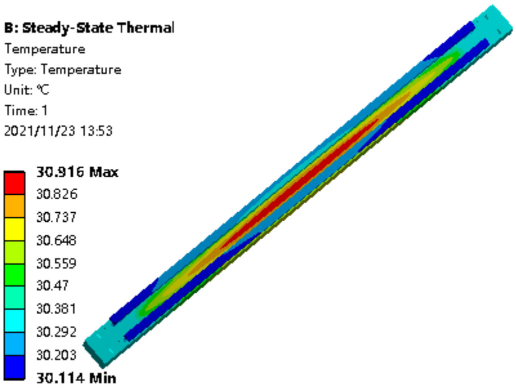

200 eV 15mrad

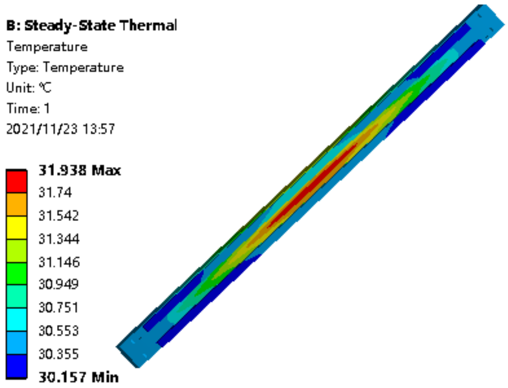

400 eV 15mrad

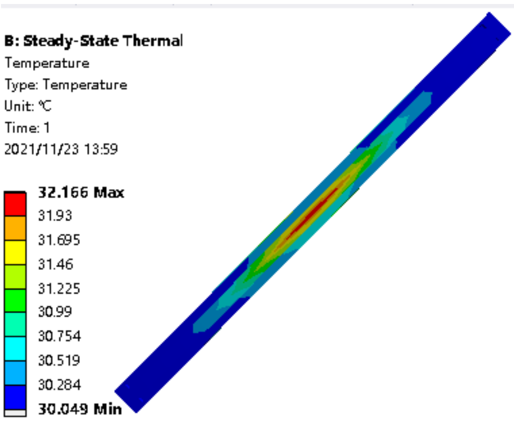

900 eV 15mrad

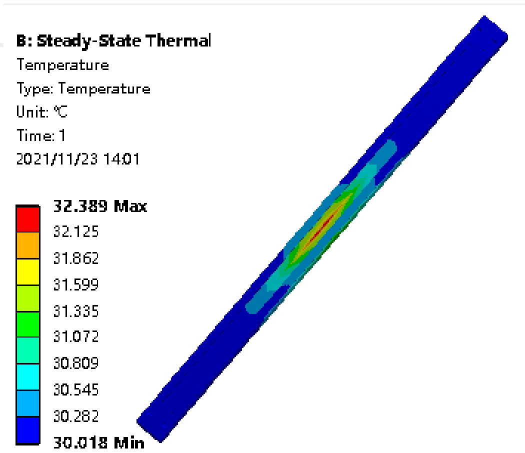

2000 eV 15mard

Fig. 4.1-23 Temperature distribution of the KB focusing mirror at 15 mrad grazing incidence and double tube forward discharge

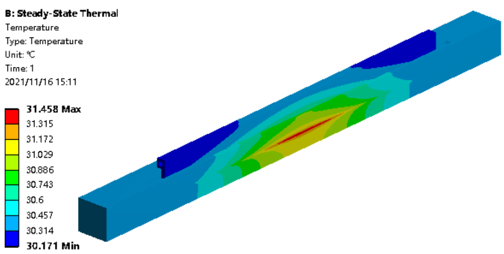

2000 eV 9mrad

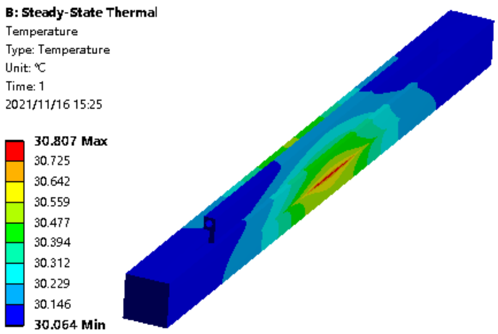

3000 eV 9mard

Fig. 4.1-24 Temperature distribution of KB focusing mirror on 9mrad grazing incidence and single-tube side-mounted conditions

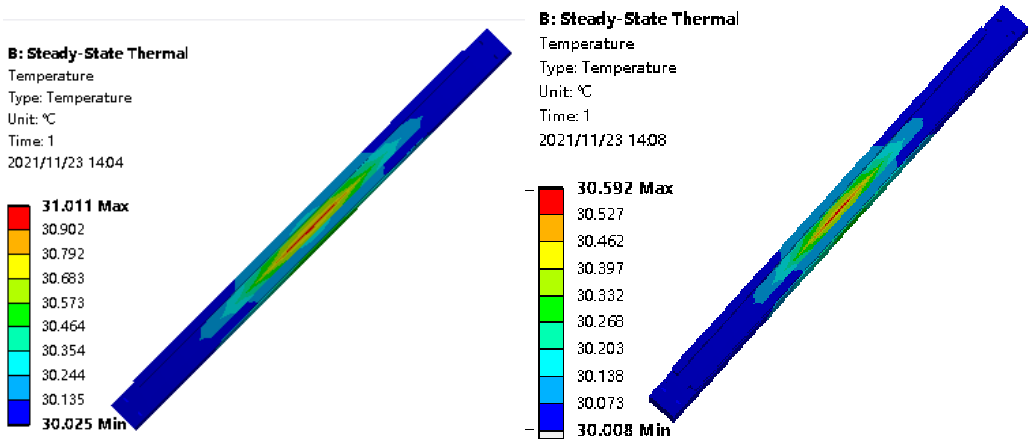

2000 eV 9mrad 3000 eV 9mard

Fig. 4.1-25 Temperature distribution of KB focusing mirror at 9mrad grazing incidence with double tube forward discharge

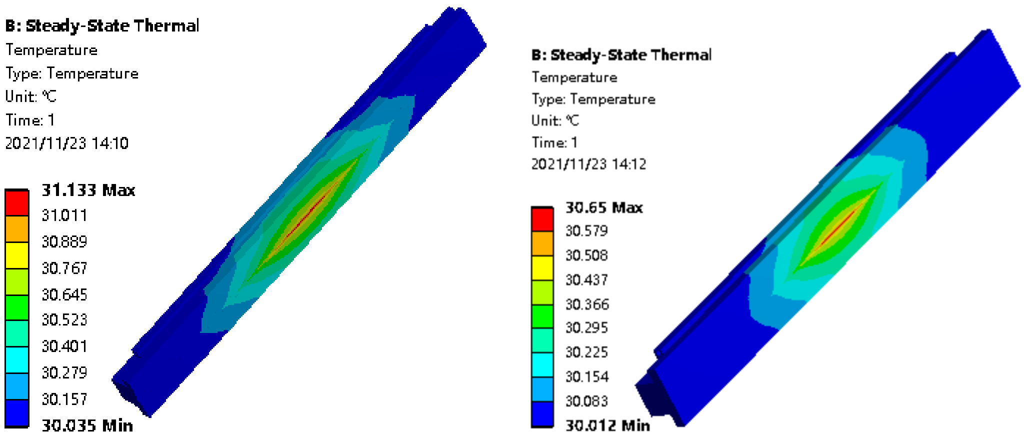

2000 eV 9mrad 3000 eV 9mard

Fig. 4.1-26 Temperature distribution of KB focusing mirror on 9mrad grazing incidence and double-tube inversion

The deformation of the KB mirror is shown in Fig. 4.1-27, 28, 29, 30, and 31

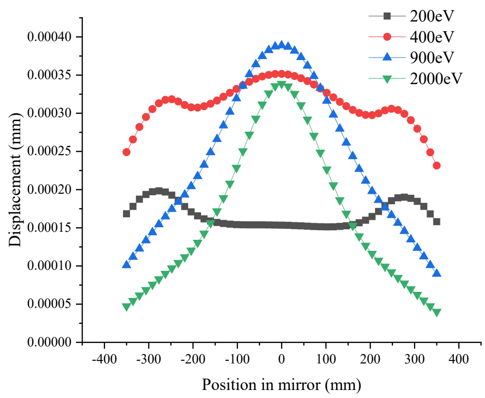

Figure 4.1-27 Deformation of horizontally deflected KB focusing mirror at 1MHz repetition rate at 1MHz and at different energy points in High charge mode at 15 mrad grazing incidence

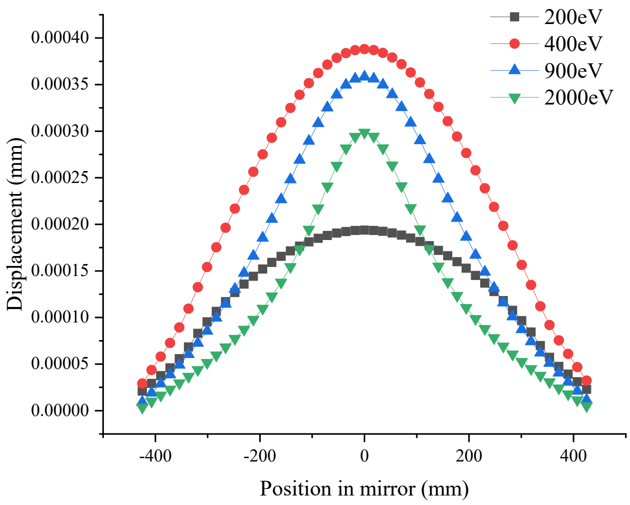

Figure 4.1-28 The deformation of the vertically deflected KB focusing mirror at 1MHz repetition rate at 1MHz and at different energy points in high charge mode at 15 mrad grazing incidence

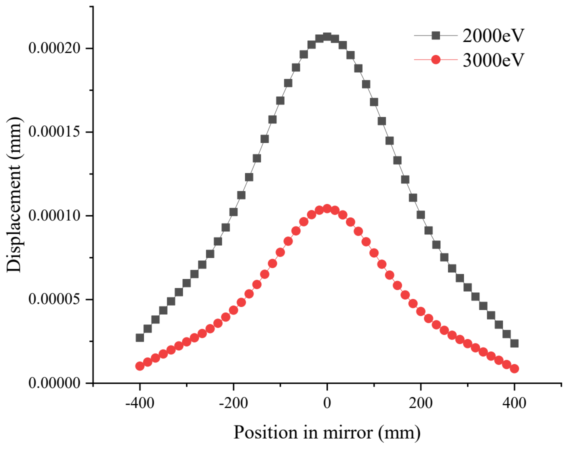

Fig. 4.1-29 Deformation of horizontally deflected KB focusing mirror at 1MHz repetition rate at high charge mode at 9mrad grazing incidence

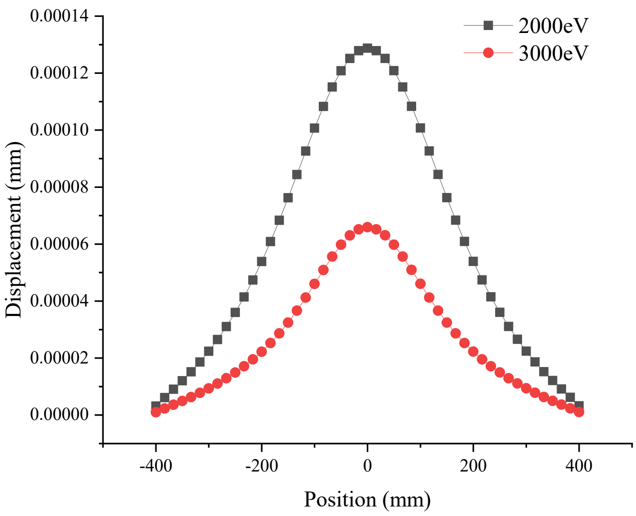

Fig. 4.1-30 The deformation of the vertically deflected (face-up) KB focusing mirror at 1MHz repetition rate at high charge mode at 9mrad grazing incidence

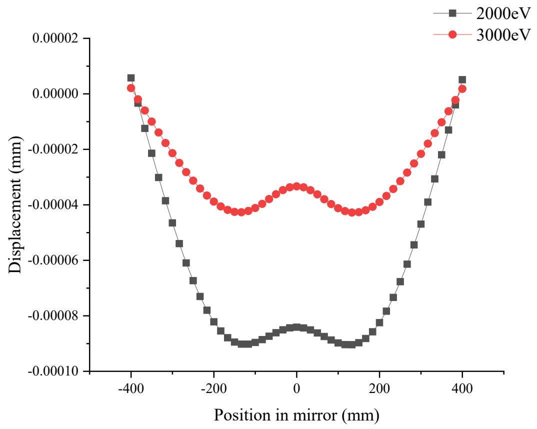

Fig. 4.1-31 The face-down deformation of the KB focusing lens at 1MHz repetition rate at high charge mode at 9mrad grazing incidence

When the accelerator is operated at different FEL repetition frequencies, the error of the equivalent radius of curvature of each optical element on the beam line and the residual height after deducting the surface shape is shown in Table 4.1-4

Table 4.1-4 Equivalent radius of curvature and residual height error of KB focusing lens at 1MHz repetition rate

	CPH				P/B ratio					
Photon energy (eV).	400	900	2000	3000	400	900	2000	3000	2000	3000
Grazing angle of incidence (mrad).	15	15	9	9	15	15	9	9	9	9
Deflection direction	level				vertical (face-up)	vertical (face-up)	vertical (face-up)	vertical (face-up)	vertical (face-down)	vertical (face-down)
Equivale	5452	1581	134.9	122.19	3191	3130	188	231.88	70.79	83.03

nt radius (km).										
Residual height error (nm, rms).	0.36	0.2	1.02	0.39	0.18	0.22	0.77	0.31	30.39	12.53

As can be seen from the above table, for the MONO branch, the KB mirror can be operated at a repetition rate of 1MHz, which can meet the requirements even when the taper mode is taken into account. However, for the Pink branch, horizontally deflected and vertically upward-facing KB mirrors can be operated at 1MHz repetition frequency, but vertically downward KB mirrors are allowed at a maximum allowable repetition rate of 30 kHz.

In summary, Table 4.1-5 shows the allowable operating repetition frequency of each optical element in different accelerator operating modes

Table 4.1-5 Allowable operating repetition frequency of each optical element in the FEL-II beamline in the operating mode

Optics	**Work re-frequency**	
	High charge mode	**High charge +taper mode**
Offset mirror	100 kHz	30kHz@10mrad
	1MHz	300 kHz@5mrad
PGM	350kHz	100 kHz
M3	800kHz	200 kHz
KB-AMO	500kHz	160kHz
KB-IEB	30kHz	10kHz
KB-SES	1MHz	1MHz
KBH-SSS	1MHz	1MHz
KBV-SSS	1MHz	1MHz

4.2 Radiation damage

Single pulse damage is one of the most critical issues in beamline design, and the dose absorbed by a single atom on an optical element can be calculated by:

$$D_A = E_{pulse}(1 - R)/A_{proj}l_{att}n_a$$

where latt is the attenuation length, R is the reflectivity, Epulse is the pulse energy, A is the spot area, and na is the atomic density. As shown in Figure 4.2-1, when the accelerator is running in high charge mode, the absorbed dose of a single atom on the optical element in the all-energy range is less than 0.007 eV/atom. Therefore, the dose absorbed by single atoms on the optical element is much lower than the damage threshold of 0.7 eV/atom for B4C and the safety threshold of 0.1 eV/atom adopted by international practice.

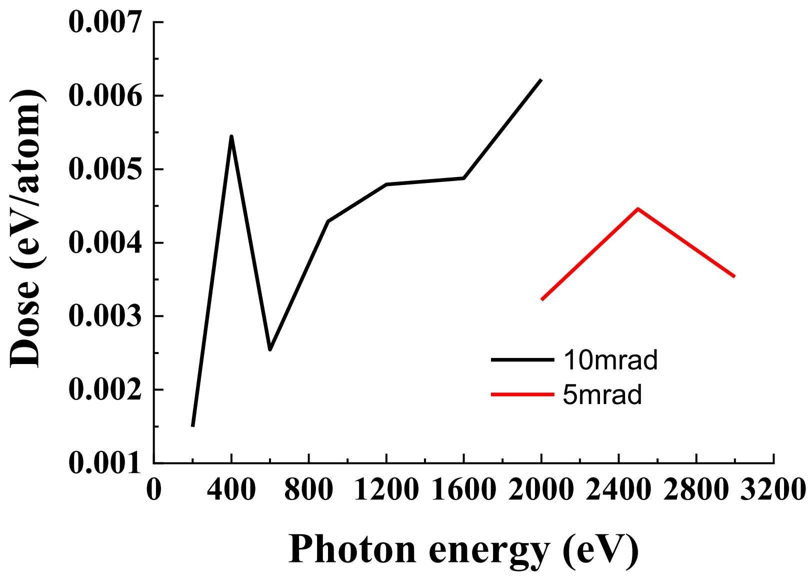

Figure 4.2-1 Absorbed dose of a single atom on an M1 mirror

The absorbed dose of a single atom on the pre-mirror corresponding to different gratings in the grating monochromator is shown in Figure 4.2-2. As mentioned above, for 200l/mm gratings, when the photon energy is lower than 1100 eV, the monochromator front mirror works under the B4C coating, and when the photon energy is higher than

1100 eV, the monochromator front mirror works under the Pt coating. For 500l/mm grating, when the photon energy is lower than 1000 eV, the monochromator front mirror works under the B4C coating, and when the photon energy is higher than 1000 eV, the monochromator front mirror works under the Pt coating. For 1200 l/mm gratings, the monochromator front mirror operates under the B4C coating when the photon energy is lower than 900 eV, and the monochromator front mirror operates under the Pt coating when the photon energy is higher than 900 eV. Therefore, for Pt coatings, the absorbed dose of a single atom is less than 0.07 eV/atom in the photon energy range in which it operates. For B4C coatings, the absorbed dose of a single atom is less than 0.02 eV/atom in the photon energy range in which it operates.

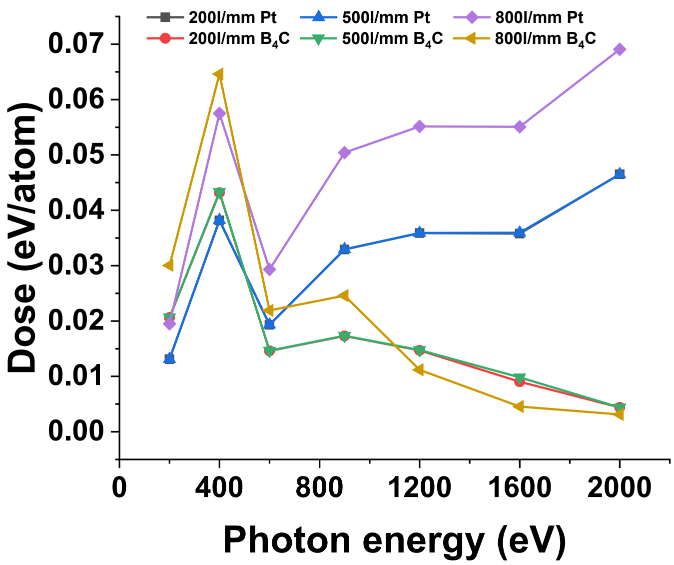

Figure 4.2-2 The absorbed dose of a single atom on the front mirror when the monochromator is working with different gratings

The absorption doses of single atoms on different linear densities are shown in Fig. 4.2-5, 6, and 7 when different grating coatings are combined with plane mirror coatings in the grating monochromator. For 200 l/mm grating, if B4C is selected for grating coating, the maximum single atomic absorption dose on the grating is less than 0.02 eV/atom, and if Pt is selected for grating coating, the maximum single atomic absorption dose on the grating is less than 0.1 eV/atom. For 500 l/mm grating, if B4C is selected for grating coating, the maximum single atomic absorption dose on the grating is less than 0.01 eV/atom, and if Pt is selected for grating coating, the maximum single atomic absorption dose on the grating is less than 0.08 eV/atom. For 600 l/mm grating, the maximum single atomic absorption dose on the grating is less than 0.01 eV/atom if B4C is selected for grating plating, and less than 0.07 eV/atom if Pt is selected for grating coating.

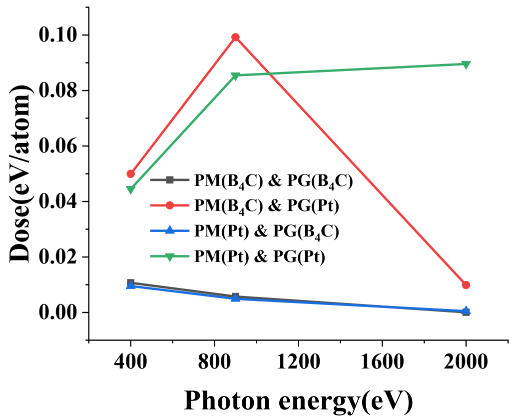

Figure 4.2-5 Absorbed dose of a single atom on a 200 l/mm grating of a monochromator in a grating

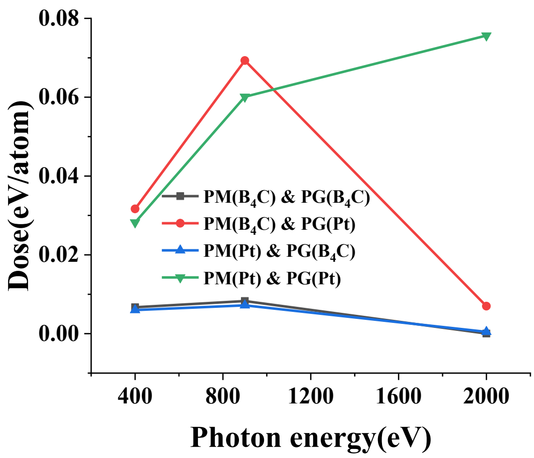

Figure 4.2-6 Absorbed dose of a single atom on a 500 L/mm grating of a monochromator in a grating

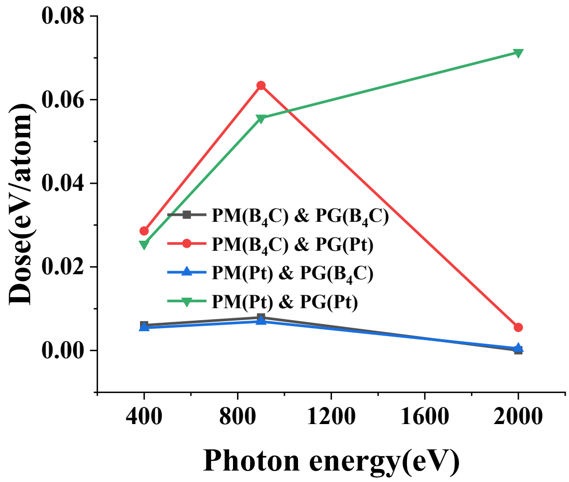

Figure 4.2-7 Absorbed dose of a single atom on a 600L/mm grating of a monochromator in a grating

5. Summary

The theoretically calculated beamline performance indexes can reach the acceptance indicators of the beamline, as shown in Table 5.0:

Table 5.0 Summary of beamline performance indicators

	Nominal	Objective	Design
Photon energy	0.2-3keV	0.5-2keV	0.2-3keV
Energy resolution	>15000@867eV	>10000@867eV	65000@867eV
Single-pulse photon transmission efficiency	30%@1keV（No monochromators）	15%@1keV（No monochromators）	50%@1keV（No monochromators）
Spot size at the sample	<10μm x. 6μm（H x V, FWHM）	<20μm x 12μm（H x V, FWHM）	2μm x 2μm（H x V, FWHM）

In the above results, the working repetition frequency of the beamline is ： 30Hz@high charge +taper mode， 100Hz@high charge mode。

6. List of beamline devices

	Device	Distance from the source point (m)
1	FE_ fixed aperture	83
2	FE_Imager	83.62
3	FE_ photon shutter	84.29
4	γ absorbers	85.1
5	FE_ safety shutter	85.67
6	Fast valve	108
7	Fixed aperture	110.36
8	Slit1	112
9	GMD/HAMPs 1	115.5
10	PES	120
11	Gas attenuator	135
12	Collimator 1	160
13	BLM 1	160.5
14	Imager 2	161.1
15	M1	165
16	Imager 3	166.1
17	M2a	168
18	Imager 4	169.1
19	M2b	172.05
20	Imager 5	173.17
21	Collimator 2	176
22	Wavefront sensor	184.4
23	BLM2	195.22
24	Imager 6	195.6
25	Stray-beam aperture	196
26	PGM	200
27	Exit aperture	203.5
28	Imager 7	207.4
29	M3	267

30	Imager 8	270
31	m_ photon shutter 1	294.4 (Branch)
32	Exit Slit	295 (branch).
33	m_ monochromatic beam energy resolution diagnotic	295.7 (branch).
34	Photon shutter 1	297.34
35	Solid attenuators	298
36	BLM3	311.2
37	m_BLM3	311.2 (Branch)
38	m_HAMPs-2	331.6 (Branch)
39	GMD/HAMPs 2	314
40	m_ collimated laser	316 (Branch)
41	Standard sample chamber	316.7 (Branch)
42	Slit 2	319.3
43	m_PAM 1	321.7 (Branch)
44	KBV-SSS	323 (Branch)
45	m_ laser beam combining chamber	324 (Branch)
46	SSS Experimental Station	325 (Branch)
47	KB-SES	331 (Branch)
48	m_ photon shutter 2	333.6 (branch)
49	m_PAM 2	335 (Branch)
50	SES Experimental Station 1	337 (branch)
51	Imager 9	340.2
52	SES Experimental Station 2	341 (Branch)
53	KB-AMO	342
54	m_beamstop 1	343.5 (Branch)
55	AMO Experimental Station 1	345
56	AMO Experimental Station 2	346.8
57	PAM 2	347.85